Alma Mater Studiorum - Università di Bologna

DOTTORATO DI RICERCA IN

SCIENZE E TECNOLOGIE DELLA SALUTE

Ciclo 34

**Settore Concorsuale:** 09/G2 - BIOINGEGNERIA

**Settore Scientifico Disciplinare:** ING-IND/34 - BIOINGEGNERIA INDUSTRIALE

# PERCUTANEOUS CEMENT DISCOPLASTY: BIOMECHANICAL AND CLINICAL ASSESSMENT OF A MINIMALLY INVASIVE TREATMENT OF LUMBAR INTERVERTEBRAL DISC DISEASE

**Presentata da:** Chloè Techens

**Coordinatore Dottorato**

Marco Viceconti

**Supervisore**

Luca Cristofolini

**Co-supervisori**

Aron Lazary

Peter Endre Eltes

**Esame finale anno 2022**

*To Ghaya,*

*Who planted a seed fifteen years ago*

# *Abstract*

This PhD project was part of a European-funded Marie Skłodowska-Curie Actions innovative training network called SPINNER (grant No. 766012.) gathering orthopaedical surgeons, engineers, and scientists to provide a complete approach of spine surgery challenges.

The spine is a complex structure and is still partially unknown. Over 80% of the population in developed countries suffer or will suffer from Low Back Pain at one stage of their life. This symptom can be caused by several spine conditions including intervertebral disc degeneration. With the continuously increasing longevity, the social and economic burden of this disease is meant to raise and therefore requires the development of surgical techniques to treat the large numbers of patients. In that context, a minimally invasive technique, Percutaneous Cement Discoplasty (PCD), has been developed to treat the oldest and poly-morbid patients who are not suitable for an open surgery, which is currently the gold standard.

In the literature, a series of works investigated the patient outcome in order to estimate the pain relief and the improved ability to perform daily activities following PCD. Changes in spine alignment were also assessed post operatively by Prof. Varga's group in Budapest, measuring the main clinical spine parameters in the frontal and sagittal planes of CT scan images. Moreover, in order to improve the surgery outcome, indications of PCD were studied by the group of Dr. Sola in Buenos Aires, resulting in a new classification qualifying the vacuum phenomenon (VP) advancement state in the disc which will help surgery planning and is intended to minimize the postoperative complications. Finally, a softer alternative to bone cement as a disc filler was tested *in vivo* and mechanically characterized *in vitro* by the group of Prof. Wu in Xingtai. However, a complete evaluation of PCD or any improvement of the technique would include the study of the spine biomechanical behaviour for a better assessment of potential failure.

The aim of this PhD thesis is to bridge the clinical experience with *in vitro* methodologies to provide a multilateral evaluation of PCD outcome and a better understanding of its impact on the spine biomechanics, and of its possible contraindications.

Firstly, the project focuses on the development of a suitable *in vitro* model to test the biomechanics of discoplasty by comparing specimens in the preoperative and postoperative conditions. In a preliminary study on porcine segments, the VP was mimicked performing a nucleotomy, while discoplasty was reproduced by filling the disc with acrylic cement. Once the model was validated, the biomechanics of spine segments after percutaneous cement discoplasty were investigated on cadaveric human segments. The main objective of discoplasty is the increase of disc height, however the surgery had been studied

in supine patients which is not the only loading configuration presenting a risk for the disc height. That is why the *in vitro* specimens were mechanically investigated in flexion and extension, where a DIC system quantified the range of motion, disc height, and strains on the disc surface.

The second part of the thesis consists of going beyond the *in vitro* evaluation of the spine biomechanics and is providing a versatile measurement of the discoplasty impact which could be applied both to clinical and experimental work. For that, a 3D geometrical method was clinically developed by the research group to assess the foramen volumetric change caused by PCD from CT scans. *In vivo*, the measurements were performed in supine position, while measurements performed with the *ex vivo* specimens completed the spine overview by bringing results under loaded positions. For that, the 3D geometry of the unloaded specimens reconstructed from CT scans (CT pose) was aligned in the loading configuration (experimental pose) using DIC data. This study showed the promises of such methodologies combining clinical know-how with experimental testing for a more complete investigation of discoplasty.

In conclusion, the project highlighted the benefits of percutaneous cement discoplasty in the treatment of advanced cases of intervertebral disc degeneration. Furthermore, it also emphasized the importance of transverse dedicated methodologies and tools to improve the analysis of the surgical outcome. Although this project completed the understanding of PCD biomechanics, in the next years a focus should be brought on the assessment of the integrity of the anatomical structures of the disc following discoplasty to assess possible risks of complications. This should include exploring the internal biomechanics of the treated disc, understanding the disc failure mechanisms, and proposing improvements of the surgical technique.

# *Content*

**1 Introduction** ..... 8

1.1 Overview of the spine ..... 9

1.1.1 Anatomy of the vertebrae ..... 9

1.1.2 Anatomy of the disc ..... 10

1.1.3 Ligaments and facet joints ..... 11

1.2 Degeneration of the disc disease ..... 12

1.3 Why are the treatments of disc degeneration disease limited? ..... 14

1.4 Aims and outline of the project ..... 15

**2 Critical review of the state of the art on lumbar Percutaneous Cement Discoplasty** . 17

2.1 Introduction ..... 18

2.2 Methods ..... 19

2.2.1 Search strategy ..... 19

2.2.2 Data collection process ..... 20

2.3 Results ..... 22

2.3.1 Results of the literature search process ..... 22

2.3.2 Evaluation of the operative technique ..... 23

2.3.3 Overview of the follow-ups ..... 26

2.3.4 Biomechanical assessment of the effects of discoplasty ..... 29

2.3.5 Alternative materials for PCD ..... 30

2.3.6 Limitations and risks of discoplasty ..... 30

2.4 Conclusions ..... 31

**3 Testing the impact of discoplasty on the biomechanics of the intervertebral disc with simulated degeneration: an *in vitro* porcine study** ..... 33

3.1 Abstract ..... 34

3.2 Introduction ..... 35

3.3 Methods ..... 36

3.3.1 Specimens ..... 36
3.3.2 Surgical procedure ..... 36
3.3.3 Nucleotomy ..... 37
3.3.4 Discoplasty ..... 37
3.3.5 Mechanical testing ..... 38
3.3.6 Displacement and strain with DIC ..... 39
3.3.7 Data analysis and statistics ..... 39
3.3.8 Cement distribution ..... 40
3.4 Results ..... 41
3.4.1 Posterior disc height ..... 41
3.4.2 Range of motion ..... 41
3.4.3 Stiffness ..... 42
3.4.4 Strain distribution ..... 43
3.4.5 Cement distribution ..... 44
3.5 Discussion ..... 45
3.6 Conclusion ..... 48
**4 Biomechanical consequences of cement discoplasty: an *in vitro* and *in vivo* study on thoraco-lumbar human spines** ..... 50
4.1 Abstract ..... 51
4.2 Introduction ..... 52
4.3 Methods ..... 52
4.3.1 Compliance with Ethical Standards ..... 52
4.3.2 Overview of the study ..... 53
4.3.3 Cadaveric specimens ..... 53
4.3.4 In vitro surgical procedure ..... 54
4.3.5 Clinical cohort and CT scan acquisition ..... 55
4.3.6 Cement geometry visualization and thickness measurement ..... 56
4.3.7 Biomechanical testing ..... 57
4.3.8 Data analysis ..... 59

4.3.9 Statistical analysis ..... 61
4.4 Results ..... 61
4.4.1 Posterior disc height ..... 61
4.4.2 Range of Motion ..... 62
4.4.3 Stiffness ..... 64
4.4.4 Strain ..... 65
4.4.5 Visualization of the cement geometry and thickness measurement ..... 67
4.4.6 Correlation between cement geometry and biomechanical parameters ..... 71
4.5 Discussion ..... 71
4.6 Conclusion ..... 74
4.7 Appendix: Cement geometry visualization and thickness measurement ..... 75
**5 Assessment of foraminal decompression following discoplasty using a combination of *ex vivo* testing and numerical tools** ..... 77
5.1 Abstract ..... 78
5.2 Introduction ..... 79
5.3 Methods ..... 80
5.3.1 Acquisition of ex vivo data ..... 80
5.3.2 Post processing of the DIC data ..... 81
5.3.3 CT scan data acquisition and processing ..... 81
5.3.4 Registration of the DIC and CT data ..... 82
5.3.5 Measurement of the neuroforaminal 3D geometry ..... 84
5.3.6 Characterization of the DIC surfaces ..... 84
5.3.7 Evaluation of the measurement quality ..... 85
5.3.8 Statistical analysis ..... 85
5.4 Results ..... 86
5.4.1 Evaluation of the registration procedure ..... 86
5.4.2 Characterization of DIC surfaces and correlation with registration precision ..... 87
5.4.3 Foramen decompression induced by discoplasty ..... 88
5.4.4 Correlation between cement volume and foraminal decompression ..... 90

5.5 Discussion ..... 90
5.6 Conclusion ..... 92
5.7 Appendix ..... 93
**6 Conclusions** ..... 98
**Appendix 1: The effect of intervertebral disc simulated damage** ..... 101
A1.1 Introduction ..... 102
A1.2 Methods ..... 102
A1.2.1 Specimens, imaging, and preparation ..... 102
A1.2.2 Incremental creation of the defects in the disc ..... 103
A1.2.3 Mechanical testing and measurement of displacements and strains with DIC ..... 104
A1.2.4 Data analysis and statistics ..... 104
A1.3 Results ..... 105
A1.3.1 Posterior disc height ..... 105
A1.3.2 Range of Motion ..... 105
A1.3.3 Stiffness ..... 106
A1.3.4 Strain distribution ..... 108
A1.4 Discussion and conclusion ..... 110
**Appendix 2: *In vivo* assessment of the cement distribution after percutaneous cement discoplasty** ..... 111
A2.1 Abstract ..... 112
A2.2 Introduction ..... 113
A2.3 Methods ..... 114
A2.3.1 Clinical cohort and CT scan acquisition ..... 114
A2.3.2 Definition of pre- and postop motion segments' 3D geometry ..... 114
A2.3.3 PMMA geometry visualisation and thickness measurement ..... 116
A2.4 Results ..... 116
A2.4.1 Evaluation of the segmentation procedure ..... 116
A2.5 Conclusion ..... 116
A2.6 Appendix ..... 118

**Bibliography**..... 119

**Acknowledgement**..... 127

*Chapter 1*

# Introduction

## 1.1 Overview of the spine

The spine is a fundamental structure of the anatomy whose health can impact almost each part of the body. Composed of an alternation of vertebrae and intervertebral discs (IVD), the spine is one of the most complex parts of the skeleton to treat (Fig. 1.1). The whole structure is stabilized by ligaments. In the next sections I will not extensively describe the whole spine anatomy, but I will present the main elements of the lumbar part, and their biomechanical function in the spine.

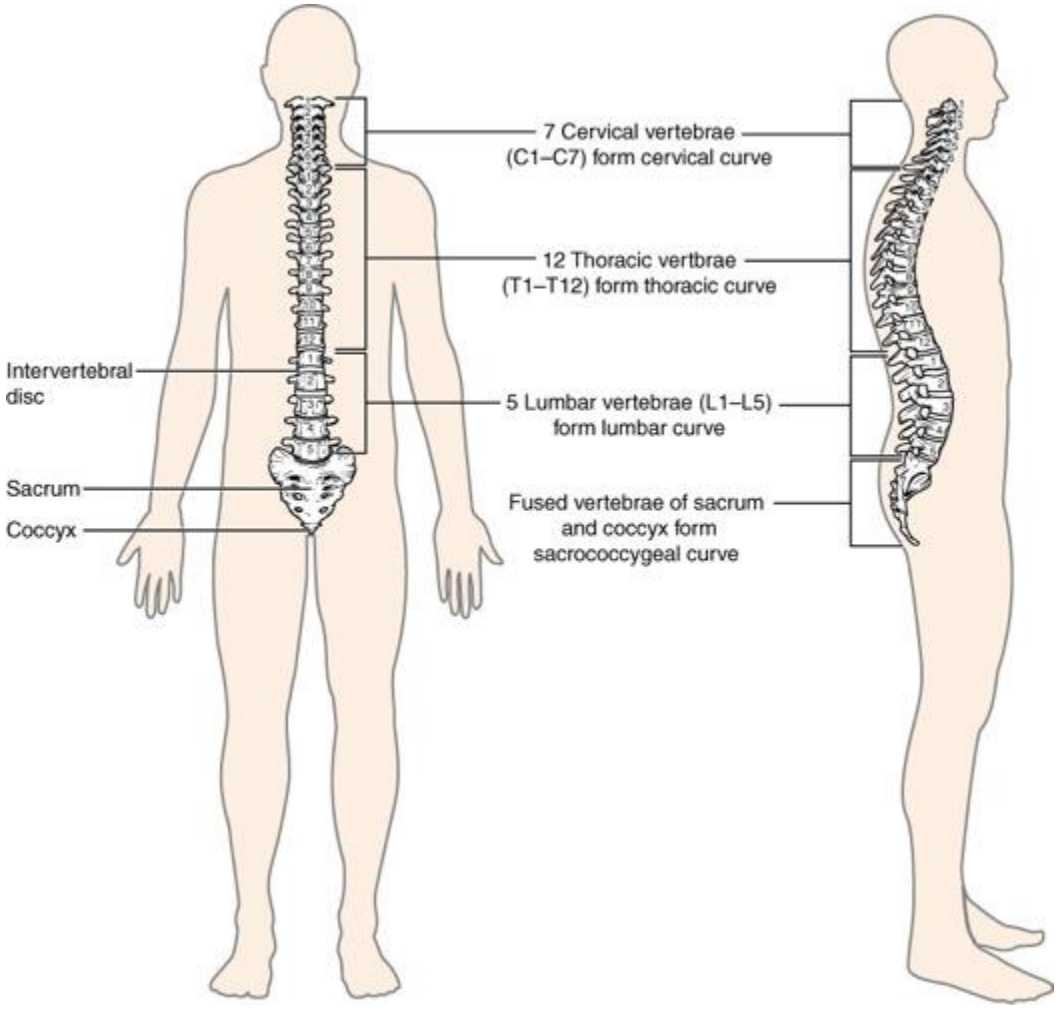


***Fig. 1.1 –*** *Spine column structure (image from: OpenStax College, CC BY 3.0, via Wikimedia Commons)*

### *1.1.1 Anatomy of the vertebrae*

Vertebrae are irregular bones whose anatomy varies depending on their spine level, the loading, the pathologies, etc. Each vertebra is composed of a vertebral body and a posterior vertebral arch, consisting of lamina and pedicles, which surrounds the spinal cord (Fig. 1.2). Consecutive vertebrae form an empty space between their pedicles called the foramen space where the nerves connected to the spinal cord before passing to the rest of the body. The vertebral body consists of trabecular bone surrounded by

cortical bone whose thickness is larger in the posterior arch. Vertebrae are the rigid part of the spine, while flexibility of the structure is ensured by the soft tissues (joints and ligaments). The lumbar vertebra functions are to protect the spinal cord and nerve roots, to support the upper body, and to distribute the weight during movement.

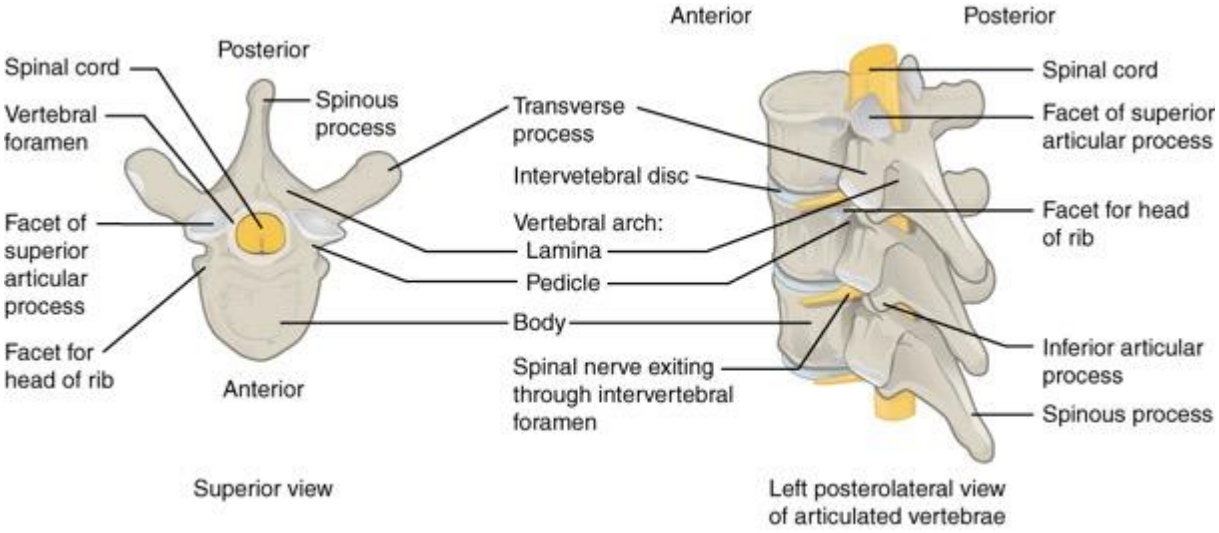


***Fig. 1.2 –*** *Structure of the vertebra. The nerves are passing through the neuroforamen to join the spinal cord. (Image from: OpenStax College, CC BY 3.0, via Wikimedia Commons)*

### *1.1.2 Anatomy of the disc*

Vertebral bodies are separated by intervertebral discs, fibrocartilaginous pads composed of three parts. Located in the centre, the nucleus pulposus (NP), a gel-like material, is surrounded by the annulus fibrosus (AF) in the transverse plane. The junction of the IVD with the vertebral body is made through the cartilaginous endplates (CEP) at both the cranial and caudal extremities of the IVD. Each of the IVD components fulfils distinct functions.

The nucleus pulposus is a highly hydrated tissue (70-90% of its weight) due to its high content of proteoglycans in the extracellular matrix [1]. Indeed, proteoglycan attracts and binds with water molecules. Its hydration level creates a hydrostatic pressure in the NP which increases under compression and generates tension in the surrounding tissue. NP is also made up of collagen type II creating a loose fibre network maintaining the unity of the nucleus [2]. Its high content in NP results in its incompressible gelatinous texture characterized by an effective modulus of 1.0 MPa and bulk modulus of 1720 MPa in confined compression [1].

The annulus fibrosus is composed of 15 to 20 concentric layers of anisotropic tissue. Each layer contains oblique collagen type I fibres oriented between ±25-45° to the transverse plane. Angulation of the fibres is shifting from positive to negative between two consecutive layers and increases towards the nucleus. Lamellae are interconnected by a collagen-based network which induces shear resistance between layers and elastin which favours the recovery after large deformations. The AF also has a large water content

(65-70% of its weight). The AF greatest stiffness in tension was found along the fibre axis and circumferentially, with a failure strain of 0.3 in the latter direction [1].

Finally, the cartilaginous endplates (CEP) are made of hyaline cartilage about 0.6 mm thick connecting the disc to the bony endplates of the vertebrae. The endplates are also highly hydrated (60% of the weight is water) and its dry main components are collagen type II and proteoglycans [2]. The collagen meshwork allows the endplates to contain the water expulsed by the NP under compression. The disc tissue is avascular however, the cartilaginous endplates are in contact with the capillaries in the vertebral body and bring nutrition to the disc cells mainly located in the nucleus. Although the CEPs do not behave linearly, an elastic modulus was estimated at 23.8 MPa [3].

The disc main functions in the spine are 1/the transmission and regulation of load between the vertebrae, 2/ the mobility of the spine, and 3/the shock absorption in case of heavy and brutal loading to protect the vertebrae [2].

### *1.1.3 Ligaments and facet joints*

The vertebrae are also connected by spinal ligaments (anterior longitudinal (ALL), posterior longitudinal, ligamentum flavum, facet capsular ligament, intertransverse ligament, interspinous ligament, supraspinous ligament) (Fig. 1.3). Spinal ligaments are bands of connective tissue made of collagen fibres. Their role is mainly to keep the spine alignment and to avoid excessive motion by connecting vertebrae, although each ligament has its own specific function.

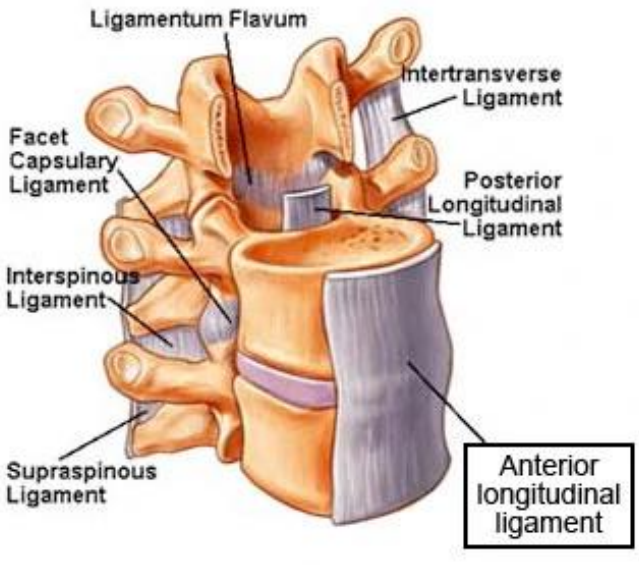


***Fig. 1.3*** *- Description of the principal ligaments on spine (Image from: http://ranzcrpart1.wikia.com/wiki/File:PicA2.jpg)*

## 1.2 Degeneration of the disc disease

With age, the spine loses its mechanical abilities due to the modification of the biological composition of the tissue as well as its anatomical shape (bones lose their density becoming osteoporotic, ligaments calcify, osteophytes appear, etc). I will not describe in detail all the changes happening in the spine due to aging, but I will focus on the disc degradation.

Disc degeneration is a natural process due to ageing. When associated with low back pain (LBP) and leg pain (LP), it is considered a pathology : Intervertebral Disc Degeneration Disease [4]. The disease affects a significant part of the population of developed countries (the prevalence of disc degeneration grade 3 on Kellgren-Lawrence scale was estimated at 47% of the population over 45 years old across Europe [5]). Depending on the study, the prevalence was higher in males or females, therefore no link can be formally established between the disease and sex. With population ageing, the prevalence of disc degeneration is likely to increase [6]–[8] as well as economic and social costs. Indeed, back pain is a leading cause of work incapacity and limits daily activities [9]. This imposes a social and economic burden at the individual, industry, and government scale, to provide patients with home care, treatments, and indemnities.

Disc degeneration appears to be an endless process of degradation which involves three main actors (the disc cells, the extracellular matrix of the disc tissue, and the biomechanics of the disc) impacting each other (Fig. 1.4) [10].

At the cellular level, the notochordal cells present in the nucleus pulposus since embryonic development, progressively convert into nuclear chondrocyte cells [11]. Notochordal cells are involved in proteoglycan synthesis. Thus, changes at the cellular scale directly lead to a change of the tissue material composition. In addition to a decrease of proteoglycan content, the reduction of notochordal cells also induces a drop of Collagen type II expression while Collagen type I synthesis increases [12]. Thus, the predominant collagen type evolves with time.

The change of extracellular matrix composition modifies the biomechanical properties of the disc tissue. The decrease of proteoglycan leads to a reduction of the nucleus hydrostatic pressure. The water content drops in the nucleus which becomes more fibrous [13]. Hence, the intradiscal pressure is reduced on the surrounding tissue, leading to the decrease of the disc height [14]. These changes alter the load distribution in the AF. In addition, Collagen type I provides resistance in tension whereas collagen type II mesh as in NP can withstand large compressive loadings. A potential change of the NP mechanical response to loading could be expected and would also disturb the stress distribution applied on the annulus and the endplates.

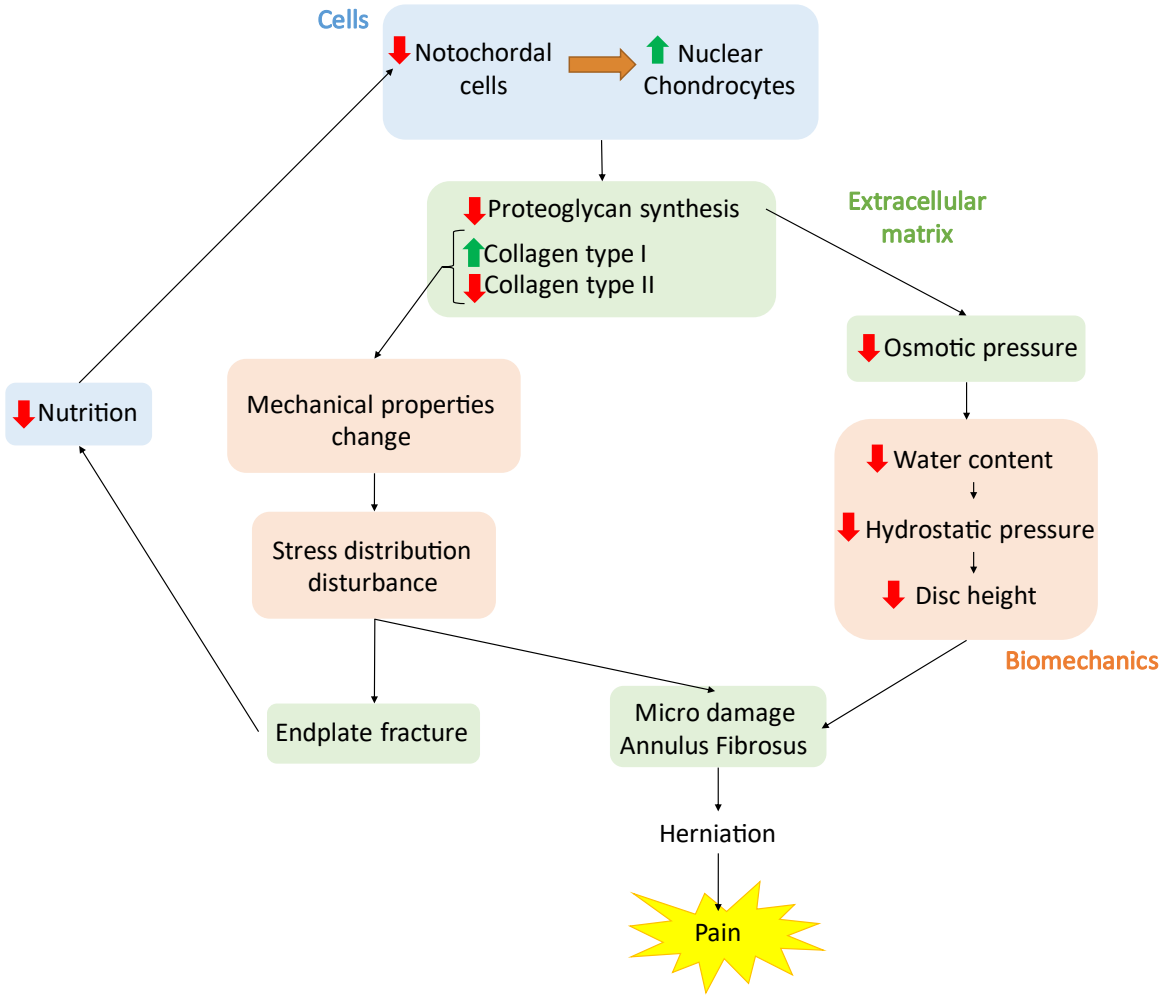


***Fig. 1.4 –*** *Disc degeneration is a complex self-sustained cycle impacting the disc at all scales (cellular, extracellular, and tissue levels). Trends in the degeneration process: reduction (red, down arrow) and increase (green, up arrow). The figure was inspired from two studies [4], [10]*

In degenerated discs, axial compliance is reduced and radial bulging is increased [15]. The changes of biomechanical properties directly impact the integrity of the tissue surrounding the nucleus. Micro damages of the annulus fibrosus such as delamination, tears, etc. will result from an abnormal loading. Once the integrity of the AF is compromised, the nucleus is not encapsuled anymore and herniation of the disc is likely to happen, causing pain if the leak occurs close to the nerves. This is one mechanism causing low back pain since the causality between disc degeneration and LBP is complex [16]. A disturbed stress distribution also increases risks of endplate fracture.

Finally, damage to the extracellular matrix also favours the degenerative process at cell level. As stated before, the disc is avascular however nutriments are transmitted through the vertebral endplates to the nucleus cells. In case of fracture but also disease of the CEPs, nutriment intake is reduced which compromises cell life expectancy and reduces notochordal cells proportion in NP, perpetuating the cycle.

Disc degeneration is a complex process which does not stop. Pfirrmann's scale is a widely used classification of disc degeneration [17]. Five grades are defined based on the visual aspect of the disc on radiographies. In the most advanced stage, Vacuum Phenomenon (VP) is observed when the nucleus disintegrates, and the space is filled with a low-pressure gas [18]. The total disappearance of NP is associated with a strong loss of the disc height leading to the reduction of the cranial-caudal diameter of the foramen causing nerve compression.

## 1.3 Why are the treatments of disc degeneration disease limited?

Disc degeneration is a common disease which can be treated in diverse ways depending on its stage. Starting with physical therapy rehabilitation, spinal manipulation, and analgesics, the most desperate cases require a stabilization surgery (interbody fusion) in which the disc is removed and replaced by a cage implant with transpedicular instrumentation. The surgical procedure aims to recover disc height and then fuse the vertebrae to restore stability at the corresponding disc level. However, the surgery has a long operative time and requires general anaesthesia and a long recovery including some monitored time at the hospital. It therefore represents a high economic cost for both the patient and the healthcare system (medication, hospital stay, rehabilitation care, medical leave salary compensation, etc.) and brings discomfort to the patient (scar, temporary disability, rehabilitation, etc.). Moreover, an open surgery is associated with high risks of excessive bleeding for the patient. All these constraints limit the patient population susceptible to take the surgery. Because disc degeneration worsens with age, some of the patients are polymorbid or elderly, not suitable for general anaesthesia or the risks associated with fusion surgery.

On the other hand, Minimally Invasive Surgeries (MIS) have been developed to treat patients while limiting surgical risks, collateral damage to the body, and economic costs. They are also associated with less complications and reduced surgical morbidity due to the minimal interaction with the patient. For all these reasons, minimally invasive surgeries are a promising research field of spine surgery which needs to be consolidated [19]. In order to treat lumbar disc degeneration in patients unsuitable for interbody fusion surgery, a MIS called Percutaneous Cement Discoplasty (PCD) was presented by Varga *et al*, in 2015 [20] and still remains partially investigated. The MIS consists of injecting polymethylmethacrylate (PMMA) cement in the disc space to replace the VP. Once the cement has hardened, it acts as a stand-alone spacer implant, restoring the disc height to relieve the LBP. Investigated in clinical studies, PCD showed good results on patients' cohorts with significant improvement of the pain level and of the ability to perform daily activities [20]–[22] (more details in Chapter 2). Spine alignment was also measured following discoplasty [21] however spine biomechanics as well as the real effect on the spine anatomy has not been investigated yet.

## 1.4 Aims and outline of the project

By integrating clinical experience and *in vitro* biomechanical testing, the aim of the project was to improve the understanding of percutaneous cement discoplasty as a treatment of disc degeneration. For that, the first objective was to investigate the surgically augmented spine to provide a better understanding of the biomechanical impact of discoplasty, such as flexibility of a two-vertebrae segment or the strain distribution in the disc tissue after augmentation. Then, the project aimed to bridge the clinical knowledge with the biomechanical evidence to propose a multidisciplinary perspective of the discoplasty concerns and improvements using a numerical approach.

The thesis starts with a review of the published knowledge about PCD as a surgical treatment in the lumbar spine in order to identify the gaps in discoplasty knowledge (Chapter 2). It established a strong rationale of the operative technique, its impact on patient condition, and the other studies whose topic is related. The state of the art also highlighted the gaps of the research on discoplasty and the forthcoming investigation topics.

The work was split into two topics of research: the *in vitro* biomechanical testing of the augmented spine and the numerical treatment of imaging data following clinical experience. Each area was divided in several steps to reach the thesis objectives.

For the *in vitro* biomechanical testing:

- To develop a reliable method to model *in vitro* the PCD surgery and to apply it on animal spine segments mechanically tested in order to measure their biomechanics. The disc height, the mobility of the specimens and the disc strains were measured in flexion, extension and lateral bending (Chapter 3).
- To quantify the biomechanics of the surgically augmented human spine after PCD. The disc height, specimen mobility and disc strains were also investigated and the impact of discoplasty was related to the characteristics of the operative technique measured *in vivo* in terms of cement thickness, volume, etc. (Chapter 4).

For the numerical investigation of clinical and biomechanical data:

- To apply a clinical method developed and used *in vivo* by the research group to *ex vivo* data to extend the assessment of foraminal space to other critical spine alignments. Geometrical evidence of decompression was correlated with characteristics of the operative technique to highlight the mechanism behind discoplasty benefits. (Chapter 5).

A side study was conducted in additional spine levels in order to assess the limitations arising from the annulus fibrosus damage performed in the *in vitro* discoplasty model. The biomechanics of the spine

segments were quantified with incremental annulus defect to determine the bias observed in Chapter 3 and 4 (Appendix 1).

The original published study including the *in vivo* measurements of the operative technique characteristics presented in Chapter 4 was presented in Appendix 2. Because the whole study covered more than these measurements and was performed by the research group, only the sections of the published research linked to my activities were included for completeness.

General conclusion including the forthcoming steps in PCD investigation (Chapter 6).

*Chapter 2*

# Critical review of the state of the art on lumbar Percutaneous Cement Discoplasty

from the manuscript:

**Critical review of the state of the art on lumbar Percutaneous Cement Discoplasty**

C. Techens, P. E. Eltes, A. Lazary, L. Cristofolini

Pre-print of a paper being submitted in Frontiers

## 2.1 Introduction

The ageing of the global population due to the increase of life expectancy directly increases the prevalence of spine disease and in particular the lumbar Intervertebral Disc (IVD) degeneration [7]. With time, the IVD water content decreases which leads to tissue breakdown and the loss of the disc height [10]. Consequently, the foramen space between adjacent lumbar vertebrae is reduced, creating neural stenosis and inducing low back pain in some cases [23]. Pfirrmann *et al.* established a 5 levels classification based on spine imaging of the IVD [17]. In the most extreme levels of disc degeneration, a vacuum phenomenon (VP) appears instead of the nucleus and creates a large instability of the spine segment and an extreme compression of the nerves [24].

Lumbar IVD degeneration treatments range from physiological exercises to surgical procedure. Interbody fusion with the insertion of a cage and bone graft combined to posterior fixations restores the intervertebral height and stabilizes the spine. Despite being the gold standard, this surgical technique is a constraining long procedure requiring a general anaesthesia and a long recovery. It is also associated with high risks of bleeding and complications. Therefore, this surgery can be contraindicated for elderly and polymorbid patients. For those unsuitable patients, the absence of efficient treatment led to the development of minimally invasive technique called Percutaneous Cement Discoplasty (PCD) [20].

PCD is dedicated to treat patients with advanced disc degeneration exhibiting a VP. The procedure consists in the injection of an acrylic bone cement within the disc to fully fill the cavity. The cement mass is then acting like a stand-alone implant, restoring the disc height.

Historically, a similar technique was implemented in the cervical spine as an alternative to interbody fusion cages for spine segment stabilization. Injection of bone cement in the disc was introduced by Roosen [25]. The technique was then replicated *in vivo* [26], [27] and *in vitro* [28]–[30] to investigate the surgical outcome and biomechanical consequences of such a treatment on the cervical spine in comparison to cages. It was found that bone cement stabilized the spine similarly to other cages [26]–[28] and showed a lower subsidence in adjacent vertebrae [29], [30].

Thus, PCD is a promising technique for spinal repair, however the knowledge around the surgery and its consequences on the lumbar spine is still under investigation. Studies were published on several aspects of PCD, from clinical cohort studies to engineering studies on biomechanics and biomaterials. No previous review on the topic was written yet, so there was a need to present an overview of the research related to PCD.

The review aimed to present the various research areas under investigation related to PCD to provide a clear view of the covered topics. The review also aimed to assess the efficiency of this technique in term

of clinics for the patient but also in term of objective parameters such as spinal behaviours and spine stability.

## 2.2 Methods

### *2.2.1 Search strategy*

The review included papers of all types from articles to letters to the editor in peer-reviewed journals. No precise study design was specified since the review aimed to collect all PCD-related publications. No time frame was defined although first publications mentioning lumbar PCD were published in 2015. Only revised and published publications with an English version were considered.

The review intended to establish a state-of-the-art about PCD. Therefore, the inclusion criteria rather targeted the qualificatives of PCD to ensure both quantitative and qualitative papers to be retrieved. The review focused on surgical practices applied on the intervertebral discs of the thoracolumbar spine and consisting of injecting polymethylmethacrylate within a vacuum disc. Studies about vertebroplasty were excluded as well as surgeries including external fixations.

The study search was performed on the electronic databases PubMed and Scopus. Additionally, the references of the screened papers were reviewed to search potential related studies. Other studies the authors were aware of could also been added (Fig. 2.1).

Once the studies collected from the databases, the duplicates were removed. A first screening was performed based on the studies' title and abstract to identify if the spine segment or the surgery type had been respected. The final eligibility of the studies was performed based on the full text content to fully assess all criteria. This process was only performed by one author, but the results were approved by others. Among the eligible studies, separation was performed between qualitative studies assessing the characteristics of the surgery and its consequences and the studies including statistics on PCD which are used for a meta-analysis.

| | |
|---|---|
| Keywords: | |
| | Percutaneous cement discoplasty / discoplasty / cement injection / percutaneous intervertebral-vacuum polymethylmethacrylate injection |
| AND | Degeneration / vacuum / nucleotomy |
| AND | Intervertebral disc / spine / lumbar / thoracolumbar |
| NOT | Vertebroplasty |
| LIMIT TO | English |

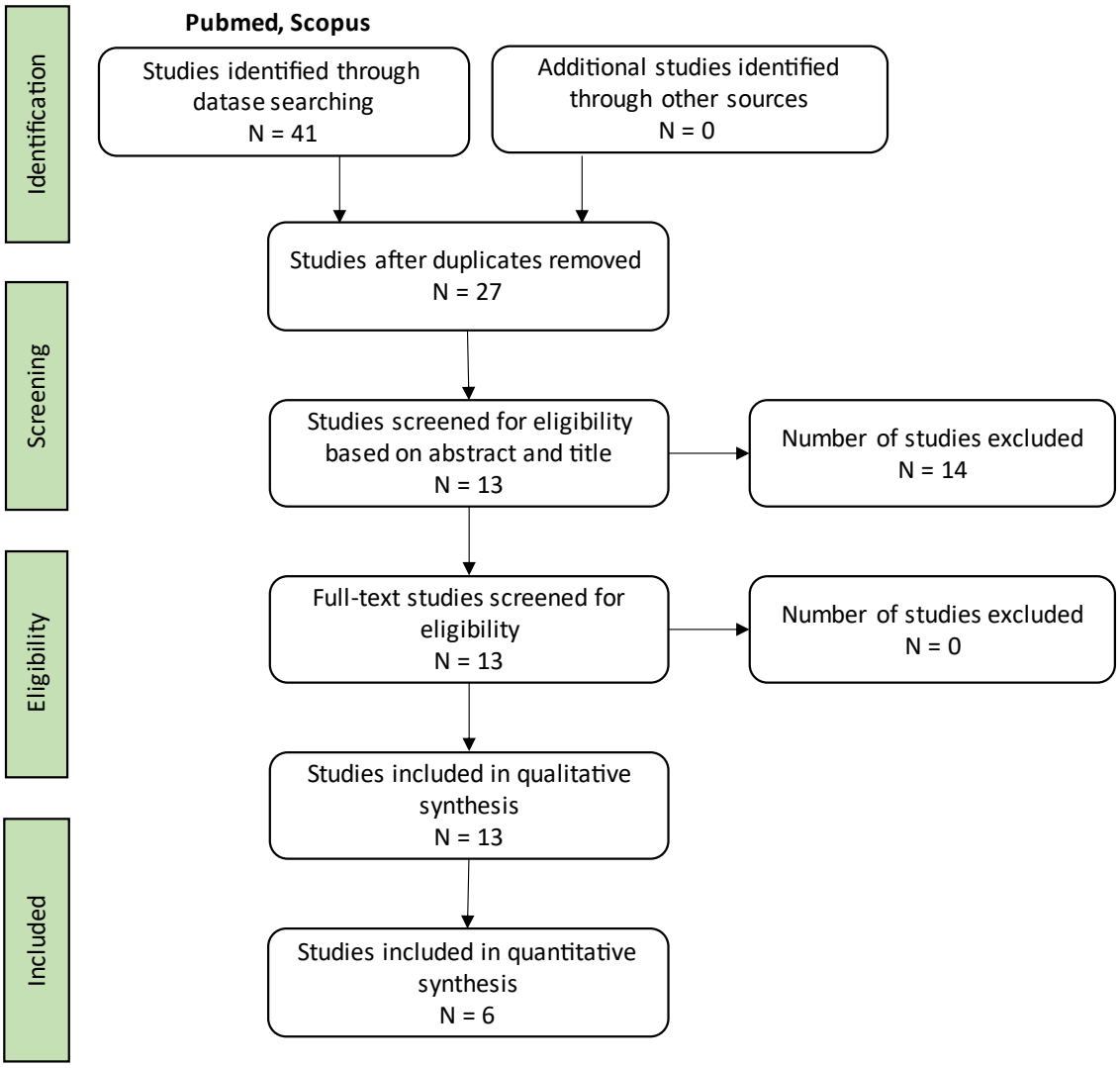


***Fig. 2.1 -*** *Workflow of the search strategy*

### *2.2.2 Data collection process*

Qualitative and quantitative data were then extracted from the studies using a form established by the authors to assess the quality of the studies and their content. The variables sought in all studies were:

- Type of the study (cohort/retrospective/prospective/*in vitro*/numerical)
- Presence and clarity of the inclusion criteria of specimens/patients in the study
- Presence and clarity of the exclusion criteria of specimens/patients from the study
- Clarity of the selection process of the participants (specimens/patients)
- Presence of comparison between groups of persons/patients undergoing two different treatments

As the review covered various types of studies from clinical to mechanical papers or exchanged letters, additional variables were investigated with more specific focus on some of the types listed above:

- Presence and duration of a follow-up
- Period of the study
- Number of persons in the cohort/specimens
- Inclusion/exclusion criteria for the persons/specimens
- Variables observed and corresponding parameters measured
- Frequency of measurement
- Nature of the parameters' outcome (index, scale, cases)
- Presentation of the operative technique
- Monitoring of the surgery
- Surgical approach chosen
- Use of preliminary medium to assess the volume of cement to inject
- Volume of cement injected
- Duration of the surgery
- Discharge of the patients
- Post-operative treatment/recommendation
- Presence of case presentation
- Complications/limitations

In particular, the review investigated patient outcomes, the operative technique, and potential risks induced by PCD on the spine depending on the type of article collected. For that, a particular interest was brought to:

- Patient feelings in terms of pain, mobility, etc.
- Patient mobility assessed objectively
- Vertebral alignment
- Mechanical behaviour of spine
- Disc height / foramen size changes
- Complications / risks

Risk of bias was also verified both at the study level (related to fundings for instance) and at the outcome levels. Among the practices recommended to decrease the risk of bias, one can mention the use of an independent observer or a double-blind, the repeatability of measurements, the reproducibility of the measurements by two operators. On the contrary, auto scaling of the patient feelings would represent subjective results although it is a crucial tool in clinics. This review did not intent to hierarchize some results over others but to make the reader aware of potential weaknesses and limitations of the data in

order to adapt to his own need. Each field of research has its own tools which fill the field needs and complete each other.

Qualitative data were reported, gathering into groups the studies presenting similar values. For quantitative parameters, the mean values of the studies will be compared using the same scale. To quantify patient's quality of life and pain, Oswestry Disability Index (ODI) and Visual Analogue Scale (VAS) scores will be graded using a scale from 0 to 100. Spine alignment and stability will be quantified by anatomical parameters in terms of angles and distances.

## 2.3 Results

### *2.3.1 Results of the literature search process*

The search on PubMed and Scopus with the keywords stated above resulted in respectively 21 and 20 papers from all types. The first screening of the abstracts and titles provided 27 eligible papers. The full-text reading established that 13 publications were qualified for this review on PCD, all written since 2015. Among them, 11 were identified as journal articles covering both clinical and engineering investigations, and 2 as letters to the editors commenting some of the retrieved articles.

The articles found included five prospective studies [1–5], one case study [6], two diagnosis studies [7, 8], one retrospective study [9], and two biomechanical studies [10, 11]. Following the case study presented by Sola *et al.*, a letter to the editor was written by Wang *et al.* to require more details about the operative technique and its outcome [31]. The content of the answers from Willhuber and Sola was published in another letter [32].

Except for the case study and the diagnosis study, all papers provided quantitative data tackling the patient outcome and/or biomechanical parameters. All studies acknowledged their risks of bias and tried to limit them.

One must note that the term Percutaneous Cement Discoplasty was not universally used in the literature since Yamada *et al.* reported the surgical technique in their two papers under the name percutaneous intervertebral-vacuum polymethylmethacrylate injection (PIPI). In this review, the surgery was named after the most common term: percutaneous cement discoplasty.

Among the recorded 13 publications, six studies used human participants. Yamada *et al.* compared groups undergoing PCD to other treatments, whereas the others focused on a preop/postop comparison. For *in vivo* studies, the selection process of the participants was explicitly detailed in the text at minimum, with additional scheme to summarize in Yamada *et al.* and Kiss *et al.* studies.

The review aimed to gather all publications linked to PCD, whether they covered the patient outcome or the operative technique. Data collected *in vivo* and *in vitro* were separated below.

### *2.3.2 Evaluation of the operative technique*

#### *2.3.2.1 Presentation of the in vivo studies*

Eleven publications tackled *in vivo* PCD applied to patients from the surgical planification to the operative technique itself and the patient outcome. Historically, cement injection in the IVD was primarily introduced to stabilize the cervical spine [25], [28]. In 2015, Varga *et al.* presented the operative technique applied for the first time to the lumbar spine [20], followed in 2018 by Sola *et al.* [33]. Four papers included a case study presentation [20], [33]. Willhuber *et al.* focused one study on the development of a methodology to fine-tune the diagnosis of cases requiring PCD as a treatment [34]. Eltes *et al.* developed a methodology to quantitatively evaluate the impact of the surgery in patient anatomy using medical imaging [7]. Finally, six papers included a follow-up of the patients [20]–[22], [35]–[37]. While Kiss *et al.* and Varga *et al.* investigated PCD as treatment of disc degeneration without distinction, Yamada *et al.* applied PCD to specifically treat scoliosis resulting from disc degeneration. The study compared the clinical outcomes of two groups: patients treated with PCD and patients treated with physiologic therapy. Willhuber *et al.* addressed the matter by comparing the treatment outcome in patients with and without degenerative scoliosis [36]. Another study by Willhuber *et al.* compared the PCD outcome between three groups of patients depending on their previous spine surgical history at the treated level [37].

#### *2.3.2.2 Surgical planning*

Generally, all studies defined the same indications for surgery. As a minimally invasive surgery, PCD first aims to treat patients not suitable for an open surgery. Patients must suffer from a Disc Degeneration Disease in an advanced stage (Pfirrmann's grade V) resulting into a VP due to the disappearance of nucleus pulposus. Evidence of foraminal stenosis directly inducing back pain is also required: LBP must increase with standing activity and be relieved after resting.

Pfirrmann's scale evaluates the intervertebral disc degeneration stage however PCD principally depends on VP and the surrounding tissue state. For that reason, surgery planning was refined to identify patients having the most suitable biological condition of the disc and the endplates [34]. A new classification of VP, established from Computed Tomography scans, identified four levels of VP based on the rate air/disc tissue and two sub-levels depending on the presence of subchondral stenosis. In the study, Willhuber *et al.* suggested that PCD should be only recommended for partial or complete VP to reduce risks of disc protrusions during cement injection. Additionally, the presence of subchondral stenosis would limit risks of adjacent fractures, in particular in osteoporotic patients.

Few contraindications were presented by Sola [33]:

- Severe osteoporosis could jeopardize the integrity of the vertebral bodies after the surgery. Following Wang's letter to the editor [31], Willhuber and Sola specified that no direct measure

of lumbar osteoporosis was used as a threshold to discriminate patients suitable for PCD [32]. However, patients with a bone mineral density T-score -2.5DS in hip of history of bone fracture were referred to endocrinologist for anti-osteoporosis treatment. In their papers, Yamada *et al.* defined a bone density threshold of 70% under which the surgery is not recommended.

- Severe deformity of the spine would exclude patients from receiving PCD as this surgery does not aim to restore the spine alignment. Later, the authors specified in their answer to Wang *et al.* that degenerative scoliosis was not a contraindication since it was usually induced by disc degeneration [32]. Moreover, PCD also demonstrated a stabilizing effect on the spine.
- Evidence of tumours or infections at the corresponding spine levels
- Obesity is a limiting factor because it reduces the quality of the fluoroscopy monitoring performed during the surgery

#### *2.3.2.3 Operative technique*

PCD is a minimally invasive surgery whose operative technique was similarly described by two papers (Fig. 2.2). A radiopaque medical cement was injected to fill the vacuum through the Kambin's triangle [20], [21]. Yamada *et al.* prioritized a transpedicular approach for the injection while Sola *et al.* also recommended an entrance parallel to the superior lateral pedicle edge. Wang *et al*. confronted the difference of approaches used by Varga and Sola *et al.*, wondering the key factor allowing a homogeneous cement distribution and avoiding leakages [31]. Willhuber and Sola explained that the cannula between middle and anterior third of intervertebral was indicated. Stopping injection when bone cement reaches the posterior vertebral wall would prevent leakages [32]. If Varga *et al.* recommended local anaesthesia, PCD can be conducted under general anaesthesia as reported by Willhuber, Kiss and Yamada *et al.* [21], [22], [35]–[37]. For all studies, the volume of injected cement varied between 3-10mL depending on the patient and spine level, since cement must entirely fill the vacuum. The surgery was always performed under fluoroscopic monitoring for a better guidance of the injection and to prevent cement leakage in the neural canals. Preliminary to cement injection, one study used a medium injected in the disc to assess the volume of required cement [22]. The surgery duration varied between studies depending on the number of treated levels, from about 25 min for one level PCD to more than 1 hour for five level PCD. Willhuber *et al.* demonstrated that PCD associated with decompression surgery also provided promising outcome to treat elderly [37].

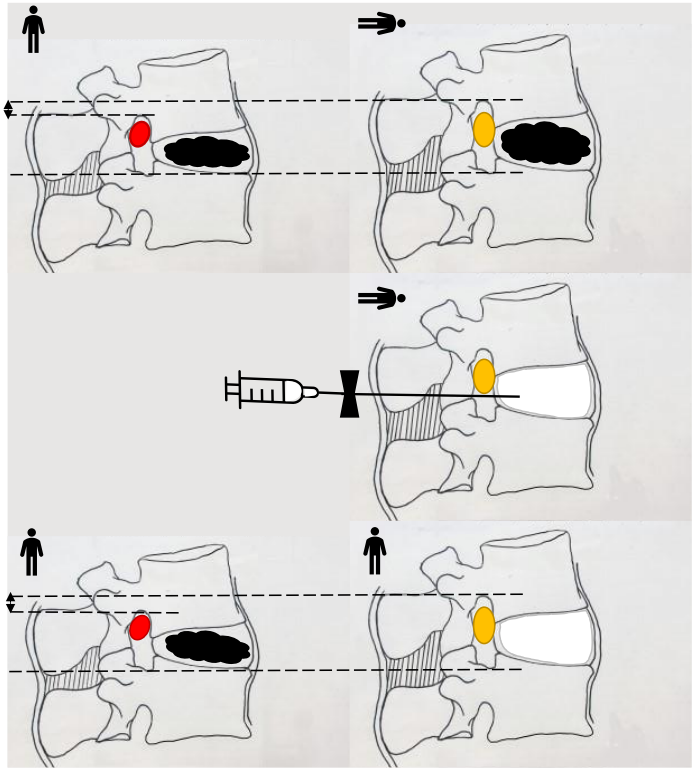

***Fig. 2.2 -*** *Operative technique of Percutaneous Cement Discoplasty. Upper row: A reduction of the neuroforamen space (arrow) is observed in the unstable spine in supine position resulting in nerve compression. Middle row: The vacuum (black) of the disc is filled by PMMA cement (white). Bottom row: After surgery, the cranial-caudal diameter of the foramen was increased by the cement mass. Red: compressed nerve, Yellow: released nerve. Adapted by permission from Springer Nature Customer Service Centre GmbH: Springer, Der Orthopade, Experiences with PMMA cement as a stand-alone intervertebral spacer: Percutaneous cement discoplasty in the case of vacuum phenomenon within lumbar intervertebral disc, Varga et al., 2015) [20]*

### *2.3.2.4 Postoperative recommendations and complications*

Patients were usually discharged within 3 days. They were encouraged to stand and walk as soon as possible [36]. In the case of the treatment of lumbar degenerative scoliosis, a brace was worn by patients for two months [22]. Willhuber's group did not recommend a brace postoperatively, since patients undergoing PCD did not have risky activities. The only recommendation was to avoid excessive flexion/extension movements and limit more than 10 kg lifting [32].

Kiss *et al.* and Yamada *et al.* reported cement leakages in 4% of the surgeries (respectively 3/63 patients and 3/80) which were treated by decompression surgery [21], [35]. In the first study, all leakages, located in the foramens, caused severe leg pain, and were treated by foraminal decompression during a revision surgery. In the second study, one leakage was localized in the intervertebral foramen, and induced a radicular pain which was treated with anti-inflammatory analgesics. Because of the reduced capacity of the disc after PCD to share the vertical stress between vertebrae, Wang *et al.* shared concerns about the increase of fracture risk [31]. In their answer, Willhuber and Sola reported one fracture over 131 treated discs. They explained that fractures were prevented by the degeneration of the endplates which resulted

in subchondral sclerosis. No endplate fracture nor cement dislodgement was reported by Yamada *et al* [22]. One deep infection and one fracture of the adjacent vertebral body were later reported by Willhuber *et al.* along with two cases of leakage in the foramen, one disc extrusion and one unexplained pain [36]. Overall, 16% of complications were reported in their last study, with only 5.7% (9/156) permanently impacting the spine [37]. Cement leakage acquainted for 3.2% and vertebral fracture for only 0.6%.

### *2.3.3 Overview of the follow-ups*

Among the six studies including a follow-up, minimal follow-ups lasted six months [20], [21]. Willhuber *et al.* presented a one year follow-up [36] and a second study of two years follow-up [37]. Yamada *et al.* first study measured patient outcome for two years [22], the second study based on the same cohort lasted about 63.7 ± 32.4 months (mean±SD) [35]. Periods over which the recruitment and the follow-up of patients was performed widely varied between studies.

#### *2.3.3.1 Selection of patients*

The first patient outcome published studies included 47 participants with complete follow-ups out of 81 initially treated patients [20]. 28 participants out of 63 were included by Kiss *et al.* in a follow-up of six months (Fig. 2.3). The first study of Yamada *et al.* enrolled 162 participants out of 252 patients [22], but was extended in a second study, resulting in a shorter cohort of 80 participants [35]. Willhuber *et al.* presented a retrospective study on 54 participants separated into 2 groups: 37 participants had a degenerative scoliosis, and 17 participants did not present any sign of scoliosis [36]. In a second study, they gathered data of 156 patients from two centres that were separated into 3 groups based on their previous surgical history (PCD only/PCD after previous lumbar surgery /PCD+decompression) [37].

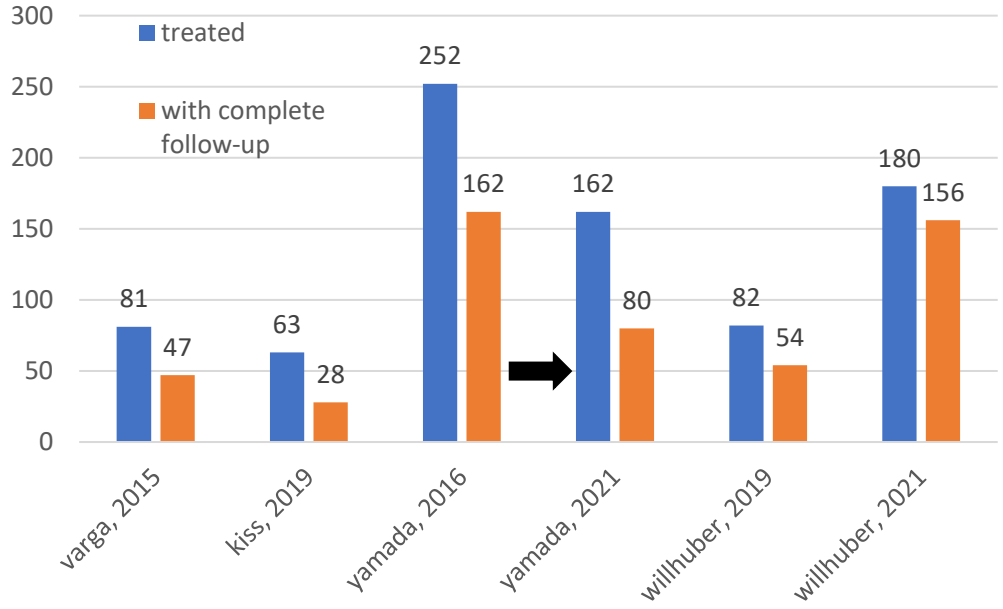


***Fig. 2.3 –*** *Patients involved in the clinical follow-up studies, from the initial recruitment to the final group.*

Among the patients treated by PCD in each study, the follow-up final participants were filtrated using exclusion criteria similar for most studies. The main exclusion criteria were:

- The absence of complete datasets [21], [36];
- The simultaneous performance of any type of spine surgery even out of L1-5 [21], [36];
- The presence of any previous surgery at the same anatomical level [22], [35], [36].

Additionally, patients with less than 1 year [36] and 2 years [37] of follow-up were excluded from Willhuber's studies.

In order to study the impact of PCD on degenerative scoliosis, patients with a Cobb angle exceeding 10°, a VAS score above 50 points, and Bone Marrow Edema visible on endplates were selected by Yamada *et al*.

### *2.3.3.2 VAS/ODI scores*

Low back pain graded by the VAS score was reported over the two years of follow-up (Fig. 2.4). In all studies, the postop VAS score was significantly reduced compared to preop, and at every step of the follow-up. In the two longest studies, the pain level increased again with time, but remained significantly reduced compared to preoperative condition. Studies reported the disability to perform daily activities following ODI variations. Similar to VAS, all studies reported a significantly reduced ODI post-surgery compared to preoperative which was still present after two years.

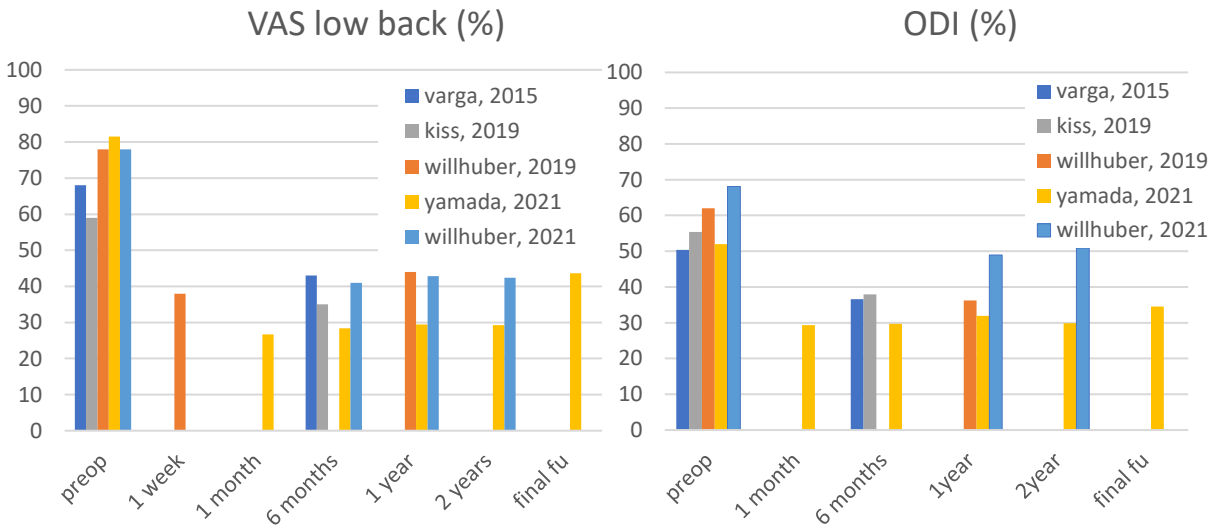


***Fig. 2.4 –*** *VAS and ODI scores chronologically reported from preoperative to two years postoperative. Fu: follow-up*

### *2.3.3.3 Radiographic parameters*

The Bone Marrow Edema (BME) score decreased after PCD and for the duration of the follow-up (>2 years) assessing the recession of the edema in the vertebral bodies (Yamada *et al.*).

The Cobb's angle was measured by Yamada *et al.* and Willhuber *et al.* preop and followed for 2 years (Fig. 2.5). After the intervention, the Cobb's angle was significantly reduced in the scoliotic group ($p=0.0006$), while the non-scoliotic group did not exhibit any change [36]. The comparison between patients treated with PCD and physiologic treatments during the follow-up showed the increasing significant effect of the surgical treatment on the Cobb's angle, however the Cobb's angle increased during the follow-up. Lumbar lordosis was not significantly impacted by PCD ($p>0.05$), while the segmental lordosis exhibited a significant increase ($p<0.05$) [21]. On the contrary, another study reported a significant increase of lumbar lordosis at one year postop ($p=0.0001$) in patient with lumbar scoliosis but no significant changes in segmental lordosis [36].

The pelvic incidence remained unchanged six months after PCD ($p>0.05$) [21]. The sacral slope significantly increased postop in two studies ($p<0.01$) and the change remained constant [21] (Fig. 2.5). The correction of sacral slope was positively correlated with the improvement of ODI. The pelvic tilt significantly decreased immediately after the intervention ($p<0.05$), and the drop remained constant after six months [21]. Lumbar lordosis was not significantly impacted by PCD ($p>0.05$), while the segmental lordosis exhibited a significant increase ($p<0.05$) [21]. On the contrary, another study reported a significant increase of lumbar lordosis at one year postop ($p=0.0001$) in patient with lumbar scoliosis but no significant changes in segmental lordosis [36].

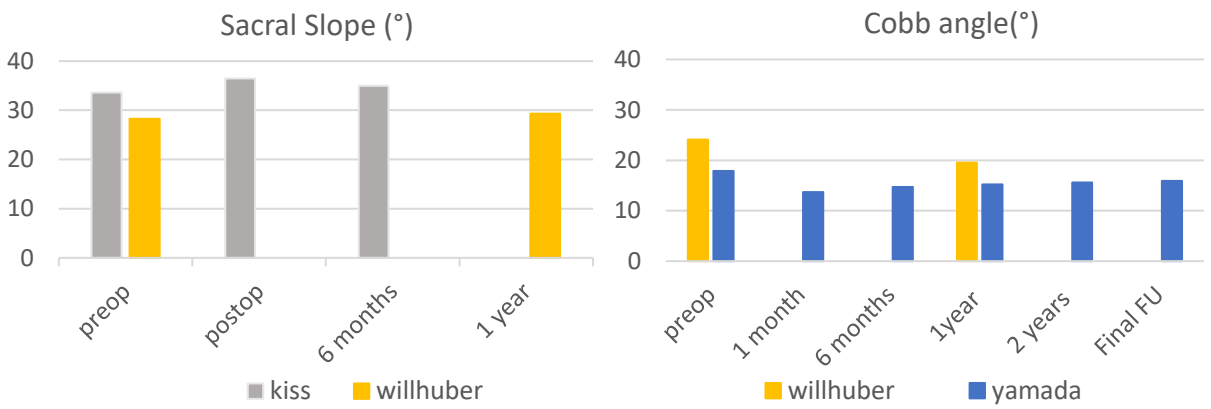


***Fig. 2.5 –*** *Impact of discoplasty on the sacral slope and Cobb angle*

Lumbar scoliosis and segmental scoliosis were significantly reduced both in segments with and without PCD [21]. The intervention significantly changed the scoliosis angle postop ($p<0.05$), but after six months no change from postop was observed ($p>0.05$).

In the sagittal plane, anterior and posterior disc height were significantly improved by PCD ($p<0.001$ for both). The interpedicular height showed a significant increase after surgery in treated segments ($p<0.001$) and the change was constant [21].

### *2.3.4 Biomechanical assessment of the effects of discoplasty*

In parallel to patient outcome investigation, *in vitro* and *in silico* studies assessed the biomechanical outcome of the surgery. The application of PCD on the low thoracic/lumbar spine being recent, apart from our studies, engineering research on the topic remained limited. Short summary of our published results is presented below; the detailed paper being extensively developed in Chapter 3 and Appendix 2.

#### *2.3.4.1 Evaluation of the operative technique*

The first interest of the technical studies was to provide objective data to evaluate the success of the surgery to match the clinical expectations. Despite relieving the pain, PCD aimed to 1/ fill VP with acrylic cement in order to 2/ increase the disc height and 3/ achieve an increase of the foramen space.

1/ *Evaluation of the cement distribution*: Postoperatively, the *in vivo* cement distribution was segmented from CT scans and characterised in term of cement mass volume and surface by Eltes *et al.* [38]. The cement axial thickness between the endplates was also measured for each disc. Cement distribution presented large variability of volume (3.8-13.1 ml range) and shape induced by the wide variations of musculoskeletal status and degeneration of each patient (Appendix 2). Improvement of the patient outcome was correlated to high cement thickness.

2/ *Measurement of Disc Height*: Techens *et al.* compared ten porcine lumbar discs in intact condition, after nucleotomy, and after simulated PCD tested in flexion and extension. In both motions, Posterior Disc Height (PDH) was significantly reduced by more than 15% after nucleotomy whereas discoplasty significantly restored it. In extension, PDH after surgery was 105% of the intact disc height. The *in vitro* investigation confirmed the disc height increase clinically observed [39] (see Chapter 3).

3/ *Measurement of the foramen space*: Eltes *et al.* developed an 3D volumetric method to quantify the preop-postop change of the foramen space from tomographic images. PCD significantly decompressed the spinal canal despite the wide difference of volumetric changes (mean= 2295 $mm^3$, SD= 1181 $mm^3$, n= 16). Foraminal decompression was favoured by higher volume, larger surface and lower surface-volume ratio [38].

#### *2.3.4.2 Biomechanical properties of the spine after discoplasty*

Although PCD does not primarily aim to spine stabilization, it is often a concern in disc degeneration. Techens *et al.* measured the *in vitro* range of motion and stiffness following PCD on porcine lumbar

segments. No significant changes were observed despite a decrease of the ROM in flexion and an increase in extension compared to intact discs. Discoplasty recovered the intact ROM compared to nucleotomy. The strains measured on the specimen surface showed a partial recovery after discoplasty of the distribution in intact discs. PCD also reduced the peak strains observed after nucleotomy [39].

### *2.3.5 Alternative materials for PCD*

More than the clinical outcome of PCD, research on PCD also covered improvements of the technique to provide a better stabilization of the spine and improvement of patient's condition. Osteogenic mineralized collagen (MC) modified polymethylmethacrylate (PMMA) cement was investigated by Yang *et al.* as a substitute to PMMA for PCD. With MC particle size ranging between 300 and 400µm, injectability, hydrophilicity, and mechanical properties of PMMA-MC were characterised [40]. After implantation in goat surrogates, PMMA-MC showed a significant better osteointegration than pure PMMA cement in term of circumferential contact index with bone. Moreover, PMMA-MC triggered a limited reaction from the immune system, in comparison to PMMA which exhibited a large fibrous encapsulation in *in vitro* experiments. Due to its decreased mechanical strength (Elastic modulus of 2.4-2.8 GPa for frequencies of 1-10Hz) reducing risk of bone fracture while keeping similar injectability characteristics as PMMA, MC-modified PMMA was presented as a promising alternative to pure PMMA cement for disc degeneration treatment with PCD.

### *2.3.6 Limitations and risks of discoplasty*

PCD being a minimally invasive surgical technique, it reduces the risks of clinical complications compared to the alternative surgeries in the treatment of degenerative disc disease. However, it still implies limitations and risks reported by the previous studies. Among the rare permanent complications reported by clinical follow-ups, cement leakage in the intervertebral foramen and vertebral body fracture were the most common. Contrary to leakage in the adjacent vertebrae which are passive, cement in the intervertebral foramen could jeopardize the spinal cord integrity. The cases can be limited by closely monitoring cement injection with the use of imaging devices and by adapting the site and approach chosen for the injection (see 2.3.2.4).

Vertebral fractures are naturally prevented by endplate sclerosis and by selecting patients with a certain bone density. Pre-operative treatments can also be implemented to strengthen the bone structures. Additionally, PCD allows to create a patient specific cement spacer adapted to the endplate shape which increases the contact surface transmitting compressive loads at the cement-endplate interface. Although no proper investigation of the intra-discal stress and subsidence after PCD has been conducted so far, an increased bearing surface is intended to reduce the pression on the endplates compared to other non-specific devices previously used to space the vertebrae [41]. Finally, vertebral fractures could be prevented by replacing the injected PMMA cement with substitute fillers exhibiting reduced mechanical

strength. Nonetheless, no experimental study could be found testing the limits in patient's activities susceptible to cause fracture. Questions such as: "Which load could a patient safely carry? Which movement could be safely achieved?" were not investigated yet, although patients indicated for PCD were unlikely to carry heavy loads or ostentatiously exercise.

Other concerns can be raised about the interface between the cement and the surrounding tissue of the annulus. No study could be found focusing on both the short- and long-term responses of the biological tissue of the disc to the presence of the injected cement. No abnormal inflammatory activity was reported in the follow-ups. PMMA cement being biocompatible and favouring osteointegration, long-term cemented discs would be expected to fuse and stabilize the treated level. Complications arising from long-term motion such as cement loosening or wear although they have not been studied yet, would therefore seem unlikely. However, substitute filler with better osteointegration would still decrease these risks of complications.

Considering the profile of patients treated with PCD following the indications and contraindications presented before, the limitations addressed above covered only the risks linked to complications clinically reported. One should remember the frame of application of PCD and conduct more investigations in case of change of the indications of the surgery (younger, more active patients, etc.).

## 2.4 Conclusions

Disc degeneration disease has a high prevalence in the population, in particular in the elderly and is responsible for low back pain. In the most advanced cases, the disappearance of nucleus pulposus results in the presence of a VP which leads to the disc collapse, and the reduction of the clearance of the foramens. Because polymorbid and old patients are not suitable for an open surgery, they are treated with percutaneous cement discoplasty, a minimally invasive surgery. The aim of this review was to establish a state of the art of the publications related to PCD.

Thirteen papers were retrieved through two databases covering clinical and engineering approaches of the surgery. Two studies presented the operative technique and its criteria for patient selection. PCD consists in filling the intradiscal space with injectable PMMA cement to replace the VP by a cemented spacer. Thus, the disc height is expected to be restored and the foramen space enlarged to release nerve compression and relive patient pain. Patients were usually discharged between one and three days after surgery. PCD was mainly contraindicated in case of severe osteoporosis and severe spine deformity although it stabilized degenerative scoliosis. Cement leakages in the vertebral bodies or the foramen were the most common complications but with a low prevalence (4% of the treated discs) and the pain was treated.

Six clinical studies included patient follow-ups lasting between 6 months and 2 years. All follow-ups concluded that PCD significantly reduced low back pain immediately after surgery and that the decrease lasted until the end of the follow-up. Similarly, the quality of life reported by patient clearly improved post-surgery and lasted until the end of the study. The disc height was restored by PCD, validating the main objective of surgery. PCD significantly reduced the postoperative Cobb's angle and pelvis tilt while increasing the sacral slope. The changes remained constant during the follow-up except for Cobb's angle which slowly restored. PCD significantly reduced the scoliosis angle which stayed stable along the follow-up although the surgery is not primarily recommended to treat scoliosis.

Among the investigations on PCD, one research axis questioned the filling material and its properties. A variation of bone cement (PMMA-MC) exhibiting mechanical properties closer to bone tissue was investigated. Its ability to favour osteointegration and limit the immune system reaction compared to pure PMMA made it a valuable candidate for PCD.

Despite the limited number of studies published about PCD, the clinical follow-ups lasted up to two years and investigated both the patient's feelings and the spine alignment. The possibilities of improvements in the surgery planning as well as the injected material were also considered. From the reviewed papers, percutaneous cement discoplasty is an efficient surgery and has some promising further development axes, however apart from our research, only clinical follow-ups and one material study were published, exhibiting a large gap for biomechanical studies. Indeed, the spine biomechanical behaviour under various loadings, including spine mobility, kinematics, but also the biomechanical answer of each component of the spine segment were omitted. This results in a major restriction: only the supine and standing positions (loaded with the upper body weight) were really investigated through clinical studies, but axial compression is not the only challenging loading configuration for disc height and foramen space. Indeed, a focus on other loading configurations as well as the measurement of different parameters would be needed to complete a rational on the benefits and limitations of percutaneous cement discoplasty.

# *Chapter 3*

# Testing the impact of discoplasty on the biomechanics of the intervertebral disc with simulated degeneration: an *in vitro* porcine study

from the manuscript:

**Testing the impact of discoplasty on the biomechanics of the intervertebral disc with simulated degeneration: an *in vitro* porcine study**

C. Techens, M. Palanca, P. E. Eltes, A. Lazary, L. Cristofolini

Published in: *Medical Engineering and Physics, 2020, 84: 51–59, 10.1016/j.medengphy.2020.07.024*

The authors wish to thank Medical Engineering and Physics for providing the permissions to re-use the manuscript titled “Testing the impact of discoplasty on the biomechanics of the intervertebral disc with simulated degeneration: an *in vitro* porcine study” in the present PhD thesis (*https://www.elsevier.com/about/our-business/policies/copyright#Author-rights).*

## 3.1 Abstract

Percutaneous Cement Discoplasty has recently been developed to relieve pain in highly degenerated intervertebral discs presenting a vacuum phenomenon in patients that cannot undergo major surgery. Primarily applied in cervical spine, little is currently known about the biomechanical effects of discoplasty in the lower spine. This study aimed at investigating the feasibility of modelling empty discs and subsequent discoplasty surgery and measuring their impact over the specimen geometry and mechanical behaviour. Ten porcine lumbar spine segments were tested in flexion, extension, and lateral bending under 5.4 Nm (with a 200 N compressive force and a 27 mm offset). Tests were performed in three conditions for each specimen: with intact disc, after nucleotomy and after discoplasty. A 3D Digital Image Correlation system was used to measure the surface displacements and strains. The posterior disc height, range of motion (ROM), and stiffness were measured at the peak load. CT scans were performed to confirm that the cement distribution was acceptable. Discoplasty recovered the height loss caused by nucleotomy ($p=0.04$) with respect to the intact condition, but it did not impact significantly either the ROM or the stiffness. The strains over the disc surface increased after nucleotomy, while discoplasty concentrated the strains on the endplates. In conclusion, this preliminary study has shown that discoplasty recovered the intervertebral posterior height, opening the neuroforamen as clinically observed, but it did not influence the spine mobility or stiffness. This study confirms that this *in vitro* approach can be used to investigate discoplasty.

**Keywords:**

Percutaneous Cement Discoplasty, Spine, Biomechanical testing, Strain



Published in: Medical Engineering and Physics, 2020, 84: 51–59

## 3.2 Introduction

Intervertebral Disc (IVD) degeneration is one of the main causes of low back pain, a large socio-economic burden for society, affecting between 60% and 70% of the population in industrialized countries at least once during their lifetimes [9]. Interbody fusion with the insertion of an intervertebral spacer after performing disc fenestration is the most common surgical treatment and has been widely studied in the literature [42]–[50]. It requires an invasive surgery which lasts for hours and is often associated with significant blood loss, long recovery, and general anaesthesia which is not suitable for elderly patients or those with significant comorbidities. Since this disease appears with age, finding minimally invasive treatments is crucial to treat the most complex cases. Percutaneous Cement Discoplasty (PCD), a surgical technique that minimizes the surgical morbidity and complication risks, is applied when a vacuum phenomenon (VP) is observed inside the IVD, resulting in the collapse of the adjacent vertebra and in nerve root compression. It consists of injecting an polymethylmethacrylate cement (PMMA) to "create individually shaped "in-site" intervertebral spacers" in order to recover the disc height and decompress the spinal canal [20]. One advantage of using PMMA to stabilize the spine is that "the load-bearing surface of the implant is fully adapted to the shape of the endplates".

PCD is a technique recently applied to the lumbar spine, the authors found very little literature on the subject. Varga *et al* presented in 2015 the technique and their clinical study on 47 patients showed significant improvement in their quality of life, correlating with a pain factor decrease at 6 month follow-up [20]. Another study reported the surgery of a patient treated with PCD [33]. Discoplasty was shown to positively affect the spinal alignment and neuro-foraminal height in 27 patients [21].

While the impact of PCD on spine has been clinically assessed by comparing pre-operative/post-operative scores, no indication about spine kinetics and kinematics has been found by the authors. Some studies investigated similar techniques on animals, performing *in vitro* testing of spines in intact condition (with a full IVD), after removal of the Nucleus Pulposus (NP), and/or after a stabilization surgery. Refilling of the disc with soft materials [51] to recover intact spine mechanics was also investigated, however it differs from discoplasty which uses acrylic cement. Only Moissonier *et al* and Wilke *et al* mimicked the PCD technique, implanting a spacer within the empty disc. The first demonstrated that nucleotomy of canine IVD increased the Range of Motion and reduced disc height, whereas the presence of a hard mass inside the disc recovered the height loss but left ROM as wide as after nucleotomy [43]. The second showed that bone cement stabilized cervical discs, reducing the ROM compared to an intact spine [28]. Moreover, using animal surrogates usually limits access to naturally degenerated discs, consequently research has also focused on the best technique to model the VP [52], [53], and the mechanical consequences of that surgery [54], [55]. In conclusion, PCD surgery relies on a weak knowledge of the mechanics of lumbar spine treated this way.



Published in: Medical Engineering and Physics, 2020, 84: 51–59

This study aims at enlarging knowledge about the mechanical consequences of PCD on lumbar spine stability. The motivations were two-fold: first, to develop a method to artificially represent a vacuum disc and the surgical technique applied to *in vitro* specimens, and to check the efficiency of this method as a model of PCD. Secondly, the study aimed at developing a methodology assessing the biomechanics of the spine before and after discoplasty. In particular, we hypothesized that PCD would recover the posterior disc height, affect the mechanical behaviour of the spine and present a damage risk for the surrounding tissue due to cement presence.

## 3.3 Methods

### *3.3.1 Specimens*

Ten functional spinal units were transected between T13 and L6 from porcine (*sus scrofa domesticus*) thoracolumbar spines. The animals were young and healthy porcine (approximately 9 months old and 100 kg) sacrificed for alimentary purposes. The specimens were cleaned using surgical tools: all soft tissues were carefully removed from the segment without damaging the vertebra, the facet joints and the intervertebral disc. In order to keep the natural kinetics of the segment while testing, the anterior, supraspinous and posterior ligaments were left intact. Each segment disc was horizontally aligned in the sagittal and frontal planes, using a six-degree-of-freedom clamp. Both segment extremities were embedded in acrylic bone cement, one after the other to make parallel pot planes. Specimens were stored frozen at -20 °C between cleaning and testing phases and between the tests which has been proven not to affect significantly the segment biomechanics [56].

### *3.3.2 Surgical procedure*

The purpose of the study is to develop a method to investigate the impact of PCD on the biomechanical behaviour of the spine by comparing IVD treated by this technique to degenerated and healthy IVDs. Thus, each specimen was tested in the three conditions sequentially:

- intact (INT) with a healthy IVD,
- after nucleotomy (NUCL) to simulate the instability of degenerated discs,
- after discoplasty (DP) (Fig. 3.1).



Published in: Medical Engineering and Physics, 2020, 84: 51–59

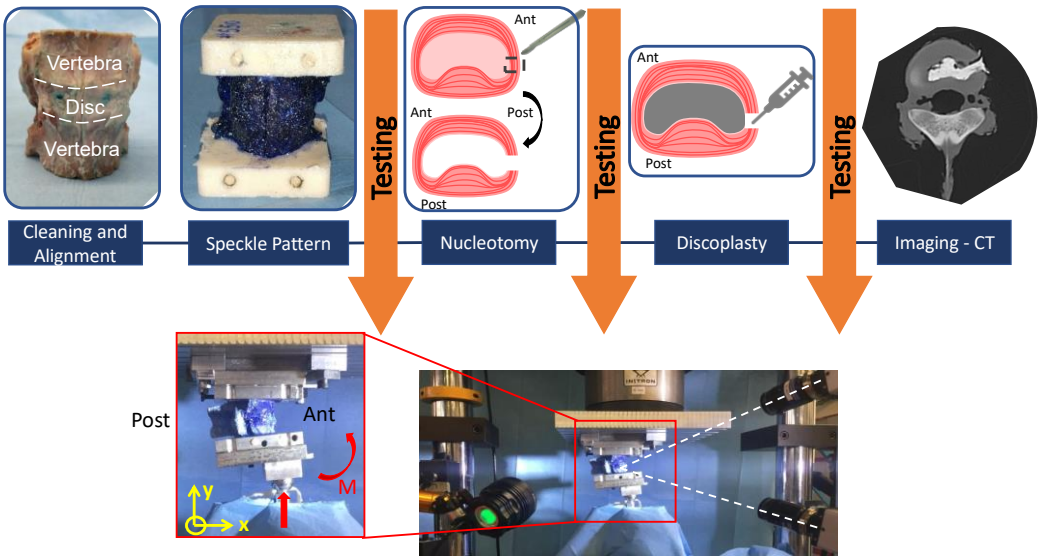


***Fig. 3.1 –*** *Experimental workflow of the study. The arrow represents the applied load and the resulting moment M.*

### *3.3.3 Nucleotomy*

Since the porcine specimens were euthanized before reaching skeletal maturation, degenerated disc instability has been manually simulated by reproducing the vacuum inside of the disc. The specimens were thawed at room temperature. A square incision was performed with a scalpel blade in the annulus fibrosus on the latero-posterior side of the disc. The nucleus pulposus, easily identified due to its softness, was completely extracted through the excision with a curette. The endplates were shaved by scratching off the soft tissue until the surfaces felt smooth. This did not weaken the endplates, as no intravertebral leakage was observed during discoplasty. The size of the incision corresponded to the disc height. The specimens were frozen at -20 °C until testing.

### *3.3.4 Discoplasty*

After being tested in degenerated conditions, the specimens were treated with discoplasty. For that, the specimens were thawed at room temperature. A high-viscosity radiopaque acrylic bone cement (10% BaSO4) (Tecres, Italy) was injected inside the disc through the incision. The cement was prepared at room temperature, mixing the powder and liquid components, and waiting as recommended by the supplier to reach the adequate viscosity before injection. Because the empty IVD was no longer in tension, the segment was distracted/stretched during the injection to avoid an underestimation of the cement volume. After injection, the cement hardened for 30 min. The specimens were frozen at -20 °C until testing. In one specimen the facet joint was unintentionally damaged at the end of the last test: checking the test results in retrospect confirmed there was no artefact.



Published in: Medical Engineering and Physics, 2020, 84: 51–59

### *3.3.5 Mechanical testing*

All the specimens underwent the same test conditions. In order to simulate *in vivo* kinetics of porcine spines, a load with offset was applied to simulate flexion, extension, and lateral bending (the same side was selected for each specimen based on the possible damages made during the preparation). This simplified loading scenario was chosen as it allows reproducible simulation of a realistic loading scenario. In quadrupeds, the choice of a side is less significant than for humans since they do not have a predisposed limb side. The specimens were mechanically tested with a uniaxial servo-hydraulic testing machine (Mod. 8032, Instron, UK) operated in displacement control. The upper pot was rigidly fixed to the top of the testing machine while the other was loaded through a spherical joint moving along a rail (Fig. 3.1). Before testing, each specimen was thawed at room temperature and pre-conditioned applying a sinusoidal loading at 0.5 Hz for 20 cycles to minimize viscoelastic creep effect. Specimens were loaded at 5.4 Nm by applying 200 N with an offset of 27 mm. The loading ramp lasted 1 s then the maximum loading was maintained for 0.3 s and the specimen was unloaded. The cycle was repeated 6 times (Fig. 3.2). Three cycles were found to be sufficient for preconditioning the data in another study [57], further cycles being nearly identical. The same trend was observed in these tests. The loading conditions were selected within the range of biological conditions, applying similar moments to other past studies [47], [58]–[60]. Besides, the selected load avoided specimen damage. Each test was repeated twice to prove the experiment repeatability. Mean of data extracted from the last cycle of both runs was derived for each specimen. Axial load and displacement were acquired by the Digital Image Correlation (DIC) system connected to a load cell (100 kN) at 15 Hz. Additionally, to have a more reliable sequence, the data were recorded with an independent computational unit (PXI, Labview, National Instruments, Aus. Texas, US) at 500 Hz. Unfortunately, some of the former records were missing for the first tests. Loads were either interpolated to have more data or smoothed with a median filter depending on the acquisition frequency.

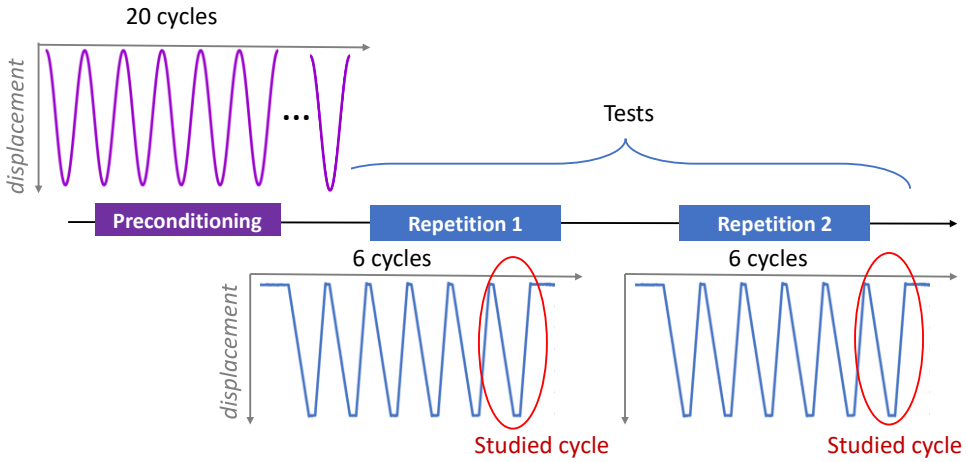


***Fig. 3.2 –*** *Workflow of the applied displacement for flexion, extension, and lateral bending.*



Published in: Medical Engineering and Physics, 2020, 84: 51–59

### *3.3.6 Displacement and strain with DIC*

For each test, the specimen surface has been studied using a DIC set-up in order to track its displacements and strains. This technique requires a high-contract speckle pattern on the region of interest. Thus, a white-on-black speckle pattern was prepared on both the vertebra and the intervertebral disc (Fig. 3.1). First, the segment was stained 3 times with a methylene blue solution to create a dark background without impacting the properties of the tissues [61]. The white pattern was then sprayed following a procedure optimized elsewhere [62]. To measure the displacements and the deformations over the specimen surface, a 3D-DIC system (Q400, Dantec Dynamics, Skovlunde, Denmark) and the associated software (Instra 4D, v.4.3.1, Dantec Dynamics) were used. Images were acquired by two cameras (5 Megapixels, 2440 x 2050 pixels, 8-bit) with high-quality 35 mm lenses (Apo-Xenoplan 1.8/35, Schneider-Kreuznach, Bad-Kreuznach, Germany) inclined at an angle of 26° (white dot line on Fig. 3.1). The field of view covered the entire specimen (about 50mm by 30mm), which gave a pixel size of about 0.02mm. The specimen was lit by cold-light LEDs. Before the tests, calibration of the DIC system was performed using a dedicated target (Al4-BMB-9x9, Dantec Dynamics). The parameters for the images acquisition and the correlation analysis have been previously optimized to minimize the error: facet size of 35 pixels, grid spacing of 11 pixels, and local filtering with a 7x7 pixels kernel. In order to investigate the biomechanical behaviour of the spine, two different acquisitions were performed:

- For extension and flexion: Lateral view of the segment with the cameras pointing at the neuroforamen
- For lateral bending; Frontal view of the specimen with the cameras pointing to the selected bending side

Images were taken at 15 Hz from the unloaded condition (reference frame, no load applied) to the end of the 6th cycle.

### *3.3.7 Data analysis and statistics*

The parameters were extracted from the last load cycle of each of the two repetitions of each loading configuration. All measurements were compared for each specimen between the three disc conditions: intact, nucleotomy, discoplasty. Peak load DIC image frame was obtained by tracking the axial translation of the free vertebra and synchronizing the cycles with the actuator displacements. In order to assess the changes in the nerve space in the neuroforamen, which is the main point in doing discoplasty, the posterior disc height was measured using DIC images: one point on each endplate was identified on the 3D profile of the disc in the back of the disc, close to the neuroforamen, where the nerve is passing. The points were aligned in the cranial-caudal direction. Their position was therefore tracked using DIC software. As a result, posterior disc height was only computed in flexion and extension, the frontal view not allowing height computation in lateral bending.



Published in: Medical Engineering and Physics, 2020, 84: 51–59

Displacements of the caudal vertebra in relation to the cranial vertebra were calculated from DIC images with a Matlab script. Assuming vertebra to be rigid bodies, the motions (translations and rotations) of each vertebra were computed based on singular value decomposition. The ROM was defined as the relative angle between the vertebra in the sagittal plane between the peak load and unloaded conditions.

A pilot study of the load-displacement curves determined that, for porcine spines, the position having a first derivative of 30 N/mm was at the limit of the laxity zone (LZ). Stiffness was defined as the slope of load-displacement relationship in LZ. Although for some specimens this method underestimated the length of the LZ, the stiffness computation was not impacted since it was within the linear region [63].

All the computations were performed with dedicated Matlab scripts (MathWorks, Inc., Natick, MA, USA). All height and strain measurements were evaluated by two independent observers. To limit inter-specimen variability influence, all stiffnesses, heights, and ROMs values were normalized to the intact condition.

In addition to posterior disc height, ROM, and stiffness calculations, the true principal strains over the specimen surface (vertebra and IVD) were measured at the peak load. In particular, the disc surface area was manually identified and the minimum, maximum and mean of the first and second principal strains were extracted. Those measurements were performed in flexion and extension because the frontal view did not allow consideration of the neuroforamen area.

For each parameter, outlying data were preliminarily tested and excluded using the Peirce criterion [64], this resulted in a 10% data exclusion at the maximum. Test parameters were computed based on the sixth cycle. Mean ± standard deviation of all the outcomes were calculated and presented by group. Due to the small specimen number, comparisons between the three conditions were made for ROM, stiffness, height, and the strain mean with a non-parametric test (Wilcoxon's sign rank, with Matlab).

### *3.3.8 Cement distribution*

In order to study the cement distribution inside of the disc, scans of the specimens have been performed after discoplasty with a clinical computed tomography scanner (Aquilion ONE, Toshiba) with 120 mA, 135 kV and a 0.5 mm voxel. The scans of nine specimens out of ten were available due to a practical mistake. The shape of the cement, its capacity to fill the disc cavity, the endplates and AF contact were visually assessed by a spine surgeon (P.E.) from the 3D reconstruction of the PMMA geometry. Segmentation process was performed in Mimics® image analysis software (Mimics Research, Mimics Innovation Suite v21.0, Materialise, Leuven, Belgium) on the 2D CT images using thresholding algorithm.



Published in: Medical Engineering and Physics, 2020, 84: 51–59

## 3.4 Results

### *3.4.1 Posterior disc height*

The posterior disc height was measured in the three conditions. At peak load, intact posterior disc height was higher in flexion than in extension. Nucleotomy significantly decreased the posterior height for flexion (p=0.006, Wilcoxon, after Bonferroni's correction α=0.025). A decrease of posterior height was also observed in extension (p=0.049, Wilcoxon, α=0.025) (Fig. 3.3). On the contrary, discoplasty restored the height. Results were normalized to the initial posterior height for each specimen. In extension, height after discoplasty was significantly higher (105% of the intact height) than after nucleotomy (81%) (p= 0.04, Wilcoxon). In flexion, posterior disc height was respectively 84% and 94% of the intact height after nucleotomy and discoplasty but the difference between the two conditions was not significant (p=0.11, Wilcoxon).

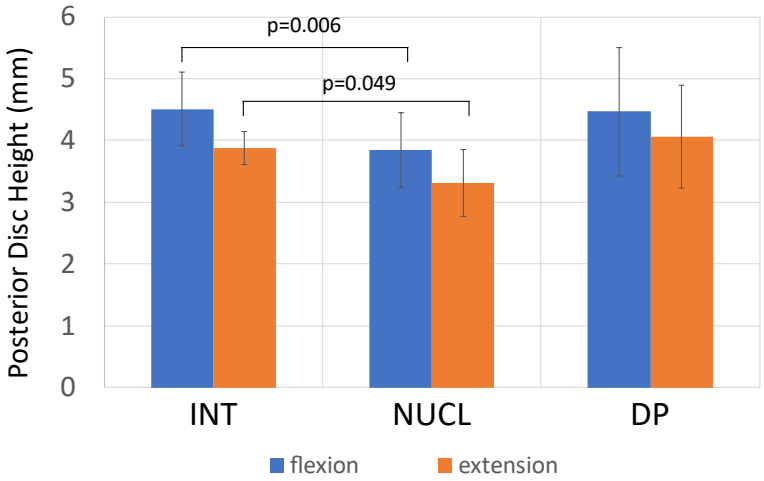


***Fig. 3.3 –*** *Intervertebral posterior disc height recorded at the peak load in intact condition, after nucleotomy, and discoplasty for both motions. Mean over all specimens and standard deviation were represented (n=10). Normalized data showed significant differences in flexion (p=0.11) and extension (p=0.04) between NUCL and DP.*

### *3.4.2 Range of motion*

Intervertebral motions in the applied direction were one order of magnitude higher compared to the other directions. Only the motions in the applied direction are reported here. In flexion and lateral bending, nucleotomy reduced the ROM (Fig. 3.4). The ROM in extension slightly increased after nucleotomy and discoplasty compared to the intact condition. The results for degenerated and discoplasty discs were normalized by the intact ROM for each motion. ROM was not significantly different between nucleotomy and discoplasty in flexion (Wilcoxon sign-rank test, p=0.57), extension (p=0.43) and lateral bending (p=0.50, Wilcoxon).



Published in: Medical Engineering and Physics, 2020, 84: 51–59

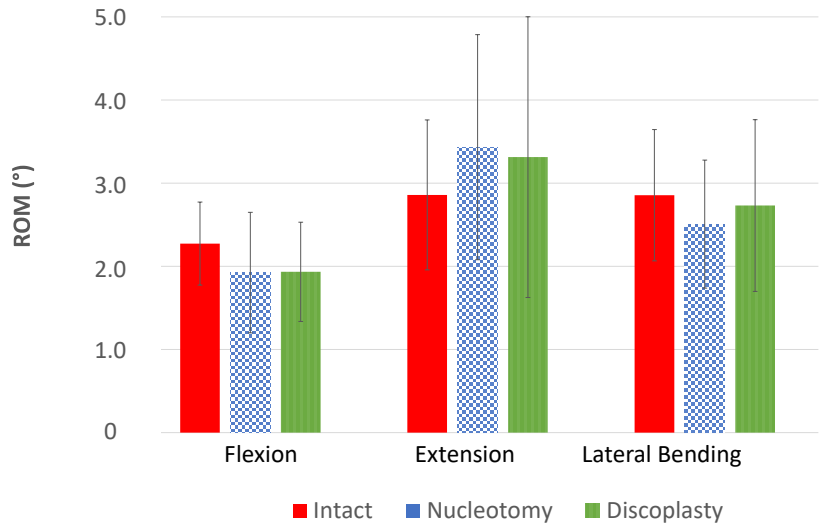


***Fig. 3.4** – Range of Motion recorded at peak load for flexion, extension and lateral bending, in all disc conditions. Normalized data were not statistically significant (p>0.1).*

### *3.4.3 Stiffness*

Stiffness was computed for only 9 out of 10 specimens due to a technical problem during acquisition. Specimens had very different behaviours regardless of the loading configuration and spinal level. The majority of the tests presented a "toe-region" before a stiff region. A recovery after discoplasty of the initial behaviour compared to after nucleotomy was also observed (Fig. 3.5). The results for nucleotomy and discoplasty discs were normalized by the intact stiffness for each loading configuration. Stiffness was not significantly different after nucleotomy and discoplasty in flexion (p=0.47, Wilcoxon), extension (p=0.95, Wilcoxon) and lateral bending (p=0.46, Wilcoxon) (Fig. 3.5).

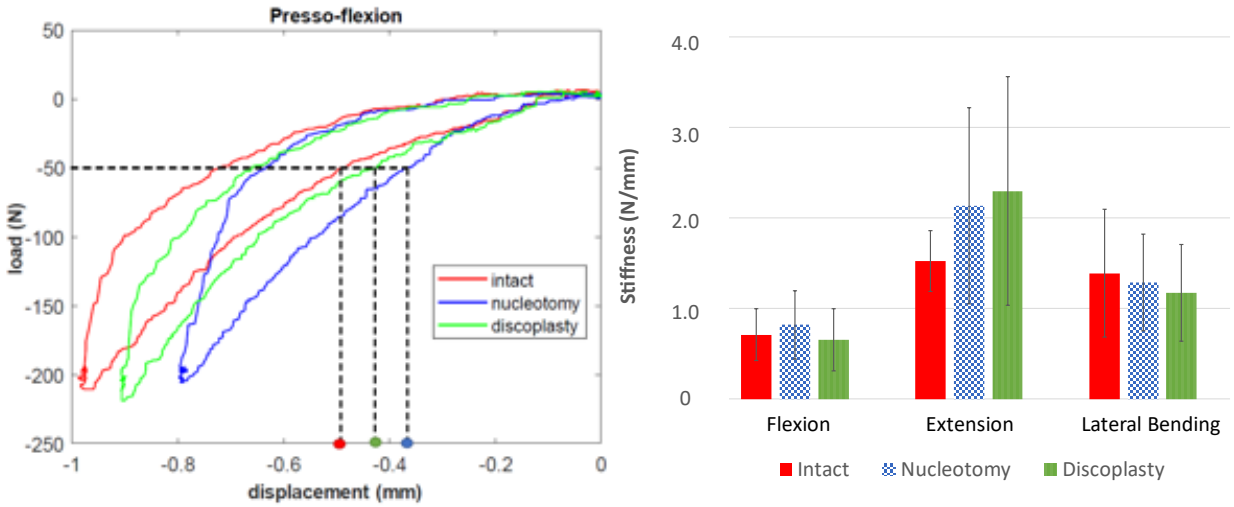


***Fig. 3.5 –** Load-displacement curve of a representative specimen tested in flexion in all disc conditions (left) – Stiffness results in all conditions for all loading configurations (right). Mean was done over all specimens. Normalized data were not statistically significant (p>0.1).*



Published in: Medical Engineering and Physics, 2020, 84: 51–59

### *3.4.4 Strain distribution*

DIC correlation has been successfully performed in flexion and extension only because the frontal view did not allow all of the disc surface to be captured. First of all, bone strains were in a [-1.5%,1.5%] range on the vertebra surface whereas they reached -17% and +11% on the discs. Moreover, IVD principal strains presented different behaviours depending on the loading configuration (Fig. 3.6). In flexion, for all disc conditions, the highest values of compressive strain are located at the cranial and caudal extremities of the IVD, starting from the anterior and spreading toward the posterior along the endplates. After nucleotomy and discoplasty, the trend was more pronounced. However, cemented discs presented lower values in this area than empty discs. The highest values of tensile principal strain were in the centre of the IVD with peak >3% of strain in the posterior region. In extension, tensile strains were larger in the anterior of the disc while high compressive strains were located in the posterior area of the disc. Discoplasty reduced the strains in most of the disc, whereas for intact and nucleotomy, high strains were found on the whole disc.

Nucleotomy seems to have a greater effect on the compressive strain in flexion and extension (Table 3.1). Meanwhile, discoplasty halved the mean tensile strain of disc surface compared to nucleotomy condition in extension ($p=0.0195$, Wilcoxon) but had similar values of second principal strain. Regarding the peak strains, discoplasty only presented a value larger than intact condition for extension. Other extreme strains were observed after nucleotomy although the differences were not significant.

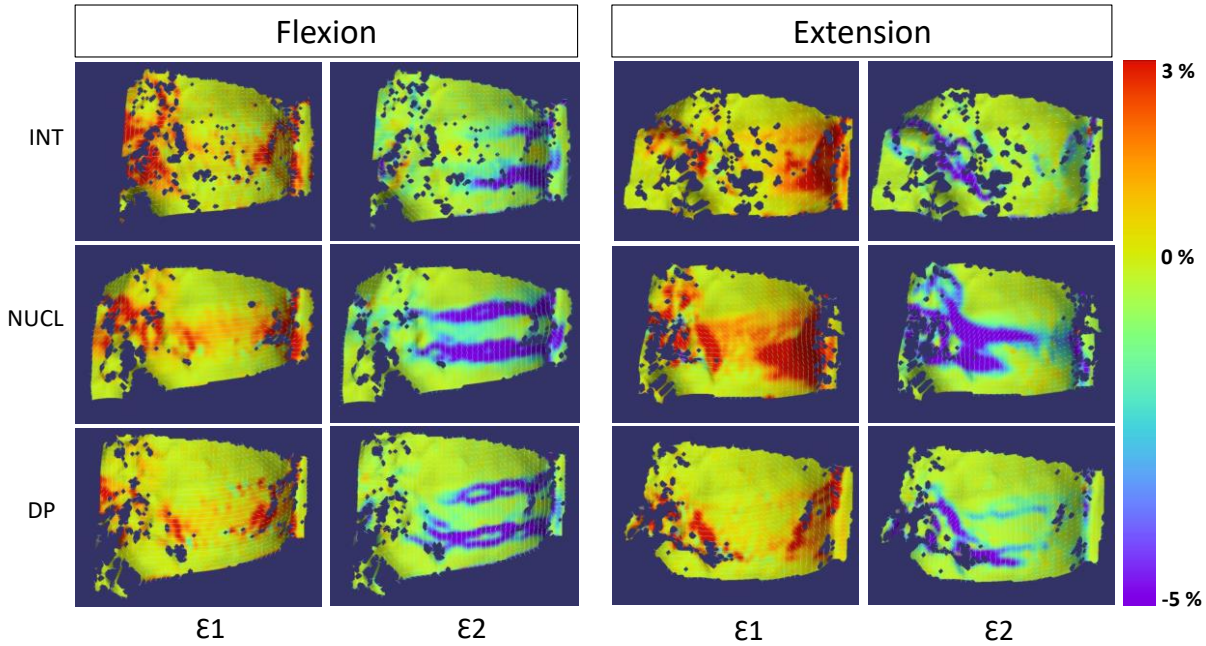


***Fig. 3.6 –*** *Showed a typical strain distribution over a specimen surface for a flexion (left) and extension (right) bending with first and second principal strains represented for each motion.*



Published in: Medical Engineering and Physics, 2020, 84: 51–59

***Table 3.1 -*** *Principal strains recorded over the disc surface in Flexion and Extension: The mean and peak (of 10 specimens) are reported for $\varepsilon_1$ and for $\varepsilon_2$.*

| $\varepsilon_1$ | Flexion | | Extension | |
|---|---|---|---|---|
| | **Mean (%)** | **Peak (%)** | **Mean (%)** | **Peak (%)** |
| Intact | 1.3±0.6 | 7.5±2.8 | 2.2±1.0 | 11.7±6.0 |
| Nucleotomy | 1.3±0.7 | 10.5±7.1 | 1.9±0.6 | 10.1±3.9 |
| Discoplasty | 1.0±0.5 | 8.7±3.5 | 1.2±0.7 | 10.0±4.1 |

| $\varepsilon_2$ | Flexion | | Extension | |
|---|---|---|---|---|
| | **Mean (%)** | **Peak (%)** | **Mean (%)** | **Peak (%)** |
| Intact | -2.0±1.2 | -17.2±6.1 | -0.5±0.4 | -8.2±7.5 |
| Nucleotomy | -2.8±1.6 | -18.7±8.9 | -1.7±1.5 | -12.5±10.4 |
| Discoplasty | -1.7±0.9 | -16.5±7.3 | -0.7±0.8 | -13.3±5.3 |

### *3.4.5 Cement distribution*

Nine specimens have been scanned to control cement distribution within the discs. Visual assessment of the specimen scans focused on the position of the cement mass within the intervertebral disc in the sagittal and frontal planes, whether it was in contact with endplates and AF, the shape of the distribution, and the ratio of disc filling. The majority of specimens had a cement volume located in the posterior of the disc (9/9 specimens), centred in the lateral direction (8/9 specimens), in contact with the endplates (8/9). Only two specimens did not present contact between the cement and the AF (Fig. 3.7).

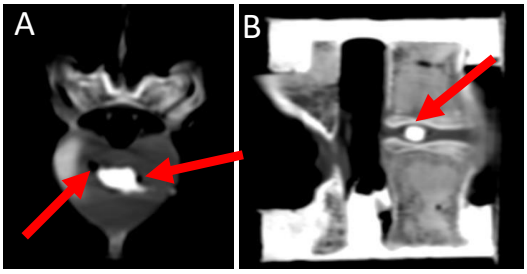


***Fig. 3.7 –*** *Sub optimal cement distribution. CT scans of porcine specimens in axial (A) and sagittal (B) planes. PMMA did not reach the annulus and the endplates (arrows), leaving vacuum.*

The NP cavity was fully filled with cement in 5 specimens, three discs were almost filled at >80% of the NP volume, and one at less than 80%. Among the specimens, seven were validated by a clinician as discoplasty models compared to cement distribution after human surgery taking porcine anatomical specificities into account, and two were sub-optimal (Fig. 3.8).



Published in: Medical Engineering and Physics, 2020, 84: 51–59

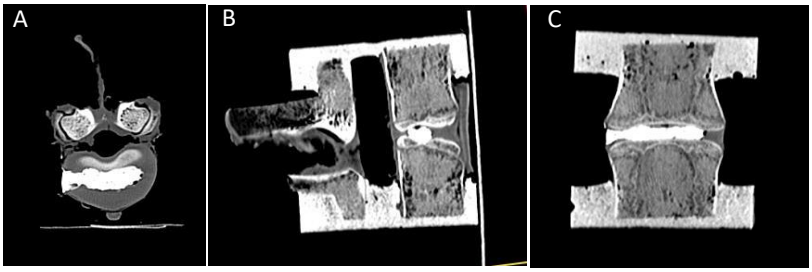


***Fig. 3.8 –*** *Ideal distribution of the PMMA in the porcine model. CT scan of the porcine specimen, A (axial plane) the PMMA filled out the empty space after nucleotomy, B (sagittal plane) and C (coronal plane) the PMMA reached the two endplates and adapted to the geometry.*

No outlier corresponded to the sub-optimal cemented specimens. All specimens presented a smaller cement volume than in human surgery (Table 3.2).

***Table 3.2 -*** *Surface area and volume of the injected cement after segmentation.*

| Specimen | Spine level | Cement surface area ($mm^2$) | Cement volume ($mm^3$) |
|---|---|---|---|
| #1 | T13-L1* | 257.8 | 282.8 |
| #2 | L3-L4 | 465.8 | 476.7 |
| #3 | T13-L1* | 211.6 | 143.5 |
| #4 | L5-L6 | 623.7 | 673.9 |
| #5 | T13-L1* | 712.3 | 750.3 |
| #6 | L3-L4 | 552.0 | 608.7 |
| #7 | L3-L4 | 742.2 | 776.5 |
| #8 | L3-L4 | 557.6 | 505.4 |
| #9 | T15-L1* | 592.7 | 685.0 |
| **Mean (SD)** | **-** | **524.0 (184.2)** | **544.8 (215.7)** |

** Porcine spines have a variable number of thoracic vertebrae (between 13 and 15).*

## 3.5 Discussion

According to clinical observations [20], a loss of disc height due to disc degeneration would result in a reduction of the neuroforamen where the back nerves are passing, compressing them and creating pain for the patient. This animal *in vitro* study aimed at exploring the feasibility of assessing the mechanical consequences on spine stability after discoplasty surgical procedure. An *in vitro* experiment was successfully conducted to establish posterior disc height, ROM, stiffness, and strains over porcine specimen surfaces.

After nucleotomy a decrease of the posterior disc height of 15% was measured. This result validated such *in vitro* nucleotomy as a simulation of degenerated disc. Furthermore, nucleotomy was associated with a decrease of ROM (not statistically significant in our sample). After discoplasty, the injected cement acted like a spacer resulting in a significant recovery of the posterior height (105% of the intact height in extension). This trend supported the clinical observations [20] and confirmed that PCD



Published in: Medical Engineering and Physics, 2020, 84: 51–59

recovered the disc height and enlarged neuroforamen space, which is the main objective of this surgery. ROM and stiffness did not show any significant difference between the degenerated and treated cases for any loading. Thus, discoplasty did not significantly impact spine flexibility in this experimental setup.

To the authors' knowledge, this was the first study addressing the consequences of discoplasty on the distribution of strain on the disc surface. The strain distribution measured after nucleotomy showed a specific pattern with intense regions, while discoplasty reduced this abnormal distribution with more moderate strain values.

DIC results showing the AF principal strains can be related to the ROM and the posterior disc height. After nucleotomy, because of the reduced posterior height and because the annulus is no longer constrained from inside, the annulus fibres bulged more, leading to intense tensile strains at the apex of the bulging. At the same time, this more pronounced bulging at mid-height caused a more pronounced concavity at the disc cranial and caudal extremities, which led to larger compressive strains in this region. After discoplasty, the injected cement spaced the endplates, and even if the cement did not stretch radially the disc fibres as the NP would do, the overall bulging was more limited, and less intense tensile strains were measured. As the cement acts as a very stiff spacer, very small strains were visible in most of the disc surface, the only highly strained region in the disc was near the endplates. Strain values after discoplasty did not exceed what the endplates underwent in nucleotomy condition. If the specimen endplates presented any weakness, this could lead to long-term damages due to the load concentration. The peak strain values increased after nucleotomy, and decreased again after cement injection, reaching intact-like values. No correlation between the strain peaks on the specimen surface and the cement distribution assessed from the CT scans was found. Even in the specimens where contact between the AF and the cement was noted, this did not result in a specific strain distribution.

The ROM measured at peak load was in the same range as other *in vitro* studies on porcine lumbar spines [58], [65]. Others studies investigating the effect of nucleotomy demonstrated that the absence of NP reduced segmental rotational stability, significantly increasing the ROM [51], [55], [59].

Discoplasty being a recent surgical technique, the authors found only one article applying a similar surgery, on dog cervical discs [43]: nucleotomy was also performed through an AF fenestration and a spacer implant was inserted. Similar to the present study, Moissonier *et al* found that nucleotomy completely disrupted spine stability, increasing significantly the ROM. Both the spacer used in their study, and the cement injected in ours failed to recover disc mobility. Similarly, the cement set in the cervical disc by Wilke *et al* reduced the ROM compared to intact disc condition. However, this study tested bone cement to anticipate interbody fusion, and the AF was not fully intact [28]. This was the major difference with soft disc filler materials which are more likely to restore intact ROM as well [51].



Published in: Medical Engineering and Physics, 2020, 84: 51–59

Although the results were normalized with respect to the intact to integrate the specimen anatomical specificity, and one outlier was removed, inter-specimen variability remained large, with no correlation with the segment level. Our tests differed from most of the literature [63] as the FSUs were tested separately in flexion and extension, therefore direct comparisons of the stiffness are not possible.

This study aimed to start exploring the biomechanical effects of discoplasty. Since this is a preliminary study, an animal model was more justifiable for ethical reasons. The use of breed porcine rather than human spines was preferred as they have less inter-specimen variation of anatomy and mechanical properties. Indeed, porcine models are commonly used to replicate human spine surgeries [66], [67]. Porcine spines could be good surrogates for *in vitro* testing, even if they exhibit larger ROM and lower stiffness [68]–[70]. Since the porcine specimens were obtained before reaching skeletal maturity, finding IVDs presenting a similar degenerated level with a vacuum as required for PCD was impossible. Nucleotomy did not aim at modelling a degenerated disc state but at creating the spine instability observed clinically based on the disc vacuum. Porcine results should therefore be qualitatively extrapolated to humans in terms of trends rather than interpreting absolute values as this study aimed at.

Vacuum volume has not been measured in this study. The importance of this parameter is unclear in the clinical practice. A recent study investigating the VP impact for PCD indication concluded that the volume of vacuum could not be used as a proper indication for this surgery [34]. Moreover, during the PCD procedure, the patient position aims at enlarging the intervertebral space by reducing the segmental lordosis. Thus, the volume of the empty disc available during the surgery is larger than the VP computed on imaging.

Usual methods to measure the disc height like Farfan or Frobin were not applied here to assess the intervertebral space. Indeed, these methods were conceived for clinical application considering the vertical height along the antero-posterior disc length on medical images, taking account of the whole disc and its orientation. This study, however, focused on the nerve space within the neuroforamen. Only the volume where the nerve passed was critical, based on clinical observations, and the discoplasty surgery was applied in first approach to re-open the foramen space by achieving indirect decompression. That is why a comparative study has been performed selecting two points at the endplates level the closest from the neuroforamen, rather than relying on a more general measurement of the disc height. The study concentrated on parameters with meaning for the clinical purpose of the surgery. Moreover, the most critical case was also investigated: physiologically when the disc is loaded in extension and the neuroforamen is the most reduced. So, measurements at the peak load were more interesting for the study.

The impact of AF fenestration during nucleotomy on the segment stability has not been assessed here, however Michalek *et al* reported alterations of IVD mechanics with disc height loss under a compressive load, following different types of incisions [71]. Disc lesions were also found to reduce the peak moment



Published in: Medical Engineering and Physics, 2020, 84: 51–59

depending on the damage shape [72]. As a consequence, our study may overestimate motion range. However, it was hypothesized that the lack of NP would destabilize the segment in larger proportion than the fenestration of AF.

Pure moment is the gold-standard loading for *in vitro* spine testing in a relevant bending condition. For spine segments consisting of several vertebrae, bending is usually associated with a follower load equipment to model the *in vivo* kinematics, including the effect of the muscles adding a compressive loading [73], [74]. Similarly, a compressive preload is found in a single FSU, but in this case a follower load cannot be implemented. In this study, an alternative loading configuration was chosen to ensure that reproducible testing conditions could be applied, thus allowing the comparison of the biomechanics of a specimen tested at different times with each of the different disc conditions. The load applied here was a combination of axial compression and bending, an alternative loading to pure bending of the spine [61], [75]–[78]. It has been demonstrated that without preload, *in vivo* stiffness of the spine segment was underestimated applying pure bending [79]. In our study, the combination of axial compression and bending allowed a more physiological spine loading with an axial component which substitutes of the preload.

## 3.6 Conclusion

So far, the only knowledge about PCD comes from clinical experience on few cases. This paper presents a feasibility study, to develop a test model and perform a preliminary investigation on the biomechanics of PCD. The study also aimed at analyzing and verifying if there is any clear mechanical risk associated with injection of cement in the cavity of a disc. No specific clinical recommendations (e.g. indication for specific patient groups) can be directly obtained from the present study. This study aimed at developing an *in vitro* surrogate to test a highly degenerated disc with vacuum inside, and to assess the biomechanical changes related to discoplasty in porcine spines. The main conclusions could be summarized in key points.

- The *in vitro* method was successfully developed to model nucleotomy.
- The *in vitro* testing protocol applied to discoplasty allowed to measure the effect of this minimally invasive surgery on the spine biomechanics.
- Nucleotomy decreased the posterior disc height. Discoplasty restored the height significantly, maintaining a gap between the vertebral bodies and re-opening the neuroforamen area as observed in clinical practice.



Published in: Medical Engineering and Physics, 2020, 84: 51–59

- The CT scans confirmed that the distribution of the cement had a similar distribution inside the disc for most specimens compared to human post-surgery observations, although the cavity after nucleotomy and the cement volume were smaller than in human cases.

- Discoplasty did not impact the ROM nor the stiffness, which remained similar to the nucleotomy condition because the cement did not directly interact with the AF nor the facets.

- Discoplasty concentrated the strains along the endplates, reducing the strain value on the middle of the disc. The mean strain over the disc was decreased after discoplasty compared to nucleotomy, limiting the risks of fibre tears.

- The goal of this preliminary study on a limited number of porcine specimens was to establish trends which could justify a larger study on human specimens.



Published in: Medical Engineering and Physics, 2020, 84: 51–59

# *Chapter 4*

# Biomechanical consequences of cement discoplasty: an *in vitro* and *in vivo* study on thoraco-lumbar human spines

from the manuscript:

**Biomechanical consequences of cement discoplasty:**

**an *in vitro* study on thoraco-lumbar human spines**

C. Techens, S. Montanari, F. Bereczki, P. E. Eltes, A. Lazary, L. Cristofolini

Adapted from a submission to: *PLOS ONE (2022)*

*With the consent of the main author, this chapter also includes my contribution to the paper:*

***A novel three-dimensional volumetric method to measure indirect decompression after percutaneous cement discoplasty***
*P. E. Eltes, L. Kiss, F. Bereczki, Z. Szoverfi, C. Techens, G. Jakab, B. Hajnal, P. P. Varga, A. Lazary*
*Published in: Journal of Orthopaedic Translation, 2021, 28: 131–139, https://doi.org/10.1016/j.jot.2021.02.003*

*Only the methods/results/figures/tables related to my contribution were included below. The corresponding sections are reported as published in appendix of the thesis (Appendix 2) for completeness, to fully describe the methods applied.*

## 4.1 Abstract

With the ageing of the population, there is an increasing need for minimally invasive spine surgeries to relieve pain and improve quality of life. Percutaneous Cement Discoplasty (PCD) is a minimally invasive technique to treat advanced disc degeneration, including vacuum phenomenon. The present study aimed to develop an *in vitro* model of PCD to investigate its consequences on the spine biomechanics in comparison with the degenerated condition. Human spinal segments (n=27) were tested at 50% body weight in flexion and extension. Posterior disc height (PDH), Range of Motion (ROM), segment stiffness, and strains were measured using Digital Image Correlation. The cement distribution was also studied on CT scans. As main result, PCD restored PDH by 41% for flexion and 35% for extension. ROM was significantly reduced only in flexion by 27%, and stiffness increased accordingly. The injected cement volume was 4.56±1.78 ml (mean ± SD). Some specimens (n=7) exhibited cement perforation of one endplate. The thickness of the cement mass moderately correlated with PDH and ROM with different trends for flexions vs. extension. Finally, extreme strains on the discs were reduced by PCD, with modified patterns of the distribution. To conclude, this study supported clinical observations in term of recovered disc height close to the foramen, while PCD helped stabilize the spine in flexion and did not increase the risk of tissue damage in the annulus.

**Keywords:**

percutaneous cement discoplasty, biomechanics, spine, digital image correlation, intervertebral disc degeneration

## 4.2 Introduction

The ageing of the global population due to increasing life expectancy [80] results in the changing epidemiology of spinal diseases and disorders [81]. In the ageing spine, the intervertebral disc degeneration (IDD) leads to biomechanical and structural changes of the spine [82]. The terminal disc degeneration is characterized by total disorganization of the intervertebral tissue, and complete resorption of the nucleus pulposus causing in many cases a vacuum phenomenon (VP) [24], [83], [84]. IDD-related structural changes lead to biomechanical malfunctions [85], such as segmental instability. Surgical treatment possibilities of segmental instability in elderly patients are limited [81]. Minimally invasive surgical (MIS) procedures are the preferred options [86]. Percutaneous cement discoplasty (PCD) is a MIS procedure, where the vacuum space in the intervertebral disc (IVD) is filled with percutaneously injected acrylic cement. The PCD procedure is expected to provide a segmental stabilizing effect and indirect decompression of the neuronal elements [20], [21], [33]. Initially PCD was biomechanically investigated on cervical discs [25], [28]. However, PCD as low-back-pain treatment has only been evaluated in terms of patient outcome by clinical studies [20], [21], [36]. If PCD appeared efficient to relieve patient's pain, biomechanics of the spine following the surgery remains unknown.

This study aims at investigating the consequences of percutaneous cement discoplasty on the biomechanics of the human spine with respect to the pre-operative degenerated condition. Therefore, the first objective was to develop a reliable *in vitro* model of percutaneous cement discoplasty. This was then used to evaluate the *in vitro* biomechanical behaviour of the treated segment. The core objective of this study was monitoring the biomechanical effects of PCD and identifying the potential links between PCD and the biomechanical outcomes in order to assess the benefits and detect potential detrimental effects. In particular, we hypothesized that PCD would increase the disc height in the posterior region with respect to the degenerated condition. We furthermore hypothesized that PCD would impact the intervertebral kinematics. Finally, we conjectured that PCD could represent a challenge for the surrounding tissue due to the perturbed stress distribution due the presence of a cement mass. We also hypothesized that the cement volume and its distribution inside the disc would impact on the biomechanical behaviour of the treated functional spinal unit (FSU).

## 4.3 Methods

### *4.3.1 Compliance with Ethical Standards*

This study was performed in line with the principles of the Declaration of Helsinki. Approval was granted by the Bioethics Committee of the University of Bologna (Prot. 76497, 1 June 2018). The cadaveric spines were obtained through two institutions: an international donation program

(International Institute for the Advancement of Medicine) and the hospital of the NCSD after ethical approval of both entities.

### *4.3.2 Overview of the study*

PCD is the ultimate treatment for polymorbid patients. This surgery does not aim to completely restore the conditions of a healthy spine, but to mechanically act on the disc foramen to relieve the pain. Thus, this study aimed to assess whether PCD would recover the disc height and impact the intervertebral kinematics in comparison with degenerated discs. FSUs were prepared for testing (Fig. 4.1). They were biomechanically tested non-destructively after simulating disc degeneration. Then percutaneous cement discoplasty was simulated. The specimens were re-tested under the same loading conditions. Kinematics and strains were measured using digital image correlation (DIC).

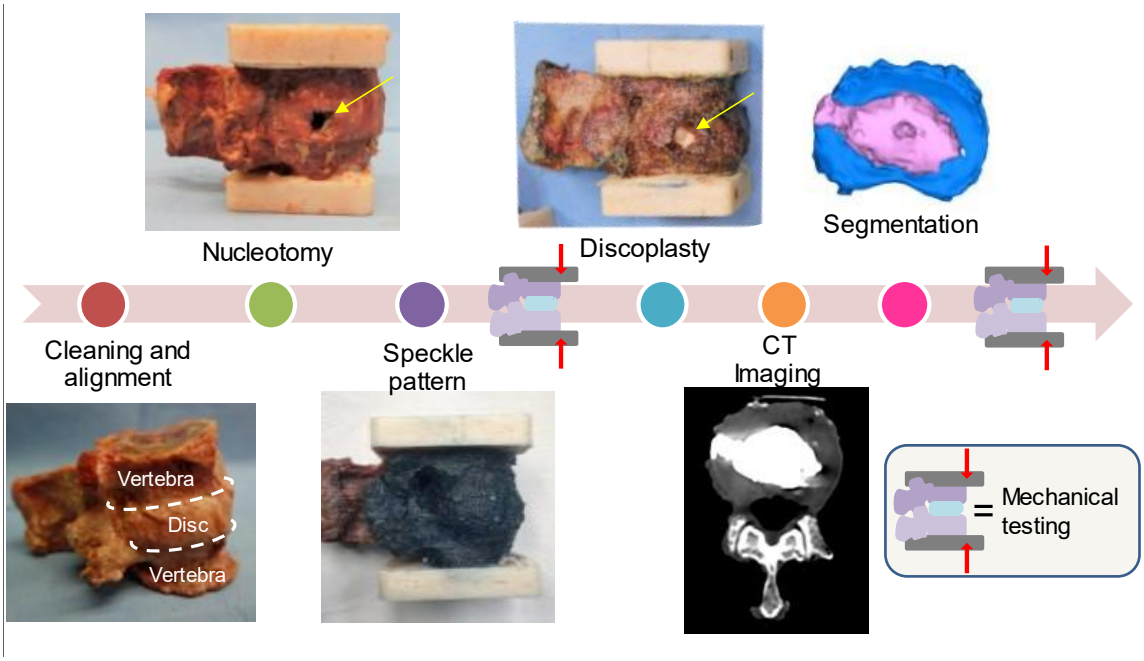


***Fig. 4.1*** *- Experimental workflow of the study. The specimens were prepared with a high-contrast speckle pattern to allow measuring displacements and strains under load with digital image correlations. Each specimen underwent biomechanical testing (under the same loading conditions) after nucleotomy and after simulated percutaneous cement discoplasty. The cement injected was investigated on CT images*

### *4.3.3 Cadaveric specimens*

For this study, 27 FSUs were extracted from 15 Caucasian lumbar spines (9 males/6 females) aged 35 to 86 years old. Death was unrelated to a spine disease. Based on computed tomography (CT) scan images, specimens with fractures or bridged osteophytes were excluded from the study by a clinician. Only specimens presenting intact endplates were selected. The selection did not consider the degree of disc degeneration. All soft tissues were carefully removed from the segment preserving the anterior, supraspinous and posterior ligaments, the facet joints, and the IVD to keep the natural kinematics of the segment [87], [88]. Each segment was aligned based on the disc orientation; both segment extremities

were embedded with acrylic cement. Specimens were stored at -28°C between cleaning and testing phases, and were thawed in physiological solution at room temperature prior to each test phase; hydration was granted during preparation and testing spraying the specimens [56].

### *4.3.4 In vitro surgical procedure*

#### *4.3.4.1 Nucleotomy*

PCD is recommended for advanced degeneration of the disc, when a vacuum is observed instead of the nucleus pulposus (NP), inducing a negative pressure within the disc [20], [33]. As donor specimens with a vacuum disc are complicated to obtain, a similar disc degeneration state was artificially created by manually emptying the disc. This degenerated disc simulation has been previously developed on animal specimens [39], [43] to provide the anatomical vacuum characteristics needed for PCD using a substitutive method. A rectangular incision as high as the disc and 5-8 mm wide was performed with a scalpel blade in the annulus fibrosus on the lateral side (Fig. 4.1), preferably on the side showing irregularities (small osteophytes, wrinkled tissues). Although it differed from the clinical posterior approach used for PCD, lateral fenestration was chosen in consideration of the loading directions as it avoided damaging the disc and ligaments in the posterior region. The nucleus pulposus was extracted through the excision and the cartilaginous endplates were shaved by scratching the cartilage off by a spine surgeon.

As the incision of the annulus fibrosus (AF) was suspected to critically affect the biomechanics of the remaining annulus, a separate methodological study was performed on eight additional specimens to quantify the consequences of this preparation (Appendix 1). Briefly, only NP removal significantly impacted the PDH. AF incision did not significantly impact the posterior disc height nor the biomechanics.

#### *4.3.4.2 Cement Discoplasty*

After being tested in a simulated degenerated condition, the specimens were treated with a highly radiopaque acrylic cement (Mendec Spine; Tecres, Sommacampagna, Italy, containing 30% BaSo4). The cement was prepared as clinically recommended [33], mixing the components at room temperature, and waiting a few minutes to obtain the desired viscosity. It was injected inside of the disc through the incision performed during nucleotomy until the cement would fill the cavity (Fig. 4.1). Because the empty IVD was no longer stretched, the disc height was manually kept constant during the injection to avoid an underestimation of the cement volume. After injection, the incision was manually closed during the cement hardening.

#### *4.3.4.3 CT scan acquisition*

In order to study the cement distribution inside of the disc, the specimens were scanned after PCD with a clinical computed tomography scanner (Aquilion ONE, Toshiba) with 220 mA, 120 kV, 0.3 mm slice thickness, 0.214 mm pixel size.

### *4.3.5 Clinical cohort and CT scan acquisition*

*[This section was adapted from Eltes et al.* [38] *and was performed by my co-authors in this paper prior to my participation.]*

In parallel to the *in vitro* study, a retrospective analysis of prospectively collected data involving 10 consecutive patients (74 ± 7.7 years old) was performed by P. Eltes' group [38]. All patients suffered from low back pain and leg pain, due to advanced disc degeneration, and underwent primary single or multilevel PCD at a tertiary care spine referral centre (Table 4.1).

Patients participating in the study were informed and their written consent was obtained. The study was approved by the National Ethics Committee of Hungary, the National Institute of Pharmacy and Nutrition (reference number: OGYEI/163–4/2019). Quantitative Computed Tomography scans were performed pre- and postoperatively, with a Hitachi Presto CT machine using an inline calibration phantom, and a protocol previously defined in the MySpine study (ICT-2009.5.3 VPH, Project ID: 269909) with an intensity of 225 mA and voltage of 120 kV [89], [90]. Images were reconstructed with a voxel size of 0.6x0.6x0.6 $mm^3$. To comply with the ethical approval and the patient data protection, anonymization of the DICOM data was performed using the freely available Clinical Trial Processor software (Radiological Society of North America, https://www.rsna.org/ctp.aspx) [91].

***Table 4.1 –*** *Clinical cohort*

| N=10 | Patient ID | Age (years) | Sex | Treated segment |
|---|---|---|---|---|
| | P01 | 83 | M | L4-L5 |
| | P02 | 59 | F | L2-L3 |
| | | | | L3-L4 |
| | | | | L4-L5 |
| | P03 | 67 | M | L5-S1 |
| | P04 | 78 | F | L3-L4 |
| | P05 | 79 | M | L5-S1 |
| | P06 | 76 | F | L1-L2 |
| | P07 | 75 | F | L2-L3 |
| | | | | L3-L4 |
| | | | | L4-L5 |
| | P08 | 66 | M | L3-L4 |
| | | | | L4-L5 |
| | P09 | 77 | F | T12-L1 |
| | | | | L1-L2 |
| | P10 | 82 | F | L1-L2 |

### 4.3.6 Cement geometry visualization and thickness measurement

*[This section includes my participation to Eltes et al.* [38] *in vivo study which was limited to the segmentation of the 3D geometries and its corresponding effect on DSI values. In order to ease the comprehension of the study results, the thickness measurements on in vivo data were included in the section even though they were not performed by me.]*

The vertebral and the cement masses were segmented with an image analysis software (Mimics Innovation Suite-v23.0, Materialise, Leuven, Belgium) on the CT slices using thresholding algorithm. Because of the extremity pots used for mechanical testing, the *in vitro* vertebrae were uniformly cropped at 3 mm from the deepest part of the endplate curvature to achieve a region of interest common to all specimens. (Fig. 4.2). All segmentations were performed by two independent operators (C.T and F.B). Segmentation repeatability was measured with Dice Similarity Index (DSI) [92].

The segmented masks were automatically converted into 3D surface meshes, and smoothed (iterations: 6, smooth factor: 0.7, with shrinkage compensation). The geometries were imported and measured (3-Matic 14.0, Mimics Innovation Suite v23.0). The vertebrae and bone cement geometries were first uniformly re-meshed (target triangle edge length: 0.3 mm, surface contour preservation, bad edges removing, split edge factor: 0.2). The endplate surfaces were manually selected. The cement thickness was defined between the two endplate surface planes, and was measured with the Midplane Thickness Analysis module of 3-Matic. Only thickness measurements of the *in vitro* cement mass were performed by me, the *in vivo* measurements were conducted by my co-authors in Eltes *et al.*

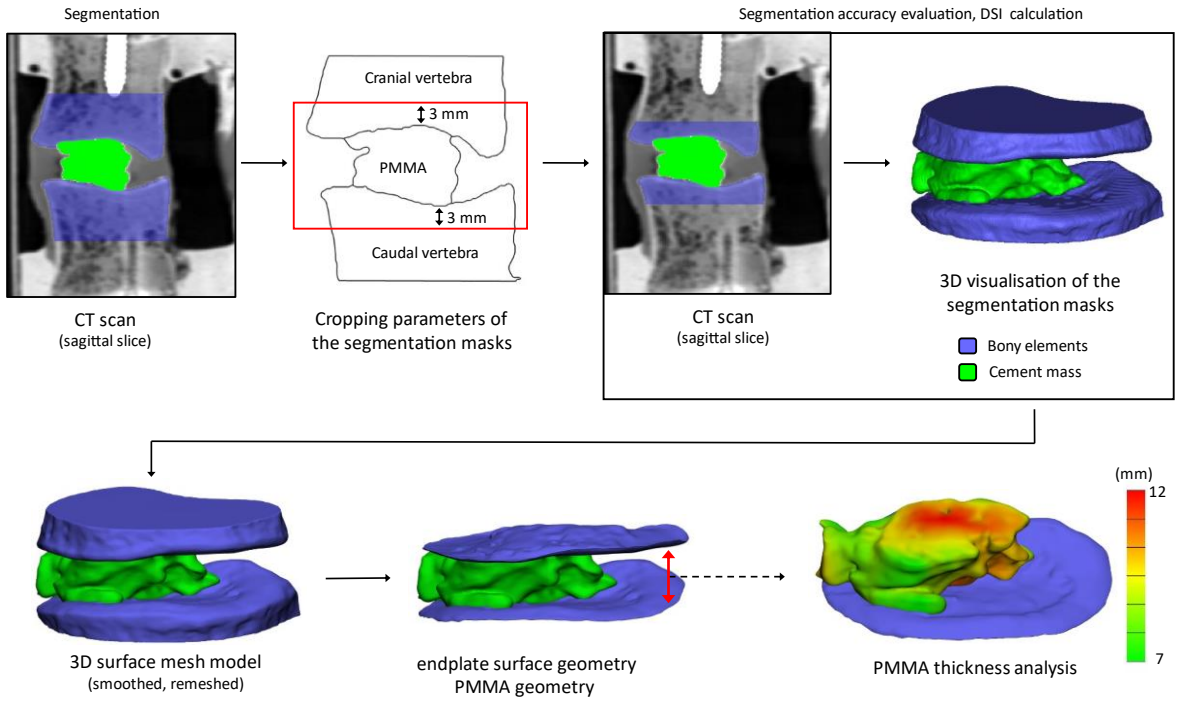


***Fig. 4.2 -*** *Workflow for the detection of the bony endplates and cement mass to visualize and assess the distribution of the cement in the intervertebral space, and to measure the cement thickness.*

### *4.3.7 Biomechanical testing*

The scope of our work was to test if discoplasty can provide relief by increasing the foramen space with respect to the degenerated conditions. *In vivo*, one of the most concerning loading scenarios for nerve compression within the foramen is related to a combination of an axial load and motions in a sagittal plane. For this reason, the specimens were mechanically tested in flexion and extension using a uniaxial testing machine (Mod. 8032, Instron, UK). For these motions, spinal specimens are usually tested under pure moments, even if it was a simplifier condition compared to the axial loading for modelling damaged or treated segments in extension [93]. Thus, one pot was rigidly fixed to the top of the testing machine. In order not to constrain the relative motion of the two vertebrae and avoid buckling, the caudal vertebra was loaded through a spherical joint moving along a low-friction rail (Fig. 4.3). This set-up allowed to reach the full load in a relatively fast loading, comparable to the speed one can expect in living subjects (file wp4_130109_1_17 from database OrthoLoad [94]).

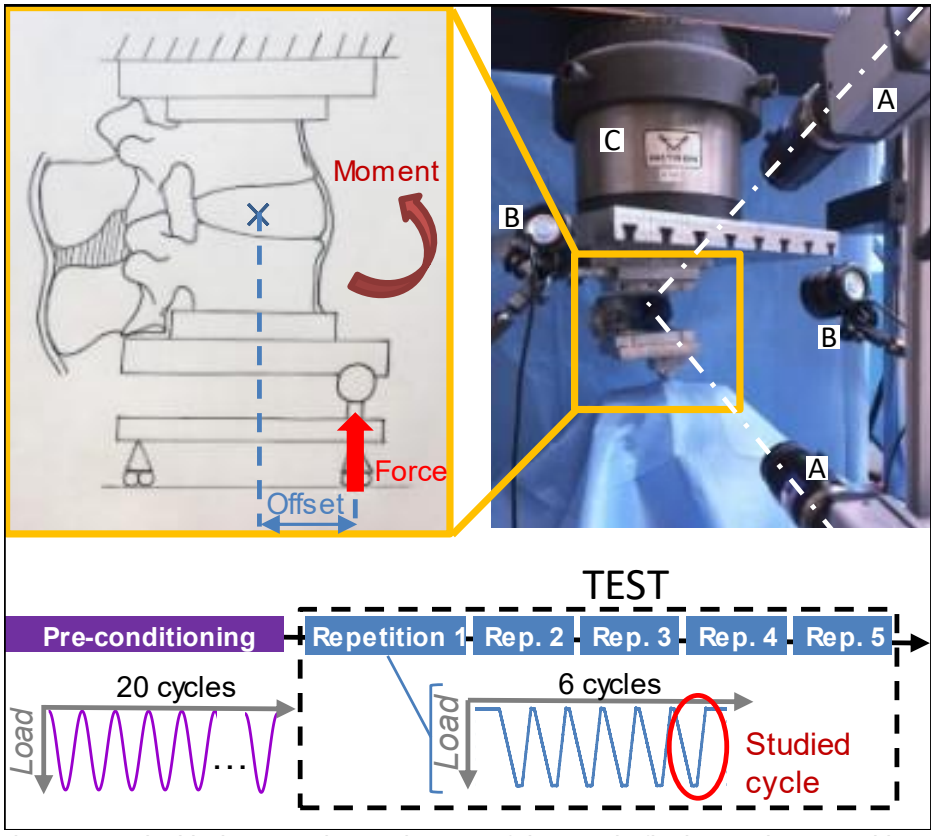


***Fig. 4.3 -*** *Testing protocol with the experimental setup of the test in flexion and composition of the test sequence. Two cameras (A) targeted the specimen, which was illuminated by high-intensity LEDs (B). The force applied by the testing machine (C) was delivered with an offset, resulting in a combination of a force and a moment*

A force of 50% of the Body Weight (BW), representing the upper body above the lumbar vertebrae, was applied with an anterior (posterior) offset, generating a combination of compression and flexion (extension) (Table 4.1). To have an anatomical definition of the offsets, the lever arms were measured with respect to the centre of the disc on CT images. As the segments are more flexible in flexion, the assigned offset was smaller (35% of the antero-posterior length of the disc) compared to extension (70%

of the length) to ensure a similar bending moment was applied in both directions. A reduced load, as close as possible to 50% BW, was applied to some specimens which exhibited a large mobility after nucleotomy, to prevent the endplates from coming in contact and possibly being damaged under the initially planned load (Table 4.2). Because the loading conditions integrated the body anatomy, the resulting moment would vary between specimens, with a standard deviation of 1.15 Nm in flexion and 2.31 Nm in extension.

***Table 4.2** – Donors' data and testing parameters for flexion and extension.*

| Specimen | Sex-Age | Spine segment | Offset (mm) | | Axial displacement variation (mm) | | Testing force (N) | |
|---|---|---|---|---|---|---|---|---|
| | | | Flexion | Extension | Flexion | Extension | Flexion | Extension |
| P01 | M-68 | T12-L1 | 12.3 | 24.5 | -0.59 | -1.35 | 402 | |
| | | L4-L5 | 14.6 | 29.3 | -0.49 | -0.35 | 402 | |
| P02 | M-79 | L2-L3 | 15.1 | 30.1 | - | -0.61 | - | 387 |
| P03 | M-53 | L2-L3 | 13.1 | 26.3 | -1.40 | -0.73 | 402 | |
| | | L4-L5 | 13.6 | 27.2 | -2.21 | -0.15 | 402 | |
| P04 | F-35 | T12-L1 | 10.4 | 20.8 | -0.37 | -0.21 | 309 | |
| | | L2-L3 | 10.7 | 21.5 | -3.20 | -0.43 | 309 | |
| | | L4-L5 | 11.0 | 22.1 | - | -0.34 | - | 309 |
| P05 | F-68 | T12-L1 | 9.1 | 18.2 | -2.06 | -0.84 | 396* | |
| P06 | M-59 | L2-L3 | 10.9 | 21.8 | 0.49 | -0.02 | 326* | |
| | | L4-L5 | 11.6 | 23.2 | 0.59 | -0.52 | 326* | 140* |
| P07 | F-78 | L1-L2 | 12.9 | 25.8 | -0.46 | -0.09 | 348 | |
| | | L3-L4 | 13.4 | 26.9 | 1.05 | -0.69 | 348 | |
| P08 | M-79 | L1-L2 | 12.8 | 25.7 | -2.02 | -1.34 | 456 | |
| | | L3-L4 | 14.8 | 29.5 | -1.22 | -0.68 | 456 | |
| P09 | F-86 | L1-L2 | 13.6 | 27.2 | -1.17 | -0.56 | 265* | |
| | | L3-L4 | 15.8 | 31.5 | -0.92 | -0.61 | 265* | |
| P10 | M-71 | L1-L2 | 11.9 | 23.7 | -1.98 | -0.38 | 343 | |
| | | L3-L4 | 13.3 | 26.5 | - | -0.40 | - | 343 |
| P11 | M-68 | L2-L3 | 12.6 | 25.3 | -0.44 | -0.11 | 319 | |
| | | L4-L5 | 13.2 | 26.3 | -1.51 | -0.01 | 319 | |
| P12 | F-80 | L3-L4 | 13.9 | 27.9 | -0.63 | -0.42 | 378 | |
| P13 | M-64 | L1-L2 | 12.8 | 25.6 | -1.62 | -0.09 | 417 | |
| | | L4-L5 | 14.9 | 29.8 | -4.31 | 0.09 | 417 | |
| P14 | M-73 | L3-L4 | 16.6 | 33.1 | -2.12 | -0.57 | 515 | |
| P15 | F-74 | L1-L2 | 12.3 | 24.6 | -1.65 | -1.01 | 412 | |
| | | L4-L5 | 15.4 | 30.7 | -1.16 | 0.24 | 412 | |

*Reduced load to avoid damages

The loading ramp lasted 1.0 second; the maximum loading was held for 0.3 seconds, then the specimen was unloaded. Each test consisted of six loading cycles, where the last one was analysed in detail (Fig. 4.3). Three cycles were sufficient for minimizing the effect of the viscous component in the response in another study [57], the subsequent cycles being nearly identical in term of loads and displacements. Each 6-cycle test was repeated five times to assess the repeatability. Before being tested, each specimen

was pre-conditioned applying the test load as a sinusoid at 0.5 Hz for 20 cycles. The specimens were tested in nucleotomy and cement discoplasty conditions for both directions of loading. The applied load and the actuator displacement were recorded by an independent datalogger (PXI, Labview, National Instruments, Austin Texas, US) at 500 Hz.

During each test, the 3-dimensional displacements and strain distribution of the specimen surface were tracked using a DIC system. This technique requires a high-contrast speckle pattern on both the vertebrae and the intervertebral disc (Fig. 4.1). First, the segment was stained with a methylene blue solution to create a dark background without impacting the properties of the tissues [95]. The white pattern was then sprayed with a water-based acrylic paint, following a procedure optimized elsewhere [95], [96]. Four white dots were manually added along the endplates to accurately identify the disc cranial and caudal borders from the images. To measure the displacements and the deformations over the specimen surface, a 3D-DIC system (Q400, Dantec Dynamics, Skovlunde, Denmark) was optimized [62] (Table 4.3) and used (Fig. 4.3). Image acquisition was performed in lateral view with the cameras pointing to the neuroforamen. Images were recorded at 15 Hz from the unloaded condition (reference frame, no load applied) to the end of the 6th cycle. In order to synchronize the DIC images with the testing machine data, the axial translation of the mobile vertebra, corresponding to the actuator motion, was derived from the images. The PXI load-displacement and axial translation curves were then temporally aligned by automatically identifying the peaks and valleys of the cycles.

***Table 4.3*** *– Material and parameters of the DIC system.*

| Material | Acquisition | Images post-processing |
|---|---|---|
| *2 cameras:* 5 Megapixels, 2440 x 2050 pixels, 8-bit. 26° between the cameras | *Software:* Instra 4D, v.4.3.1, Dantec Dynamics | *Facet size*: 35 pixels<br>*Grid spacing:* 11 pixels<br>*Filtering*: local 7x7 pixels kernel |
| *35 mm lenses:* Apo-Xenoplan 1.8/35, Schneider-Kreuznach, Bad-Kreuznach, Germany | *Calibration*: Al4-BMB-9x9, Dantec Dynamics | |
| *Lights:* cold-light LEDs | *Field of view:* 60mm x 100mm<br>Pixel size: 0.04 mm | |

### *4.3.8 Data analysis*

All measurements were compared for each specimen and each loading configuration (flexion, extension) between the two conditions: nucleotomy (NUCL), and PCD. Since PCD aims to assess the changes of the height of neuroforamen, the posterior disc height (PDH) was measured at the peak load as the cranial-caudal distance between endplates close to the neuroforamen.

Applying singular value decomposition (SVD) on rigid bodies, the motions (translations and rotations) of each vertebra were computed from DIC images with a Matlab (R2019b, MathWorks Inc., Natick,

MA, USA) script [39], [97]. The range of motion (ROM) was defined as the relative angle between the vertebrae in the sagittal plane between the peak load and unloaded conditions.

Load-displacement data were smoothed using a median filter (over 30 data points) and the last cycle of the test was isolated. Then, its loading part was fitted by a continuous curve-fitting method to characterize the specimen stiffness [98]. An exponential curve was applied to the toe region followed by a linear curve to the elastic region (Eq. 1).

$$F = \begin{cases} A\left(e^{B\delta} - 1\right) & \delta \leq p \\ E(\delta - p) + q & \delta > p \end{cases} \qquad (Eq.\,1)$$

Where:

*F* is the applied force

*d* is the measured displacement

*A*, *B*, *E*, *p*, *q* are specimen-specific parameters

The laxity (LZ) and elastic zones (EZ) were identified from load-displacement curves as respectively the region of large mobility and no loading, and the region where tissue stretched, characterizing the transition point in between (Fig. 4.4). Stiffness was characterized on the toe region by the parameters A, B and in particular their product A*B which describes the stiffness at the initial loading conditions. The elastic stiffness in the linear region starting at the transition point (p, q) is defined by the slope E of the curve.

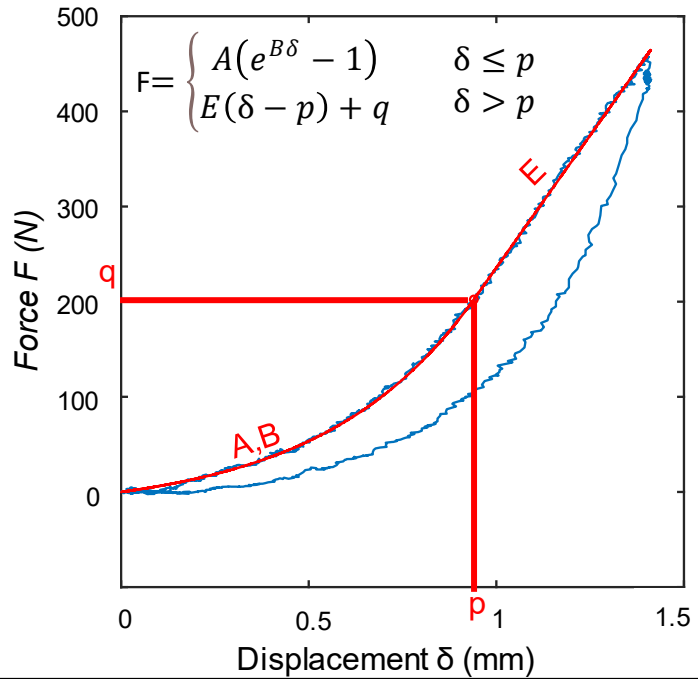


***Fig. 4.4 -*** *Typical load-displacement curve followed by the specimens in the majority of the tests (79/104): this was described with an exponential toe region, and linear elastic part which were fitted following Tanaka et al. model [98]*

The maximum and minimum true principal strains ($\varepsilon_1$, $\varepsilon_2$) over the vertebrae and IVD were measured at the peak load. Their median over the disc surface were computed, as well as their extreme values (defined as the 95%-percentile, to avoid local measurement artifacts).

All the computations were performed with dedicated Matlab scripts. To overcome the inter-specimen variability, the parameters measured after cement discoplasty were normalized to the nucleotomy condition of the respective specimen.

### *4.3.9 Statistical analysis*

Shapiro-Wilk tests were applied to all parameter distributions to assess their normality ($\alpha$=0.05). Depending on the normality assessment, comparisons between nucleotomy and discoplasty were made for ROM, stiffness, height, and the strain median with either a non-parametric Wilcoxon's test or a paired t-test. Influence of the spine level on the results was assessed with a one-way ANOVA. Finally, correlations between the cement distribution and the biomechanical parameters were evaluated with Spearman's rank correlation coefficient using SPSS Statistics 25.0 (IBM Corp., Armonk, NY, USA) with p=0.05. The interpretation of the correlation strength was based on Evans' classification [99] (less than 0.20 is very weak, 0.20 to 0.39 is weak, 0.40 to 0.59 is moderate, 0.60 to 0.79 is strong and 0.80 or greater is a very strong correlation).

## 4.4 Results

The different indicators were normalized between nucleotomy and simulated PCD for each specimen and each direction of loading. Main trends are reported here, the detailed parameter values are found in Table 4.4.

Three specimens were excluded in flexion: for one, the DIC-correlated area was too small; in another one, the posterior process broke but the specimen was unaffected in extension; a third specimen broke during the test.

### *4.4.1 Posterior disc height*

The PDH was measured from DIC correlations for flexion (n=24) and extension (n=27). The specimens exhibited a PDH increase of 41%±46% (mean±SD) in flexion (paired t-test, p<0.001) and 35%±38% in extension (p<0.001). In particular, the largest increase of PDH in both flexion and extension were respectively measured at the L3-L4 level whereas the smallest increase happened at T12-L1 (extension) and L2-L3 levels (flexion) (Fig. 4.5). However, spine level did not significantly impact PDH (ANOVA; p=0.69 in flexion, p=0.65 in extension).

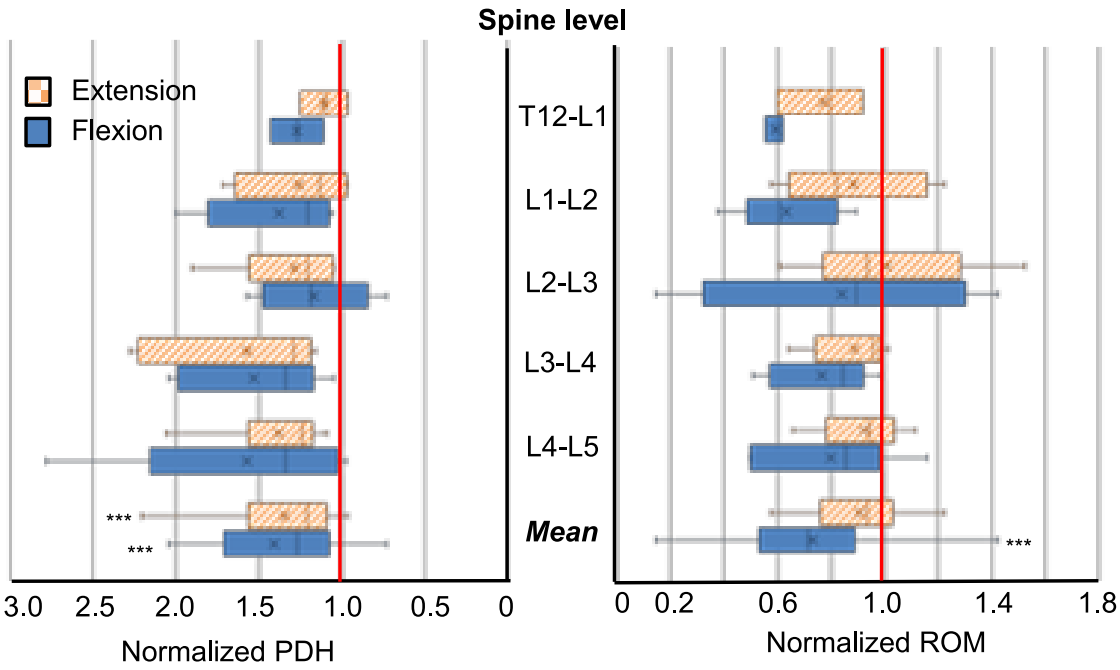


***Fig. 4.5 -*** *Changes (Mean ± SD) of the posterior disc height (PDH) and of the Range of Motion (ROM) caused by cement discoplasty at the different spine levels and as a mean of all levels. The PDH and ROM after discoplasty were normalized with respect to the value before discoplasty: a normalized value of 1.00 indicates no change; a value greater (smaller) than 1.00 indicates that the respective magnitude was increased (decreased) due to discoplasty. First quartile, median and third quartile are represented by lines. Mean is indicated by the cross and min and max values by the whiskers. Statistical significance (paired t-test, p<0.001) is designated by ****

### *4.4.2 Range of Motion*

The ROM was derived from DIC correlations in flexion (n=24) and extension (n=27). Discoplasty decreased the ROM by 27% ± 27% (mean±SD) in flexion (paired t-test, p<0.001) and decreased it by 9% ± 96% in extension (p=0.33). The different spine levels exhibited different trends in flexion with a mean ROM drop about 40% for segments between T12 and L2, whereas the low lumbar spine showed a smaller decrease about 20% (ANOVA, p=0.66) (Fig. 4.5). Conversely, similar ROM was measured in extension, independent of the spinal segment (p=0.56).

***Table 4.4*** *- Summary of the biomechanical parameters for each loading configuration (flexion and extension) and disc condition (nucleotomy (NUCL) and percutaneous cement discoplasty (PCD)). The variation trend between absolute values of NUCL and PCD is indicated with increasing ⇑ and decreasing ⇓ arrows. The mean (SD) between specimens is reported*

| | | Posterior disc height (mm)* | ROM (°) | Stiffness parameters | | | $\varepsilon_1$ (%) | | $\varepsilon_2$ (%) | |
|---|---|---|---|---|---|---|---|---|---|---|
| | | | | p (mm) | q (N) | E (N/mm) | Mean (SD) | 95-percentile | Mean (SD) | 95-percentile |
| **Flexion** | **NUCL** | 5.5 (1.4) | 4.8 (1.2) | 3.3 (1.3) | 283 (76) | 313 (126) | 1.9 (0.7) | 6.9 (2.5) | -1.3 (1.0) | -7.6 (3.6) |
| **(n=24)** | **PCD** | 7.3 (1.6) ⇑ | 3.5 (2.0) ⇓ | 2.0 (1.4) ⇓ | 259 (111) ⇓ | 400 (165) ⇑ | 1.4 (0.5) ⇓ | 5.8 (2.9) ⇓ | -0.7 (0.3) ⇓ | -5.4 (2.2) ⇓ |
| **Extension** | **NUCL** | 5.8 (1.9) | 2.3 (1.0) | 2.2 (0.8) | 327 (77) | 629 (165) | 1.1 (0.5) | 4.5 (1.6) | -0.9 (0.6) | -8.6 (4.8) |
| **(n=27)** | **PCD** | 7.5 (2.2) ⇑ | 2.2 (0.9) ⇓ | 1.6 (0.9) ⇓ | 269 (77) ⇓ | 577 (190) ⇓ | 0.9 (0.3) ⇓ | 3.1 (1.0) ⇓ | -0.6 (0.3) ⇓ | -5.1 (1.9) ⇓ |

* For both NUCL and PCD, the posterior disc height in extension is superior to flexion. Because n=24 specimens were averaged in flexion and n=27 in extension., both motions cannot be compared.

### *4.4.3 Stiffness*

The specimens showed different behaviours according to the loading configuration and disc condition (Fig. 4.6). After nucleotomy, in flexion load-displacement was described by an exponential curve for the LZ and a linear curve for the EZ in equivalent proportion. In extension, the loading phase showed a flat linear LZ associated with a sharper transition to the linear EZ. After PCD, different behaviours were observed in flexion. Some specimens exhibited an S-shaped load-displacement curve, others a very short LZ followed by a linear EZ. The rest displayed the usual exponential-linear shape already observed after nucleotomy. In extension, specimens followed an exponential-linear behaviour too.

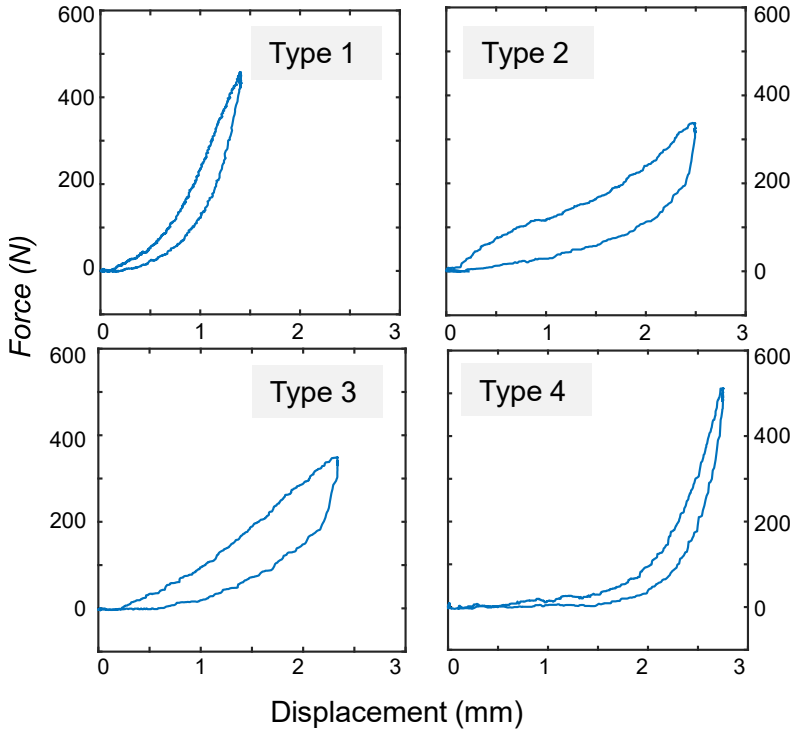


***Fig. 4.6 -*** *Typical load-displacement curves found for the 27 specimens depending on the testing conditions (disc condition, motion) resulting in 104 tests. Type 1: the majority of the tests (79/104) was described with an exponential toe region, and linear elastic part which were fitted following Tanaka et al. model [26]. Type 2: S-shaped was followed by 2/27 specimens in nucleotomy flexion and 7/27 in cement discoplasty flexion. Type 3: 1/27 specimens in nucleotomy extension, 1/27 in cement discoplasty extension, and 4/27 in discoplasty flexion followed a flat toe region and linear elastic region. Type 4: L-shaped was followed by 10/27 specimens in nucleotomy extension*

The elastic stiffness, transition load and displacement were estimated by fitting the load-displacement curves (Table 4.4, Fig. 4.7). In flexion, mean transition displacement was reduced by 38% from nucleotomy to cement discoplasty (paired t-test, $p<0.001$) while transition load was unaffected ($p=0.28$). In extension, both parameters respectively dropped by 28% and 16% (paired t-test, $p<0.001$). For both loading configurations, the LZ was larger after PCD. Finally, discoplasty increased the mean elastic stiffness at peak load by 37% (one sample t-test, $p<0.01$) in flexion but decreased it by 7% ($p=0.07$) in extension.

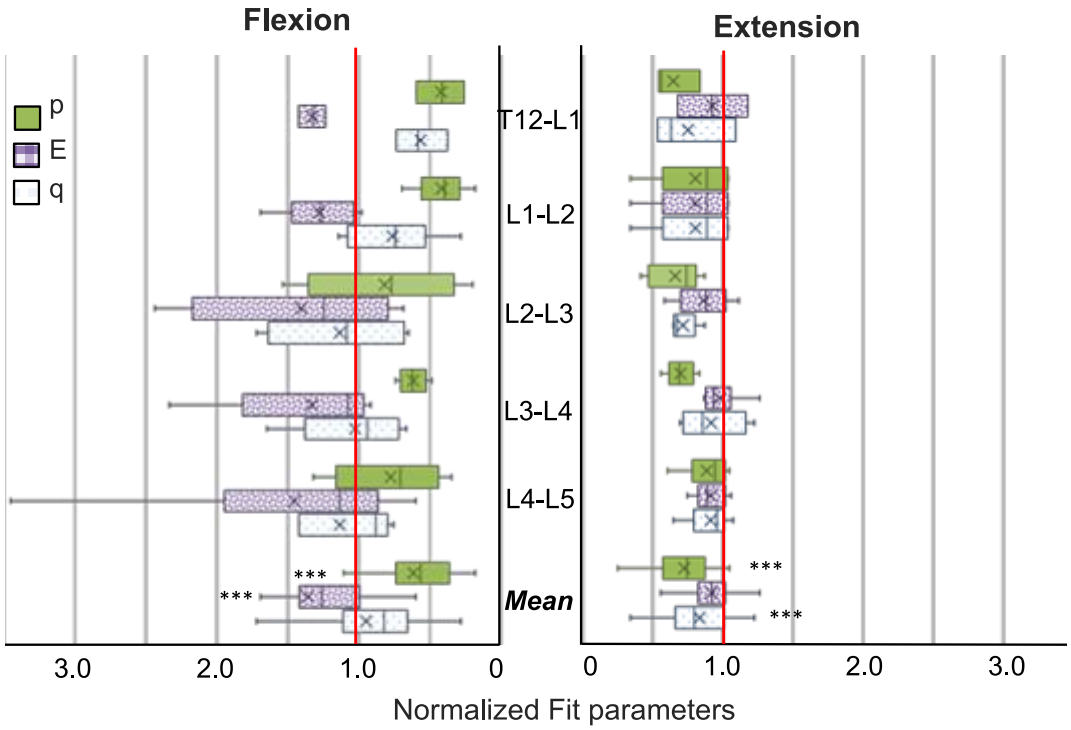


***Fig. 4.7 -*** *Stiffness parameters changes caused by cement discoplasty depending on the spine level. p: transition point displacement, E: elastic stiffness, q: transition point load. The values after discoplasty were normalized against the respective values after nucleotomy. A value above 1.00 means the parameter increased in discoplasty compared to the nucleotomy condition. A value smaller than 1.00 means discoplasty reduced that parameter. First quartile, median and third quartile are represented by lines. Mean is indicated by the cross and min and max values by the whiskers. Statistical significance (paired t-test, p<0.001) is designated by ****

When sorting the results by spine level, differences were more pronounced in flexion: the high lumbar spine showed a shorter LZ with very low variability between specimens. Similarly, the variability between specimens was smaller for high levels in flexion. Conversely, in extension, results showed similar trends for all the spine levels.

### *4.4.4 Strain*

The mean true strains were derived between specimens (Table 4.4). In flexion, the maximum strain after discoplasty was 12% (paired t-test, $p<0.05$) smaller than after nucleotomy and the minimum strain 40% higher (Wilcoxon test, $p<0.01$). In extension both strains were reduced by discoplasty by 12% (Wilcoxon test, $p<0.05$) and 14% (paired t-test, $p<0.01$). These changes of the median value after PCD were associated with a reduction of the extreme strain values, and a shrinkage of the highly strained regions. Discoplasty was associated with a migration of the maximum strains towards the endplates, while minimum strains were located at the disc mid-height (Fig. 4.8). In nucleotomy, in the compressive side of the disc the maximum (tensile) principal strains were directed circumferentially and the minimum (compressive) ones axially. After discoplasty, in the compressive part of the disc the minimum principal strains were directed axially and in the stretched part, the maximum strains were directed circumferential.

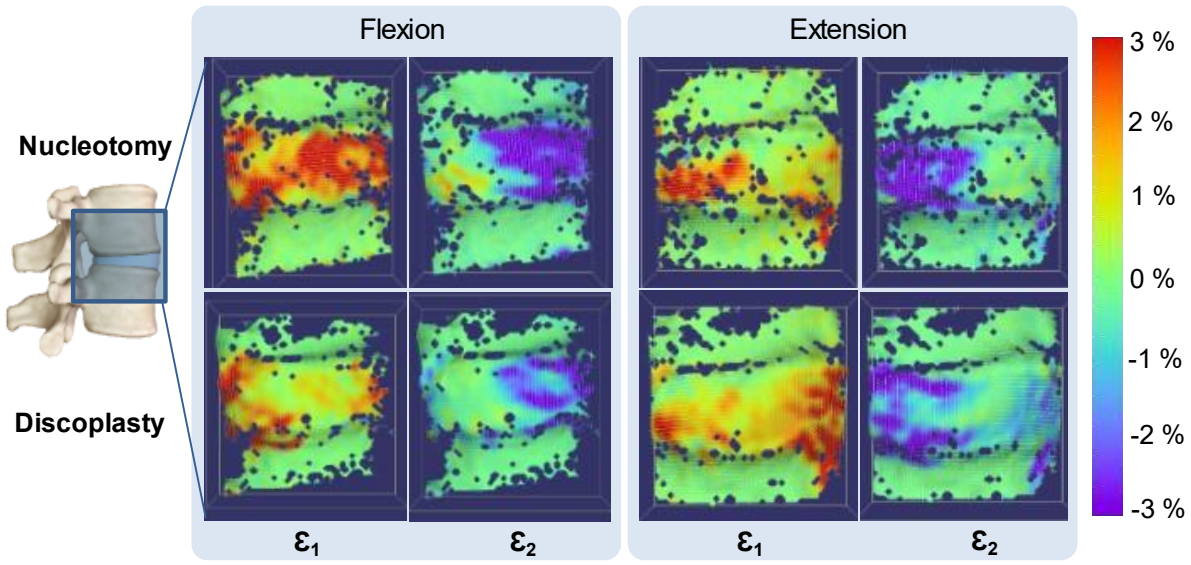


***Fig. 4.8 -*** *Typical distribution of Maximum ($\varepsilon_1$) and Minimum ($\varepsilon_2$) True Principal strains on the specimen surface in flexion and extension. The dark blue spots on the specimen surface correspond to the areas where the DIC algorithm could not correlate, in particular along the endplates. Only the disc underwent large strains*

We also analysed the number of specimens in which strains exceeded 5%, 10% and 15%. The number of specimens showing high strain values was smaller after PCD (Fig. 4.9). After discoplasty, the strains did not exceed 10% except in flexion where the number of specimens exhibiting maximum strains exceeding 10% increased. Finally, the most extreme maximum and minimum strains values measured among all specimens were respectively 13.6% and -22.9% regardless the disc condition.

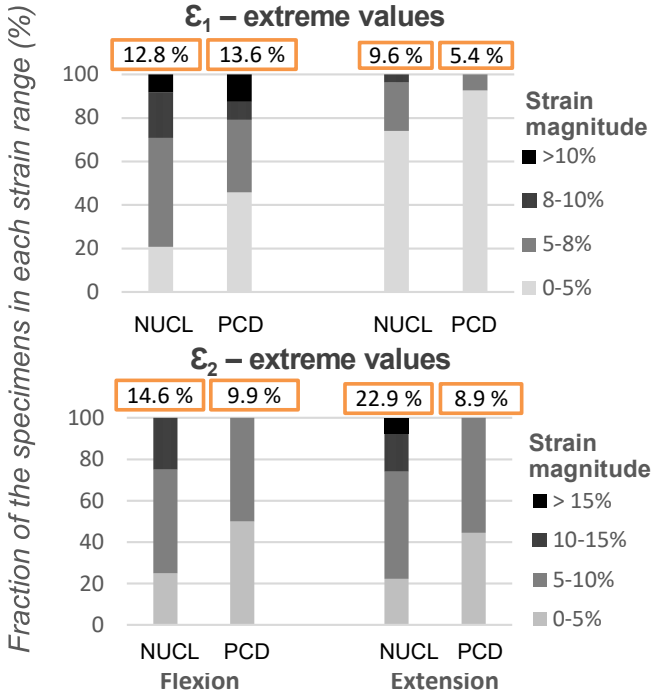


***Fig. 4.9 -*** *Analysis of the absolute extreme values of the maximum ($\varepsilon_1$) and minimum ($\varepsilon_2$) principal strains among the 27 specimens. For each disc condition (NUCL/PCD), the fraction of specimen falling in each strain range is presented, with the largest absolute strain value measured among the discs being displayed for each condition*

### *4.4.5 Visualization of the cement geometry and thickness measurement*

*[This section includes the DSI values computed from the segmentations I performed for Eltes et al. study. Thickness measurements of the in vivo study were not directly performed by me, however, since I participated to their computation process and they are relevant for the comparison with the in vitro study, I include below the results computed by my co-authors.]*

The inter-operator DSI for the cement and the vertebrae were 0.98±0.02 and 0.97±0.01 (mean±SD) respectively, indicating a high repeatability. For consistency, the cement distribution over the caudal vertebral endplate in the intervertebral space was visually assessed in the same view for all specimens (Fig. 4.12 and 4.13 in Appendix 4.7). In most cases, the cement distributions mimicked the nucleus shape, with a mean volume of 4.56±1.78 ml (mean±SD). Surfaces of both endplates and the injected cement were also measured (Table 4.5). Seven specimens exhibited leakage of cement into at least one vertebral body in different proportions (Fig. 4.10). The cranial-caudal thickness of the cement was 9.62±1.30 mm (mean±SD among specimens, Table 4.5) with larger values for specimens with perforation of the endplate (Fig. 4.13).

The inter-operator DSI values computed for the segmentation of the *in vivo* bone cement mass were high for all segmented geometries (mean: 0.93 ± 0.035, n = 16) demonstrating the precision of the segmentation method. The *in vivo* cement distribution was found to be heterogeneous with volumes varying between 3763 $mm^3$ and 13108 $mm^3$ (Fig. 4.11).

***Table 4.5** – Summary of the cement distribution analysis for each specimen. The cement thickness between the endplates was measured axially.*

| | | Cement geometry | | Cement thickness | | | | Caudal endplate | Cranial endplate |
|---|---|---|---|---|---|---|---|---|---|
| Specimen ID | Level | Surface ($cm^2$) | Volume ($cm^3$) | Min (mm) | Max (mm) | Mean (mm) | SD (mm) | Total surface ($cm^2$) | Total surface ($cm^2$) |
| P01 | T12-L1 | 18.94 | 4.18 | 4.6 | 9.3 | 7.4 | 0.9 | 15.25 | 14.98 |
| | L4-L5 | 21.77 | 4.12 | 5.6 | 13.5 | 9.5 | 1.8 | 13.99 | 13.98 |
| P02 | L2-L3 | 35.12 | 7.89 | 6.5 | 14.0 | 10.1 | 1.6 | 22.56 | 21.86 |
| P03 | L2-L3 | 23.72 | 5.05 | 6.2 | 14.3 | 9.3 | 1.4 | 17.82 | 18.44 |
| | L4-L5 | 21.67 | 5.27 | 6.8 | 15.0 | 10.5 | 1.5 | 19.90 | 18.13 |
| P04 | T12-L1 | 11.81 | 2.14 | 6.0 | 10.1 | 8.4 | 0.8 | 12.45 | 12.08 |
| | L2-L3 | 16.61 | 3.40 | 7.4 | 12.3 | 9.6 | 1.0 | 13.97 | 13.79 |
| | L4-L5 | 13.49 | 2.02 | 6.5 | 12.6 | 10.5 | 1.4 | 13.35 | 14.00 |
| P05 | T12-L1 | 12.93 | 2.34 | 3.4 | 11.1 | 6.6 | 1.3 | 8.48 | 9.44 |
| P06 | L2-L3 | 11.49 | 2.49 | 5.8 | 16.9 | 8.9 | 1.7 | 10.89 | 11.02 |
| | L4-L5 | 15.35 | 3.18 | 4.3 | 13.8 | 8.0 | 1.6 | 12.14 | 12.67 |
| P07 | L1-L2 | 21.84 | 2.86 | 7.5 | 19.8 | 10.8 | 2.4 | 21.66 | 16.58 |
| | L3-L4 | 20.03 | 5.07 | 7.1 | 16.0 | 10.6 | 1.3 | 16.34 | 15.56 |
| P08 | L1-L2 | 26.84 | 7.04 | 3.8 | 16.8 | 9.0 | 2.3 | 17.86 | 18.55 |
| | L3-L4 | 22.38 | 3.88 | 5.3 | 12.2 | 9.8 | 1.6 | 20.25 | 19.94 |
| P09 | L1-L2 | 26.12 | 6.02 | 4.6 | 13.8 | 9.3 | 1.5 | 18.81 | 18.36 |
| | L3-L4 | 38.70 | 8.89 | 5.2 | 17.2 | 9.9 | 1.7 | 19.72 | 21.35 |
| P10 | L1-L2 | 24.28 | 5.51 | 4.8 | 15.7 | 9.9 | 1.8 | 15.26 | 14.77 |
| | L3-L4 | 24.74 | 5.44 | 6.6 | 18.3 | 11.6 | 2.0 | 16.01 | 15.98 |
| P11 | L2-L3 | 16.07 | 3.36 | 6.4 | 11.6 | 9.7 | 1.3 | 15.37 | 15.20 |
| | L4-L5 | 17.03 | 3.31 | 7.1 | 13.1 | 10.4 | 1.3 | 14.32 | 14.92 |
| P12 | L3-L4 | 20.14 | 3.52 | 2.4 | 11.9 | 8.5 | 2.2 | 18.12 | 17.99 |
| P13 | L1-L2 | 22.95 | 5.69 | 7.3 | 15.9 | 10.9 | 1.5 | 15.53 | 14.89 |
| | L4-L5 | 27.29 | 5.15 | 9.3 | 16.6 | 13.2 | 1.3 | 16.00 | 16.05 |
| P14 | L3-L4 | 30.31 | 7.15 | 4.3 | 14.3 | 9.3 | 1.8 | 21.52 | 20.83 |
| P15 | L1-L2 | 16.51 | 3.57 | 5.7 | 13.9 | 9.5 | 1.3 | 14.25 | 14.67 |
| | L4-L5 | 19.40 | 4.42 | 3.7 | 14.8 | 8.8 | 2.2 | 18.25 | 18.67 |
| | **Mean (SD)** | **21.39 (6.65)** | **4.56 (1.78)** | | | **9.6 (1.3)** | | **16.30 (3.44)** | **16.10 (3.10)** |

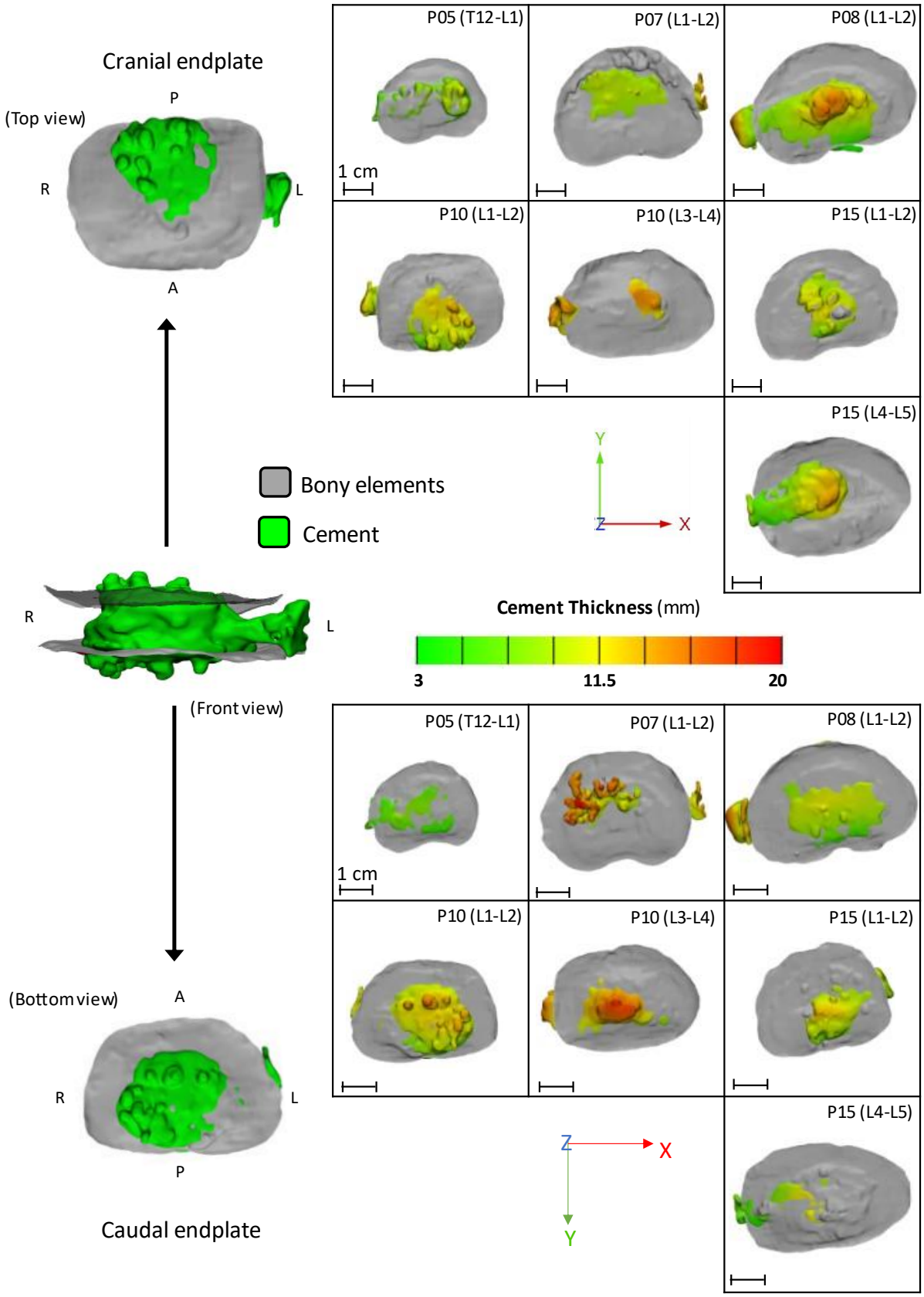


***Fig. 4.10 -*** *Visualization of the cement leakage geometry through the cranial (up) and caudal (down) endplate and thickness measurement. In the presented specimens, endplate perforation was observed. Thickness is represented by a colourmap scale ranging from green to red. The xyz coordinate system defines the view*

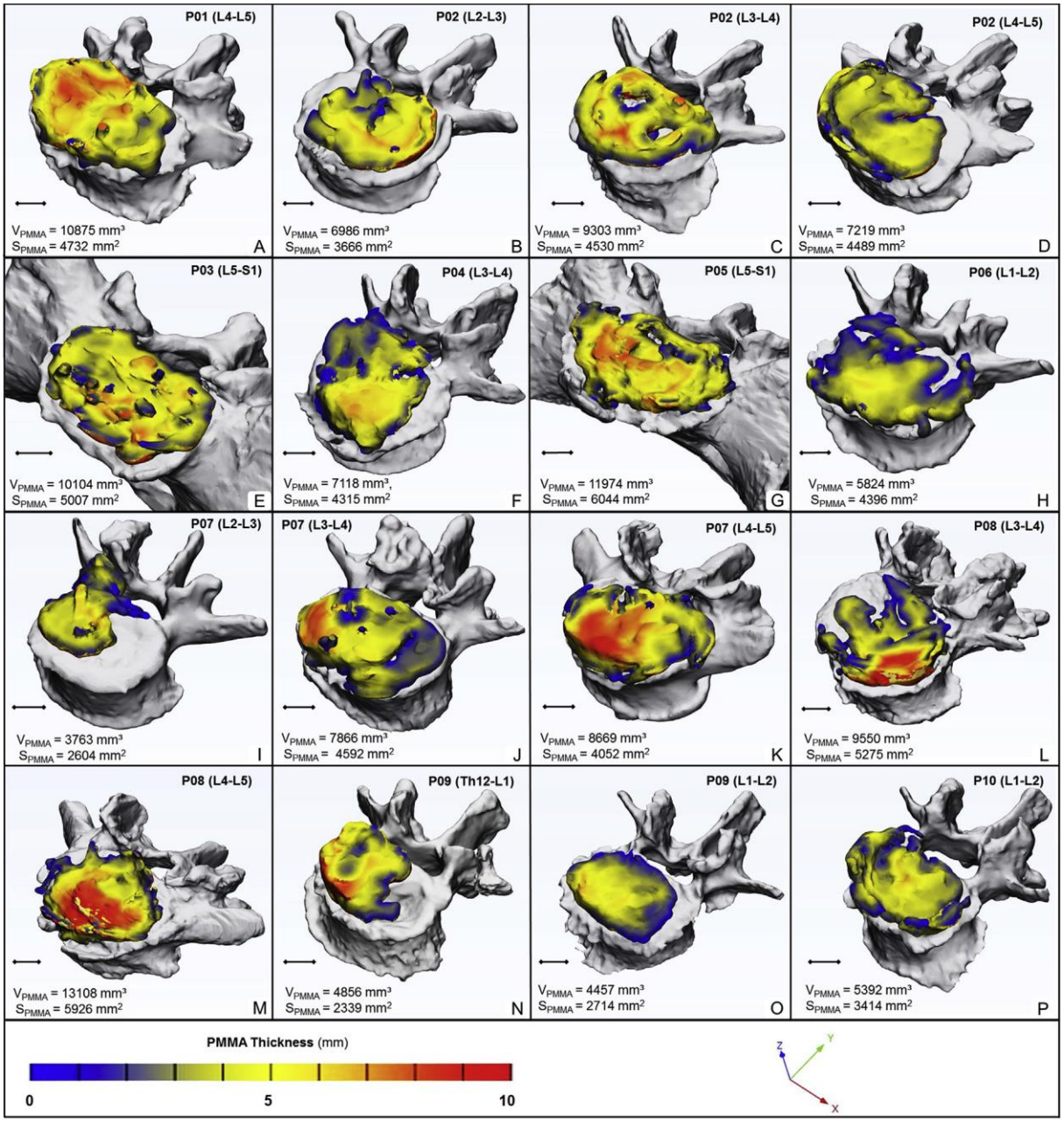


***Fig. 4.11 –*** *Visualization and thickness measurement of the in vivo cement geometry injected during PCD. (A-P) the cement geometry distribution over the caudal vertebral endplate of the investigated motion segment (the xyz coordinate system defines the view). The mean volume is 7941.59 ±2749.82 mm³, and surface is 4256.02 ±1094.20 mm². Thickness is represented by the colorbar (Blue/Green/Red), scale 0–10 mm (A–P). [Image extracted from [38] under the Creative Commons license CC BY 4.0.]*

### *4.4.6 Correlation between cement geometry and biomechanical parameters*

Relationships between cement distribution and biomechanical parameters were investigated for each direction of loading (Fig. 4.11). The mean cement thickness positively and moderately correlated with PDH after discoplasty in both extension and flexion (Spearman's coefficient $\rho$=0.410, p=0.034, C and $\rho$ =0.407, p=0.048, B). It also moderately affected the normalized ROM in extension ($\rho$ =0.432, p=0.037, A). Similarly, the maximum cement thickness strongly affected PDH in flexion ($\rho$ =0.663, p<0.001, E) and showed a moderate positive correlation with the absolute ROM in extension ($\rho$ =0.413, p=0.032, D). Relations with other parameters were not significant.

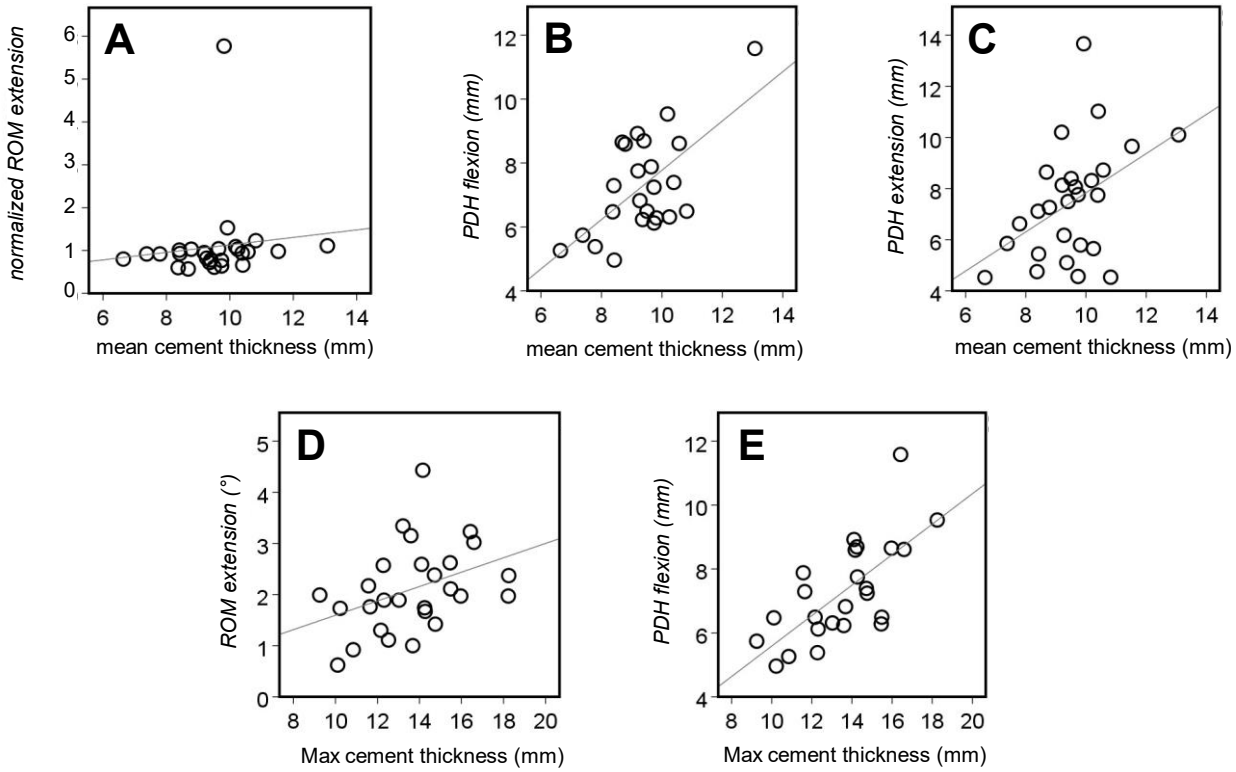


***Fig. 4.11 -*** *Statistically significant associations between the cement thickness and the biomechanical parameters of the tested specimens*

## 4.5 Discussion

This study assessed the biomechanical consequences of PCD on the spine kinematics and on the strain distribution. To investigate the effects of PCD on the intervertebral range of motion and stiffness, and on the strain distribution, 27 FSUs were prepared with a simulated disc lesion, and then treated with cement discoplasty. Simulated discoplasty was found to significantly increase the intervertebral height in the posterior region both when flexion and extension were applied.

Discoplasty also impacted the segment kinematics, significantly reducing the flexibility in flexion. This was associated with a shortening of the laxity zone and an increase of the elastic stiffness. The difference

of load-displacement behaviours after nucleotomy and after discoplasty were caused by the combination of the action of the elements of the intervertebral joint. In flexion, facet capsules and posterior ligaments were shown to transmit the load [100]. Different from nucleotomy condition, where the vertebrae are free to rotate until the posterior elements stretch (exponential+linear behaviour), the presence of cement already spaced the facets and pre-stretched the posterior ligaments. This resulted in an immediate loading of the facet capsules followed by the posterior ligaments explaining the two load increases of the S-shape.

Conversely, the cement mass did not affect the mobility in extension. It only impacted the beginning of the segment motion, shortening the laxity zone: during extension, the motion of the vertebrae, "rolling" on the cement, was only constrained by the contact of the posterior elements independently to the presence of cement. Discoplasty also modified the load-displacement behaviour. Following nucleotomy, the intervertebral joint only transmitted the load after the facets contact, resulting on a suddenly stiffening behaviour (L-shape). Discoplasty smoothed this behaviour, probably restoring part of the role of the joint elements. A study suggested that the anterior longitudinal ligament had a limited effect on load-resistance in extension attributing it to the bulk compression in the posterior of disc [100].

Discoplasty also reduced the disc tissue deformation: in average, both the maximum and the minimum strain were lower than after nucleotomy. After nucleotomy a large bulging was induced in the disc under load in particular on the compressed side of the disc, leading to both high tensile and compressive strains in the same location at mid-height. Conversely, once the disc height was restored by PCD, the anatomical elements retrieved their functions in the spine motion, with tensile strains located on the anterior longitudinal ligament in extension and in the posterior disc in flexion. The distribution of compressive strains became more defined after PCD, with concentrations along the endplates. The largest values of strain found on the surface were reduced after discoplasty. Comparing the corresponding stretches, discoplasty induced values within the same range as estimated strains *in vivo* [101]. Thus, discoplasty did not seem to present a risk of damage for AF outer tissues.

The injected cement was largely distributed in the disc space. In some cases, the injection process resulted in perforation of the endplates, due to degenerative lesions or deterioration caused by the nucleotomy. Cement perforation of the endplates is a clinically known phenomenon which does not represent a contraindication to PCD (only leakages into the spinal canal are clinically relevant [20], [33], [36]). Cement geometry directly impacted PDH and ROM. The thicker the cement, the higher PDH for both directions of loading. The thickness also induced a significant positive moderate correlation with the ROM in extension as a consequence of a larger PDH. Indeed, extension motion is restricted by the contact of the facets. A high PDH spaced the cranial and caudal facets giving a wider range of mobility in extension.

As presented in clinical studies, PCD aims to recovering the healthy disc height and neuroforamen section by creating a cement spacer between the vertebral bodies. This study supported clinical observations [20], [21], [33], presenting a significant increase of PDH under bending, which is a more critical loading scenario with a reduced foramen than in *in vivo* measurements made in supine/prone position.

Percutaneous cement discoplasty application to lumbar spine is a recent surgical technique. The only paper about *in vitro* biomechanical testing which can be found in literature was performed on porcine lumbar discs [39]. Different from the present human study, that preliminary porcine study did not report any significant change of ROM nor stiffness after PCD, but reported similar changes in the strain distribution concluding that discoplasty procedure tends to restore the deformation state of a healthy disc. The difference between the present findings and the previous study probably relates to the difference between human and porcine in terms of NP and AF, and anatomy of the facets. The ROMs measured at peak load were in the same range as others *in vitro* studies on human spines [102]–[109]. Other studies on the effect of nucleotomy demonstrated that the absence of NP reduced segmental rotational stability, significantly increasing the ROM [30, 38–40]. Only Eysel *et al*. found a drop of ROM for both motions [110]. Heuer *et al.* presented the strain map of intact IVDs, exhibiting similar distributions with the strain measured in this present study after PCD [103].

In parallel, clinical studies investigated the surgical procedure. The *in vivo* cement masses presented by Eltes *et al.* [38] almost filled the disc volume. In our case, donors were relatively old, but still had a very strong annular structure. Removing it to only have the outer layer like in advanced degeneration with vacuum was very difficult considering that the nucleus was removed by a spine surgeon using standard surgical tools. Then, the cement volumes injected in our study entirely fit the nucleus space with values close to the range of 3-5 ml clinically reported [20]. Finally, one should highlight the lack of bone cement extrusion through the AF defect at the end of testing. Indeed, extrusion of the filling material is a major concern in the research of NP regeneration techniques, particularly when the AF is damaged to allow the material insertion [51]. Therefore, PCD does not require AF repair.

One limitation relates to the simplified loading conditions applied. FSUs *in vitro* are usually subject to pure bending moments [63] sometimes coupled with a compressive preload [79], [105], [109]. The setup used in this study applied an eccentric compressive load which induced the bending, as in other spine studies [78], [111], [112]. Although the pivot point does not remain stationary during the motion, the lever arm variation during the tests was evaluated by DIC in term of relative translation of the vertebra. This resulted in a change of the bending moment between nucleotomy and discoplasty conditions of 3.2% ±2.8% (mean ±SD) in flexion and 1.1% ±1.0% in extension, making the loading conditions comparable.

Due to the diverse degeneration states of the donors' intervertebral discs and the limited number of available specimens, nucleotomy was required to establish a common condition allowing possible repetition of the study. For that, fenestration in the AF was needed, which can be suspected to compromise the biomechanics of the FSU. The impact of fenestration on the segment stability was assessed in a dedicated experiment (Appendix 1). The PDH, ROM, stiffness and strain distribution were checked. Fenestration of the AF did not significantly perturb the disc behaviour in comparison to the nucleus extraction/removal. Nucleotomy only significantly reduced the disc height. Lateral bending was not investigated because the position of the defect would have prevented the test of both bending directions.

## 4.6 Conclusion

This study was the first to investigate the impact of cement discoplasty on the biomechanics and kinematics using *in vitro* human lumbar spines. Because *in vitro* testing can only replicate some aspects of the *in vivo* conditions, the clinical integration of the result absolute values is limited. However, general conclusions can be drawn from the study and integrated into clinics.

- The cement filled the empty discs and *in vitro* distributions had similar volume and thickness as clinically observed.
- The posterior disc height was increased after discoplasty with respect to the nucleotomy condition: the cement mass acted like a spacer, supporting clinical observations.
- Stability of the segment was greater in flexion after discoplasty: the range of motion was significantly reduced, and the elastic stiffness increased.
- No indication of risks of mechanical damage on the outer disc was observed after discoplasty: the distribution of strain on the disc showed a clear decrease of large disc deformations.
- The cement geometry, in particular cement thickness, directly influenced the posterior disc height, and impacted the range of motion in extension only.

## 4.7 Appendix: Cement geometry visualization and thickness measurement

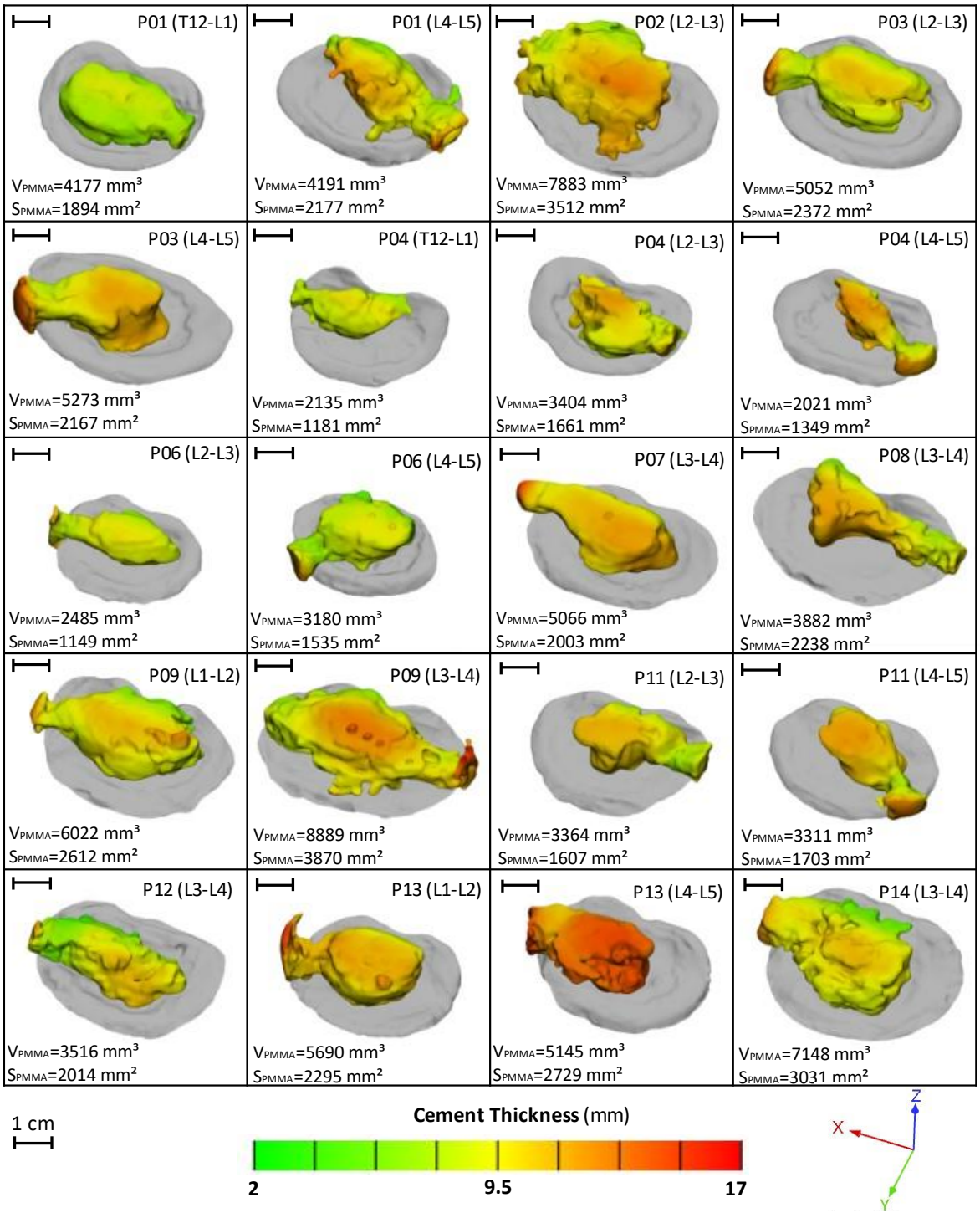


***Fig. 4.12 -*** *Visualization of the cement distribution over the caudal endplate geometry and thickness measurement. In the presented specimens no endplate perforation was observed. The mean±SD volume is 4591±1863 mm³, and surface is 2155±726 mm². Thickness is represented by a 2-17 mm colourmap scale ranging from green to red. The xyz coordinate system defines the view*

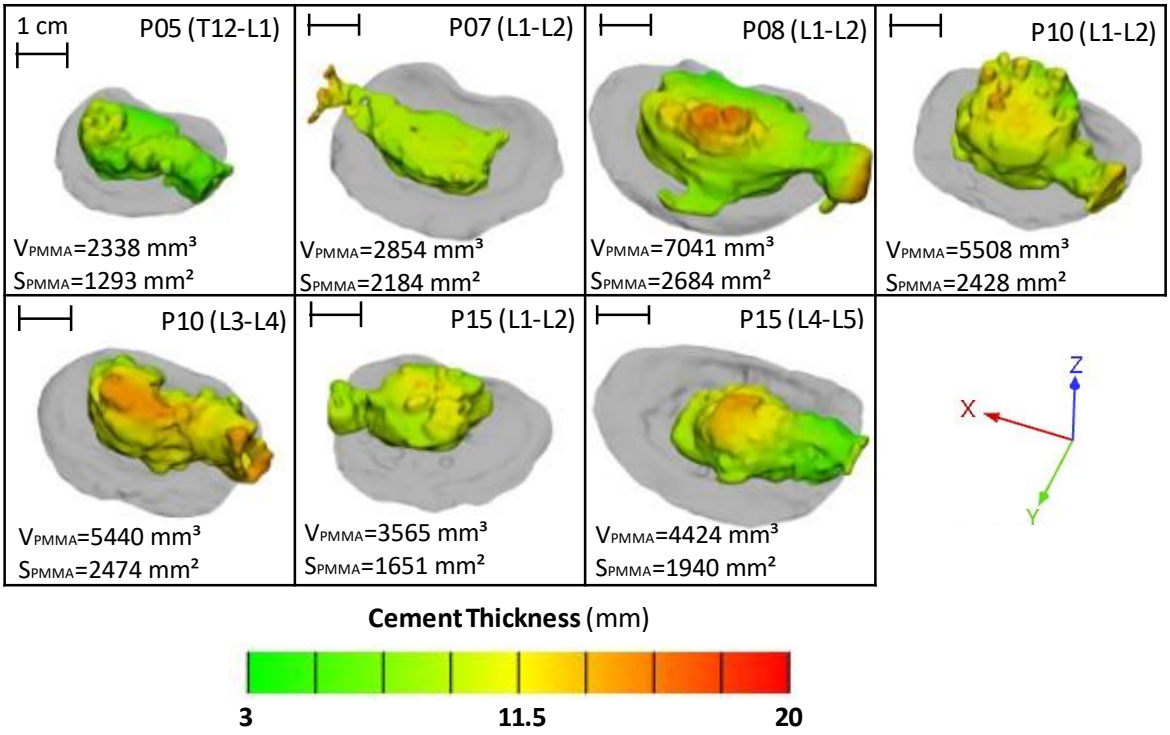


***Fig. 4.13 -*** *Visualization of the cement distribution over the caudal endplate geometry and thickness measurement. In the presented specimens, endplate perforation was observed. The mean±SD volume was 4453±1664 mm³, and surface was 2093±496 mm2. Thickness is represented by a colourmap scale ranging from green to red. The xyz coordinate system defines the view*

*Chapter 5*

# Assessment of foraminal decompression following discoplasty using a combination of *ex vivo* testing and numerical tools

from the manuscript:

**Assessment of foraminal decompression following discoplasty using a combination of *ex vivo* testing and numerical tools**

C. Techens, F. Bereczki, S. Montanari, A. Lazary, P. E. Eltes, L. Cristofolini

Pre-print of a paper being submitted in Nature SR

## 5.1 Abstract

Percutaneous Cement Discoplasty (PCD) is a minimally invasive surgical technique to treat degenerated intervertebral discs. When the disc is severely degenerated, the vacuum observed in place of the nucleus pulposus can be filled with bone cement to restore the disc height, open the foramen space, and relieve pain. This study aimed to evaluate the foramen geometry change due to PCD, in the loaded spine.

Cadaveric spines (n=25) were tested in flexion and extension while Digital Image Correlation measured displacements and deformations. Tests were performed on simulated pre-operative condition (nucleotomy) and after PCD. Registering DIC images and the 3D specimen geometry from CT scans, a 3D model of the specimens aligned in the experimental pose was obtained for nucleotomy and PCD. Foramen space volume was geometrically measured for both conditions. The volume of cement injected was measured to explore correlation with the change of foramen space.

PCD induced a significant overall foraminal decompression in both flexion (foramen space increased by 835±1289mm$^3$, p=0.001) and extension (1205±1106mm$^3$, p<0.001), confirming that the expected improvements of PCD show also during spine motion.

The foraminal space increase observed *in vivo* after PCD was still presented during spine flexion and extension, sign that the primary goal of PCD benefited also during spine motion. Furthermore, in extension when the foramen is the most challenged, the impact of PCD on the foramen was proportional to the injected cement volume.

## 5.2 Introduction

Advanced degeneration of the intervertebral disc deeply affects the biomechanics and structure of the spine. The loss of disc height associated to the degeneration leads to the reduction of the neural foramen and a compression of the nerves inducing low back pain in the patients. Percutaneous Cement Discoplasty is a minimally invasive surgical technique developed as an alternative for patients not suitable to lumbar interbody fusion surgery due to advanced age or comorbidities [20]. In particular, PCD is recommended for intervertebral discs (IVDs) exhibiting a vacuum phenomenon (VP) as the result of degeneration. During surgery, the degenerated disc is filled with injected acrylic bone cement to create a spacer between the vertebrae and indirectly decompress the nerve by restoring the disc height and the neuroforaminal space by indirect decompression [20].

The application of PCD in the lumbar spine has been mostly studied clinically. First, the effects of PCD have been assessed in term of disc height restoration on CT scans, pain relief and quality of life improvement [21]. Then, the biomechanical behaviour of the treated spine as well as its alignment under loading has been studied using *ex vivo* model to gain a better the understanding of the consequences of discoplasty in flexion and extension (see Chapter 4). Additionally, an *in silico* approach was developed by Eltes *et al.* for the quantitative investigation of the indirect changes induced by PCD inside the spinal canal and the neuroforamen in patients [38]. This patient-specific method used clinical CT scan-based images of the patient in supine position.

In spine research, *in vivo* assessments are always constrained by the need of using only non-invasive and safe acquisition tools. These tools also often fail to control the imposed conditions, and cannot measure some physical quantities (e.g. force, stress, relative motions) in the internal spine structure. Indeed, medical imaging often require the patient to be static whereas tracking the spine motion is performed externally (e.g. with stereophotogrammetry) and does not allow direct insight of the internal tissue.

This study aimed to assess the changes of foramen characteristics following PCD in the most concerning motions. It was hypothesized that (i) PCD would significantly affect the foramen space in flexion and in extension, and (ii) that the volume of cement injected would correlate with the foramen change. For that, we developed a method/workflow the *ex vivo* data of the spine segments in loaded configurations and the *in silico* tools to investigate the foramen geometry to bridge clinical and experimental approaches and widen the investigation of PCD. In particular, we aimed to measure the impact of discoplasty on the shape and size of the foramen in complex motions.

## 5.3 Methods

This study is a combination of *ex vivo* investigation of spine biomechanics [39], [113] and *in silico* image analysis similar to a clinical approach [38]. Thus, the *ex vivo* data serving here were recorded in another study (see Chapter 4).

### *5.3.1 Acquisition of ex vivo data*

Lumbar functional spinal units (n=25) were transected from 15 donors whose death was unrelated to spine condition. The specimens were cleaned without damaging ligaments and facet joints.

Because vacuum is rarely observed in the intervertebral disc, and so is among the spines available, degeneration of intervertebral discs was modelled by manually removing the nucleus pulposus and the inner layer of annulus through a square opening performed on the lateral side of the discs. Cement discoplasty was performed by injecting acrylic cement through the opening (Fig. 5.1). These experimental models have been developed in a previous study on porcine specimens [39].

Specimens were tested in both nucleotomy and simulated discoplasty conditions to assess the impact of the injected cement on the kinetics. Specimens were mechanically tested in flexion and extension applying an axial load (50% body weight) with an offset (Fig. 5.1, Table 5.7.1). During the test, DIC system monitored the lateral side of the specimens and measured the displacements of the surface. During testing, three specimens were damaged, in a way which could only affect flexion results. These tests were excluded from the results as a precaution, thus leaving n=94 tests available (see section 4.4).

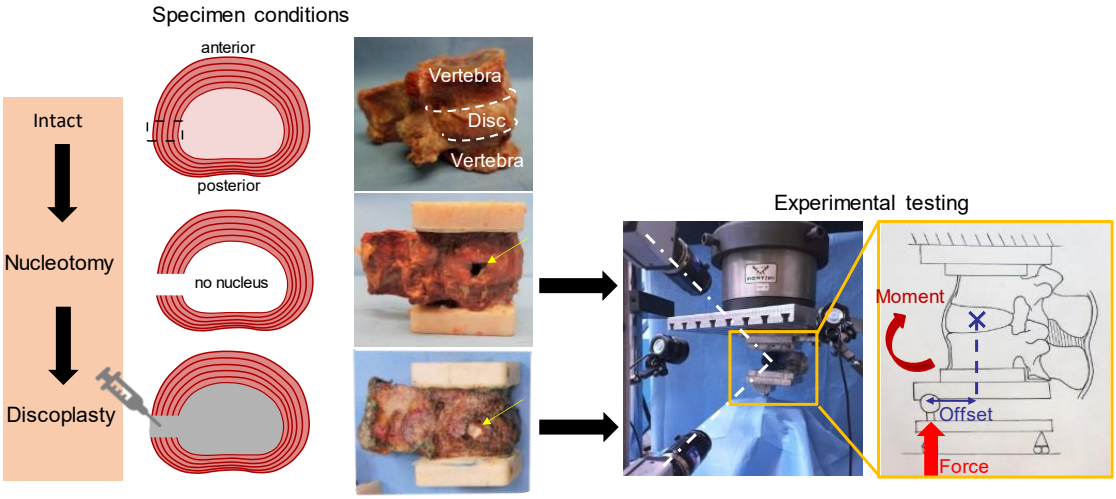


***Fig. 5.1*** *- Preparation and test of one specimen in flexion. The discs were tested in nucleotomy and discoplasty. The eccentric load was applied to create the bending moment (in flexion here) while DIC system recorded the specimen position (white dot lines)*

### *5.3.2 Post processing of the DIC data*

The DIC measurements (n=94) provided the coordinates of the specimens' surface points corresponding to the correlated area on the surface of the two vertebrae and intervertebral disc. The frame at peak load was selected for each test. The 3D correlated area converted into a point cloud using an iterative-closest-point algorithm ("icpregister", Matlab, version, MathWorks, city, state) and imported into MeshLab1.3.2 [132] (http://www.meshlab.net). In order to reconstruct the surface, the normals of the mesh vertices were estimated ("compute normal for point sets") considering a neighbourhood of 100 points. Then, the specimen surface was reconstructed from the point cloud with normals using the Ball Pivoting Algorithm (BPA) [114]. This algorithm was iteratively applied with ball radius of 0.8 mm, 1.0 mm, 1.10 mm (clustering radius: 20% of ball radius, angle threshold: 90°) in order to include the maximum of vertices and to fill the smaller holes resulting from the lack of correlation. An ultimate loop of the BPA with a ball radius of 1.25 mm was performed to fill more holes unless it led to the superposition of new mesh triangles with former ones. The clustering radius of this loop was reduced to 10% in order to avoid that issue [114]. The reconstructed surface was stored as an STL file.

In order to identify the vertebral surfaces only, for each specimen, the reconstructed DIC surfaces corresponding to the four test configurations (nucleotomy and discoplasty, each loaded in flexion and extension), were imported into a modelling software '3-matics' (Mimics InnovationSuite v23.0, Materialise, Leuven, Belgium). Using a 'brush' tool, the parts of the DIC surface corresponding to the vertebra were manually selected and copied separately as new parts (n=188) (Fig. 5.2).

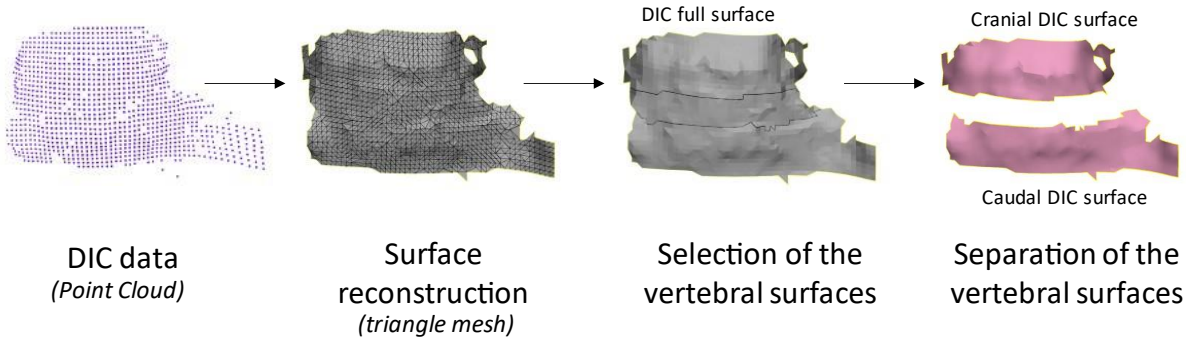


***Fig.5.2 -*** *DIC data: from point clouds to identified vertebra surfaces*

### *5.3.3 CT scan data acquisition and processing*

The specimens were scanned with a clinical computed tomography (CT) scanner (Aquilion ONE, Toshiba; with 220 mA, 120 kV, 0.3 mm slice thickness, 0.214 mm pixel size) after discoplasty before testing.

The caudal and cranial vertebrae (called BONE masks) of each specimen were segmented into Mimics® image analysis software (Mimics Innovation Suite v23.0, Materialise, Leuven, Belgium) from the DICOM images using thresholding and some manual edits to separate the vertebrae from the injected

cement. A second segmentation of the same vertebrae was performed: in order to match the surface recorded with DIC, a threshold >700 HU was applied to capture both vertebrae with the remaining soft tissue around (BONE-ST masks) (Fig. 5.3).

### *5.3.4 Registration of the DIC and CT data*

The rigid registration relied on the assumption that the two vertebrae behave as rigid bodies displacing in space (especially the cranial one, which was not constrained) while the connecting soft tissues were deformed. In order to associate the DIC surface meshes and the segmented geometries from CT scan, the first step consisted in registering the DIC surface of each vertebra on the corresponding BONE-ST masks (Fig. 5.3). For that, DIC surface meshes (n=188) of cranial and caudal vertebrae were imported into Mimics in the four tests (nucleotomy and discoplasty, each loaded in flexion and extension). A first manual alignment of caudal and cranial DIC meshes (moving element of the registration) on the corresponding caudal and cranial BONE-ST masks (fixed element of the registration) was performed in the sagittal, frontal, and transverse views using the 'reposition' tool. Then each DIC surface mesh (moving element of the registration) was globally registered on the corresponding BONE-ST mask (fixed element of the registration) using the 'STL registration' tool.

In order to move the 3D geometry of the cranial and caudal vertebrae from CT pose to the experimental pose, the segmented BONE masks were first converted into STL parts. Then, the cranial and caudal BONE parts and the cranial and caudal registered DIC meshes were copied into '3-matic' (Mimics Innovation Suite v23.0) where the DIC full surface mesh (two vertebrae + disc) was already imported. In order to align the BONE parts in the experimental pose, two rigid registrations were performed using the '3 point registration' tool (for each specimen, this process was repeated for the four tests: nucleotomy/discoplasty, each loaded flexion and extension):

- The DIC full surface mesh (moving element of the rigid registration) was registered to the caudal registered DIC mesh (fixed element of the rigid registration). The meshes being identical, the selected points were identical vertices in both meshes and the point registration was perfect.

- Similarly, the cranial registered DIC mesh (moving element of the rigid registration) was superposed to the DIC full surface mesh (fixed element of the rigid registration). In order to match the position recorded with the DIC, the cranial BONE part conjointly moved with its registered cranial DIC mesh. This resulted into the cranial and caudal BONE parts in the same position as the vertebral bodies at full load during the *ex vivo* tests.

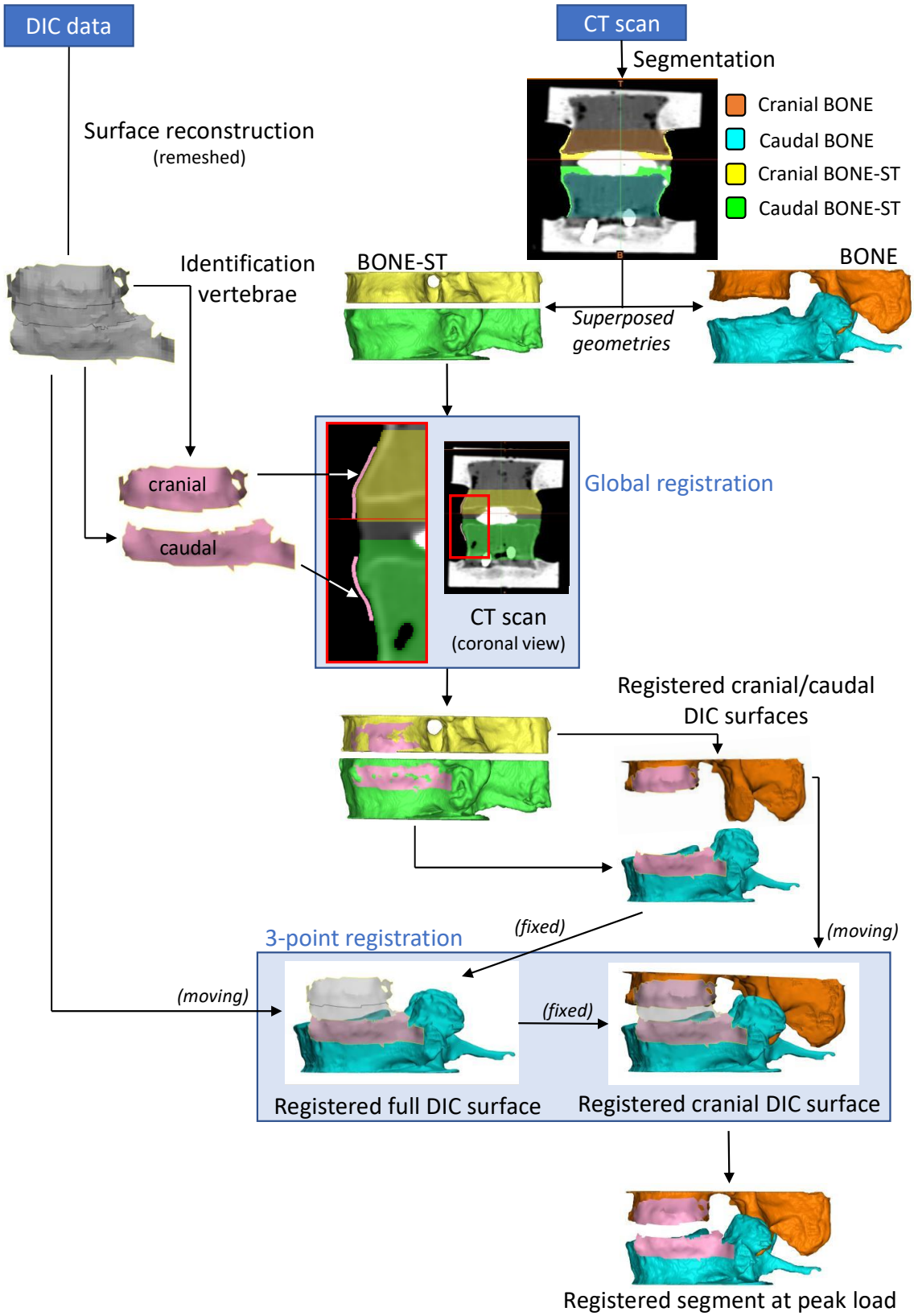


***Fig. 5.3 -*** *Registration process from the CT pose to the experimental pose. Registration of DIC meshes onto the corresponding BONE-ST segmented masks was first performed. After registration the position of DIC in the space mask remained unchanged whether BONE-ST or BONE part is considered due to the masks' superposition. The vertebrae were then aligned in the experimental pose using registration between the DIC meshes*

### 5.3.5 Measurement of the neuroforaminal 3D geometry

Once the BONE parts were correctly aligned, the neuroforamen change due to discoplasty was measured using a method developed previously for this purpose [38]. A measurement cylinder was drawn and aligned in the virtual transverse axis of the two neuroforamen in '3-matic' software (Fig. 5.4). The cylinder was 90 mm long while its radius was adjusted for each specimen and motion (flexion/extension) in order to entirely fill the foramen of both nucleotomy and discoplasty conditions (Table 5.7.5). The intersection of the vertebrae with the cylinder was subtracted from the cylinder, providing the free foramen volume $V_{nucleotomy}$ and $V_{discoplasty}$. The volumetric change ($\Delta V = V_{discoplasty} - V_{nucleotomy}$) of the foramen between nucleotomy and discoplasty was computed for flexion and for extension.

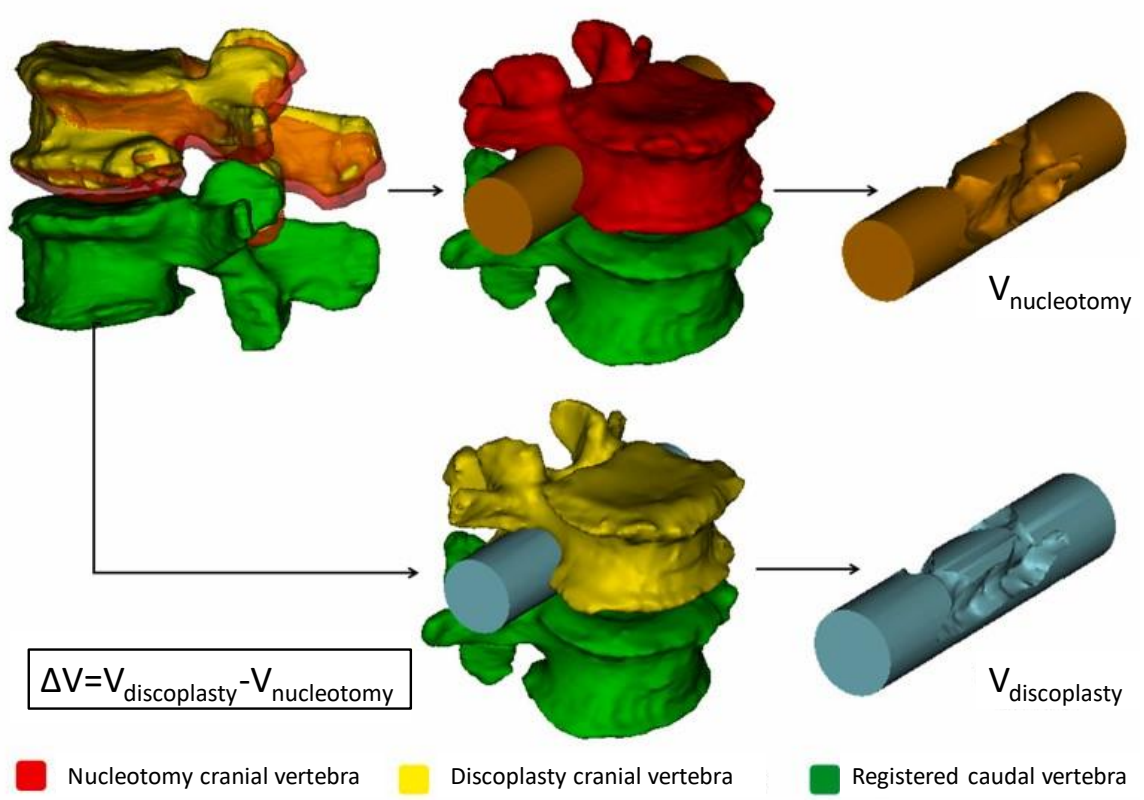


***Fig. 5.4:*** *Volumetric measurement of the foramen geometry change between nucleotomy discoplasty. This figure was adapted with the authors' consent from [38] under the Creative Commons license CC BY 4.0. The legend was adapted to the present nomenclature (Appendix 2)*

### 5.3.6 Characterization of the DIC surfaces

As it was suspected that the quality of the overall registration could be affected by the quality of the DIC acquisition, the geometry of the correlated DIC surfaces was characterized in terms of dimension and unicity. The surface of the mesh was automatically measured by '3-matic'. The total contour of the mesh was computed by adding the length of the external and internal 'bad contours' reported by the software. Finally, in order to assess the specificity of the surface, its roughness was measured. Roughness usually characterizes very small asperities however here, the evaluated geometric irregularities of the DIC-acquired surfaces were larger (of the order 1-5mm), and these features were important for the

registration. By measuring the roughness at this level, the asperities were identified on the surface and quantified by their height. For that, the point clouds of the DIC surfaces were primarily segmented into 80 000 points in CloudCompare v2.6.0 opensource software (R&D Institute EDF, Paris, France, https://www.danielgm.net/cc/). The roughness, corresponding to the distance between the point and the best fitted plane on the kernel, was computed using 'tool>other>roughness' tool. In order to target the main asperities of the DIC surface, kernel sizes in the range of the asperities were tested. A 3.0 mm kernel size was finally set, allowing the identification of the asperities characterizing the vertebra shape while excluding the noise asperities created by the remaining soft tissue. Because both the height and the number of asperities helped the manual registration, the roughness distribution histogram was extracted for each surface, and the mean and maximum of the distribution were computed. In addition, to quantify the number of high asperities (called density of asperities below), the number of mesh nodes exhibiting a local roughness >0.5 mm was derived using a Matlab script.

### *5.3.7 Evaluation of the measurement quality*

The whole workflow was reproduced by 2 operators ($O_1$ and $O_2$) who repeated it 2 times ($T_1$ and $T_2$) each. The inter operator repeatability of the segmentation was measured with DSI. Only the segmentation of the BONE masks was evaluated since it might directly impact the foramen volume. The BONE-ST mask segmentation did not involve subjective operator intervention and was not evaluated. The quality of the global registration between the DIC meshes and the segmented BONE-ST masks was measured with RMSE, indicating the average distance error between the 2 elements. To evaluate the repeatability of the entire procedure, the Hausdorff Distance (HD) of the two registrations of the same DIC surface mesh ($O_1T_1$ vs $O_1T_2$, $O_2T_1$ vs $O_2T_2$, $O_1T_1$ vs $O_2T_1$, and $O_1T_2$ vs $O_2T_2$) was measured with the MeshLab1.3.2 software (http://www.meshlab.net) Metro tool [115].

### *5.3.8 Statistical analysis*

All statistical analyses were performed with SPSS Statistics 25.0 (IBM Corp., Armonk, NY, USA) using nonparametric tests. Interrater ($O_1$ vs $O_2$) reliability was determined by Intraclass Correlation Coefficient (ICC) estimates and their 95% confident intervals (CI) were calculated based on a mean rating (k=4), absolute-agreement, 2-way mixed-effects model. Intra-rater ($O_1T_1$ vs $O_1T_2$, and $O_2T_1$ vs $O_2T_2$) reliability was determined by ICC estimates and their 95% CI were calculated based on a single measurement, absolute-agreement, 2-way mixed-effects model. ICC was applied for the foramen space measurements. The statistical significance in the change of foramen volume from nucleotomy to discoplasty was assessed by a paired Wilcoxon's test. The relationships between the mean volumetric change ($\Delta V$) and the cement volume, HD values and the DIC mesh surface, HD values and the roughness parameters were investigated with Spearman's rank correlation. P-value smaller than 0.05 were considered significant.

## 5.4 Results

### *5.4.1 Evaluation of the registration procedure*

The DSI for the segmentation of the vertebral bodies only (BONE masks) was 0.99 ± 0.01 (mean±SD), indicating a high reproducibility of the procedure and its operator independence.

The RMSE was automatically retrieved for each vertebra, disc state, and loading configuration to evaluate the matching of the DIC surface with the corresponding BONE-ST mask. Overall, the two operators $O_1$ and $O_2$ exhibited an RMSE of 0.27mm ±0.10mm and 0.24mm ±0.08mm respectively, demonstrating of the high repeatability of the method.

The reproducibility of the registration was evaluated computing the Hausdorff Distance (HD) for each DIC mask between its registration at two times ($T_1$, $T_2$), and by two operators ($O_1$, $O_2$). The HD values were computed for each node of the mask, the minimum, mean, maximum, and RMS HD values over each mask were extracted (Table 5.7.2). Both operators exhibited low HD values (mean±SD) of 0.09 ±0.19 mm ($O_1$) and 0.07 ±0.07 mm ($O_2$) which proved the intra-operator similarity of the registrations. Similarly, the mean HD values measured between the registrations of each operator were 0.17 ±0.22 mm ($T_1$) and 0.16 ±0.20 mm ($T_2$), and showed the low influence of the operator on the registration results. To more deeply assess the repeatability of the registration method, cumulative probability plots of the HD values of each mask were created for and between both operators (Fig. 5.5 A and B). Almost all the masks (~99%) had an HD value < 1 mm at 90% of the mesh nodes. One mask for $O_1$ (Fig. 5.5 C) exhibited a mean HD exceeding the others by 8 times the standard deviation (2.46 mm). The corresponding registration was considered not reliable enough to be included in the foramen measurements, and the causes of this poor registration were investigated.

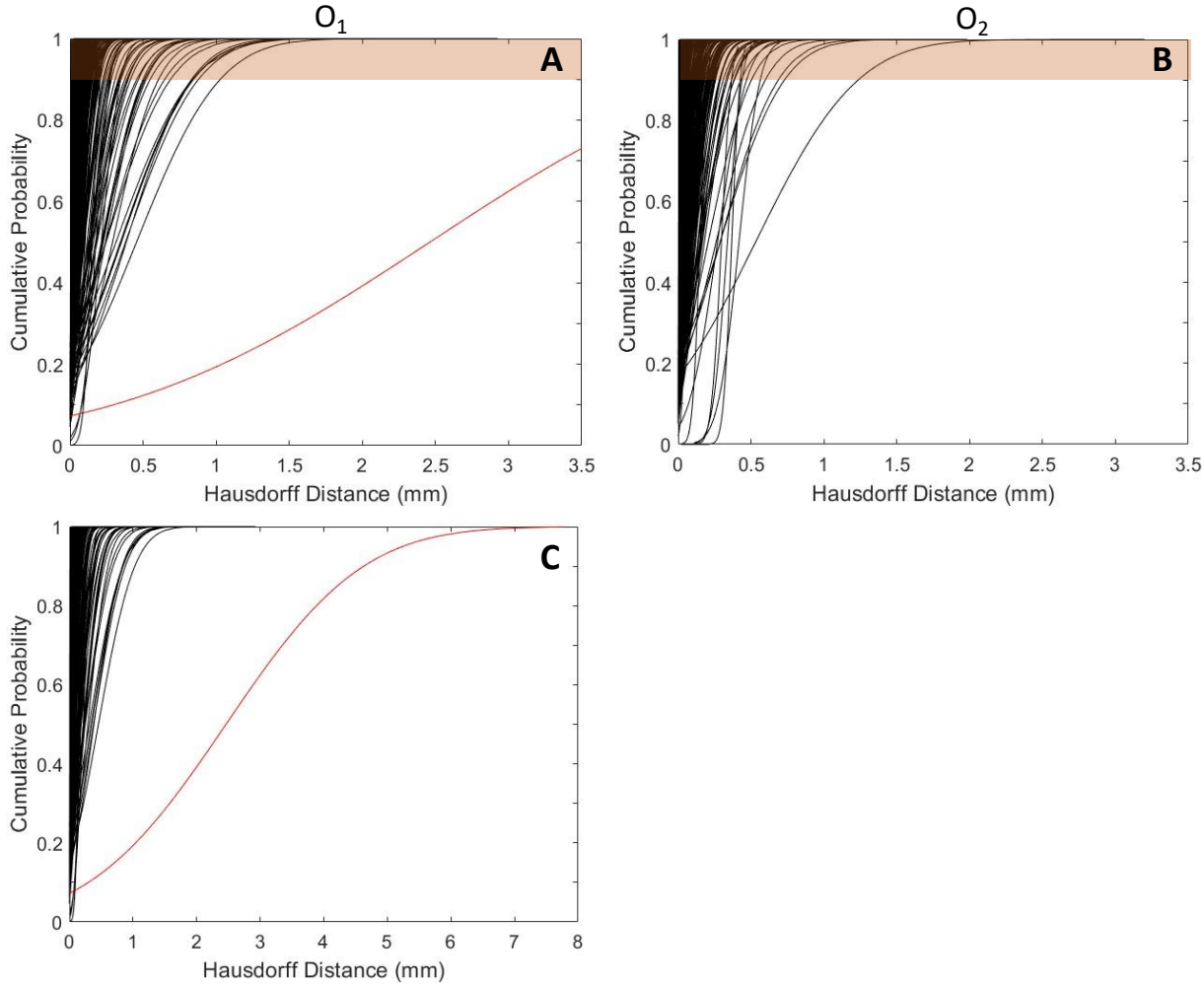


***Fig. 5.5:*** *HD cumulative probability of operators $O_1$ (A) and $O_2$ (B) for each DIC mask registration (188 curves in total corresponding to 25 specimens, with 2 vertebrae each, tested in 2 disc conditions and 2 loading configurations, with exclusion of 3 tests in flexion). One DIC mask registration showed very large HD values compared to the others (C)*

### *5.4.2 Characterization of DIC surfaces and correlation with registration precision*

In order to have a more detailed assessment of the registration accuracy, the impact on the registration of the DIC mask characteristics were investigated. In particular, the total surface and the roughness of the masks were studied. The overall DIC mask surface area in the different specimens was at 440 ± 137 $mm^2$ (mean±SD). The maximum and mean roughness over all DIC masks were respectively 1.10 ± 0.36 mm and 0.11±0.02 mm. The mean density of asperities was 7973 nodes (range 0-64521). Weak but significant negative correlations (Fig. 5.6) were found between the DIC mask surface area and the mean HD values for $O_1$ ($\rho$= -0.419, $p<0.01$), the DIC mask surface and the mean HD values for $O_2$ ($\rho$= -0.358, $p<0.01$), the DIC mask surface and the maximum HD values for $O_1$ ($\rho$= -0.379, $p<0.01$), and the DIC

mask surface and the maximum HD values for $O_2$ ($\rho$= -0.347, p<0.01). No significant correlation was found between the HD results and DIC mask roughness.

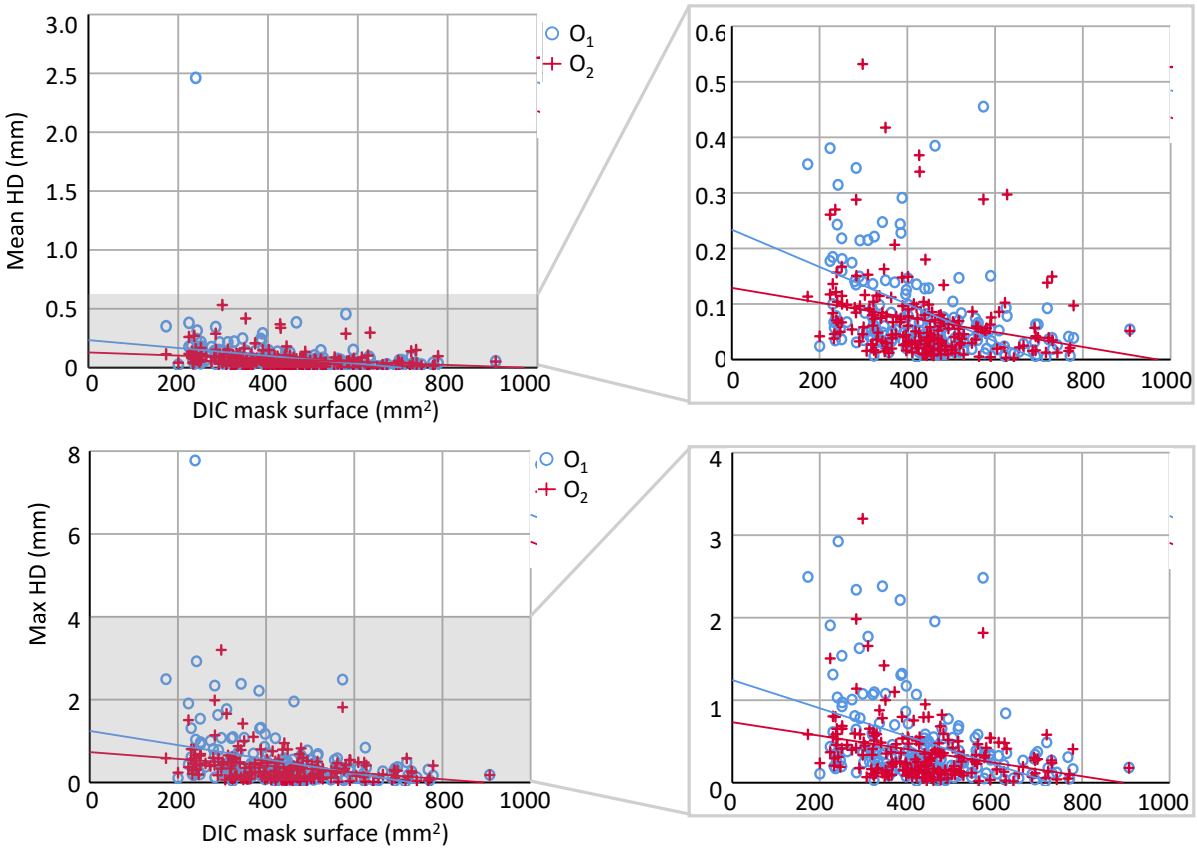


***Fig. 5.6:*** *Correlations between the mean Hausdorff Distance (top), the maximum Hausdorff Distance (bottom) measured for operators $O_1$ and $O_2$, and the surface of each DIC mask. Linear regression is plotted for all data*

### *5.4.3 Foramen decompression induced by discoplasty*

To test the reproducibility of the method, the measurements of the foramen volume after nucleotomy and discoplasty were performed by two operators repeated twice. Interrater reliability for $O_1$ mean($T_1$,$T_2$) vs $O_2$ mean($T_1$,$T_2$) was ICC=0.898 (CI 95%, Lower bound=0.828, Upper bound=0.937). Intra-rater reliability for $O_1T_1$ vs $O_1T_2$ was ICC=0.987 (CI 95%, Lower bound=0.980, Upper bound=0.991) and for $O_2T_1$ vs $O_2T_2$ ICC=0.994 (CI 95%, Lower bound=0.992, Upper bound=0.996). These results confirmed the high repeatability and reproducibility of the foramen volume measurements.

The volume of the foramen was compared after nucleotomy ($V_{nucleotomy}$) and after discoplasty ($V_{discoplasty}$) for flexion and extension. A large variability in term of foramen change ($\Delta V=V_{discoplasty}-V_{nucleotomy}$) was observed among the specimens for both operators (Fig. 5.4). Details of the decompression measured by $O_1$ and $O_2$ are reported in Table 5.7.3 and 5.7.4 in Appendix 5.7. The volume increased by 835±1289mm$^3$ ($V_{nucleotomy}$ vs $V_{discoplasty}$, p=0.001, paired Wilcoxon's test) was observed in flexion and 1205±1106mm$^3$ (p<0.001) in extension (Appendix 5.7 Table 5.7.5). The specimens were sorted by spine levels, resulting

in a larger mean volumetric change in the levels L3-L4 and L4-L5 for both flexion and extension (Fig. 5.4, Table 5.2).

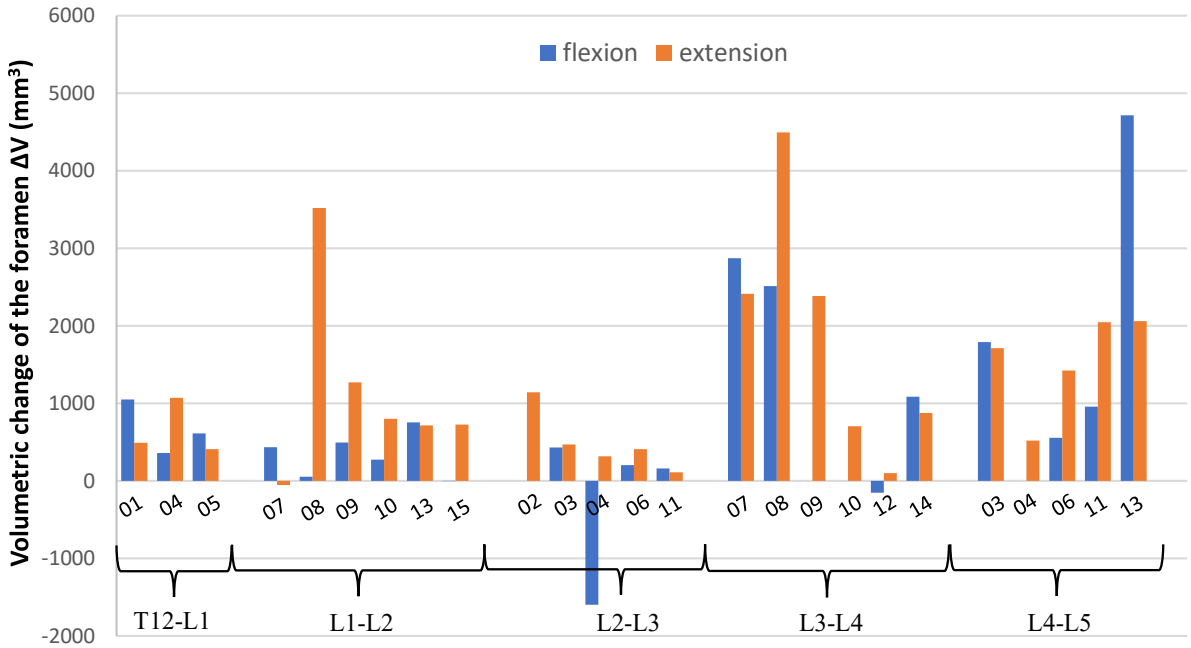


***Fig. 5.7*** *– Mean change of the foramen volume after discoplasty in flexion and extension for every specimen. The mean was computed across all operator measurements at all times ($O_1T_1$+$O_1T_2$+$O_2T_1$+$O_2T_2$/4)*

***Table 5.2 –*** *Mean and Standard Deviation of the foramen volumetric change depending on the treated spine level. Results were reported for flexion and extension*

| | Flexion | | Extension | |
|---|---|---|---|---|
| | **Mean (mm³)** | **SD (mm³)** | **Mean (mm³)** | **SD (mm³)** |
| **T12-L1** | 673 | 350 | 657 | 361 |
| **L1-L2** | 333 | 295 | 1163 | 1231 |
| **L2-L3** | -202 | 1102 | 489 | 390 |
| **L3-L4** | 1578 | 876 | 1829 | 1607 |
| **L4-L5** | 2004 | 1975 | 1552 | 635 |

### *5.4.4 Correlation between cement volume and foraminal decompression*

The cement volume measured for every specimen was 4575±1854 $mm^3$ (mean±SD). In flexion, a weak positive correlation was observed between the volume of injected cement and the ΔV of the spinal canal (Spearman's test, ρ=0.273, p=0.232, not significant). A significant moderate positive correlation was observed in extension (ρ=0.470, p=0.018) (Fig. 5.8).

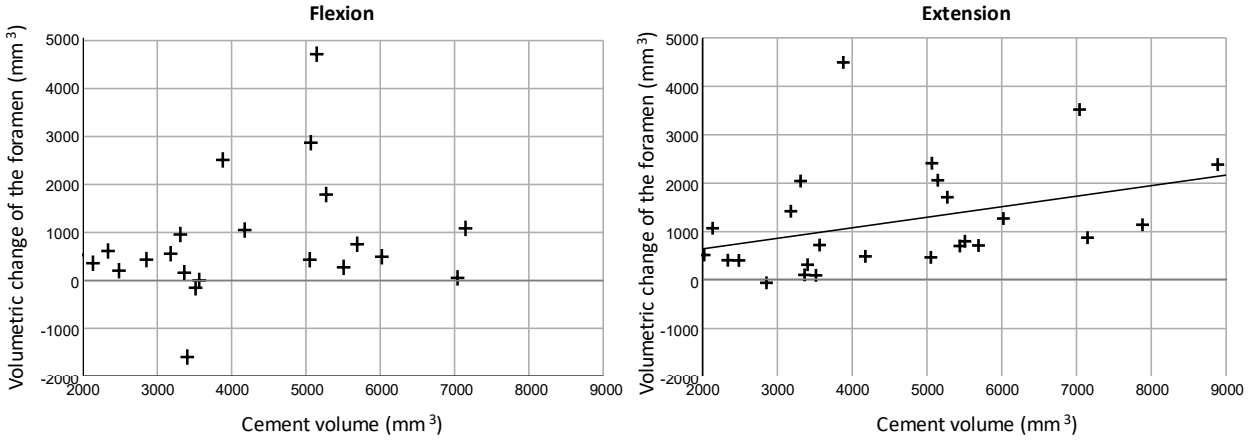


***Fig. 5.8:*** *Correlation between the volume of cement injected and the foramen volumetric change induced by PCD: in flexion (left), and extension (right). Linear regression is plotted for all data*

## 5.5 Discussion

In this paper, an investigation of the foramen geometry was conducted on *ex vivo* data in order to estimate the impact of PCD when the spine is loaded in flexion and extension. The 3D vertebra geometries were obtained from CT scans of the *ex vivo* specimens and then aligned in the experimental bending pose using registration of DIC data. The alignments were repeated for the specimens in pre- and post-operative conditions allowing the measurement of the foramen volume change implied by PCD.

The segmentation and registration methods showed low intra- and inter-operator differences showing of the repeatability and reproducibility of the workflow. In addition, registration of the DIC surface masks onto 3D vertebrae was proven to be precise, exhibiting a mean error in the range of the CT scan resolution. Thus, the combination of *ex vivo* experimentally acquired data and clinical images allowed registering the 3D geometries of the vertebrae in the actual pose under load, and to compare the condition after nucleotomy and after discoplasty.

The foramen was investigated using a method previously developed on *in vivo* data [38]. PCD significantly decompressed the foramen both in flexion and extension. The volumetric change was smaller in flexion probably because the cement mass is only indirectly involved in this direction of motion. Indeed, flexion was mainly constrained by the soft tissue (ligaments and facets) and limited by

the anterior endplate contact. The cement mass contributed to a larger stretch of the posterior ligaments and wider opening of the foramen. In extension the combined action of the injected cement and the posterior elements (facet joints) tended to constrain motion at an early stage compared to the nucleotomy condition, thus leaving more foramen space. All specimens showed an increase of the foramen volume, except one in flexion. This exception could be explained by the relative position of the cement mass within the disc and the loading application axis. As the bone cement was located anteriorly where the axial load was applied, it limited the bending rotation of the vertebrae compared to the free rotation observed after nucleotomy, resulting in a decrease of the foramen volume.

Finally, the larger volumes of cement were associated with larger increase of the foramen space in extension only due to the direct involvement of cement for this direction of motion.

To the authors' knowledge, there are very few studies addressing the impact of PCD on the foramen space [21]. The method of 3D assessment of the foramen volumetric change using a cylinder was developed by Eltes *et al.* to provide an appropriate tool to evaluate the impact of PCD on the spine on living. It was developed on *in vivo* data pre- and post-operatively acquired on patients [38]. The study confirmed that PCD increased the foraminal dimensions in neutral position. The geometrical change was also proven to have a strong positive correlation with the volume and surface area of injected cement. This could partially explain the larger change in foramen observed *in vivo* (2295 mm3 ± 1181, n = 16) than *ex vivo* since the volume of cement injected during patient surgery was in average larger than *ex vivo*.

In Eltes *et al.* [38], the impact of PCD on foraminal space was investigated on patient's CT scans recorded in supine position. Because numerous repetitions of *in vivo* tomography to investigate different patient positions is time-consuming and can increase radiation exposure, *in silico* or *ex vivo* approaches are alternative methods allowing to easily vary the poses.

However, our study also presented some limitations. Only 25 specimens were tested here: while this was sufficient to observe the general effect, a larger cohort would also allow to explore the dependence of the outcome on the spine level. Moreover, despite the high accuracy and precision showed by our method, the registration repeatability and replicability were found to be increased with large DIC mask surface areas. Although a narrow field of view is not systematically associated with poor registration, one of the tests had to be excluded from our cohort for this reason. Thus, acquiring a larger portion of the specimen surface would provide more nodes in the mesh to register, and then a decreased error. The more cameras a DIC system does include, the larger the field of view is [116]. With such set-ups, the workflow of this study could be automatized using larger DIC masks.

## 5.6 Conclusion

Following a first clinical investigation of the *in vivo* foraminal space after PCD [38], this study aimed to develop a more detailed *ex vivo* analysis of the foramen geometrical changes induced by the surgery in complex loaded configurations. For that, *ex vivo* biomechanical testing and CT imaging were combined to create the 3D geometry of the spine segments in preop- and postop- conditions. This work allowed to draw some conclusions demonstrating of PCD benefits on the foramen space.

- PCD induced a significant decompression of the foraminal space under flexion and extension, showing the efficiency of the surgery under loading.

- The increase of foramen space was positively correlated with the volume of injected cement in extension, confirming the clinical observations.

- This method could be applied for the assessment of the spine geometry under various other loading conditions as long as the DIC-acquired field of view is large enough.

## 5.7 Appendix

***Table 5.7.1** – Donors' data and testing parameters for flexion and extension*

| Specimen | Sex-Age | Lumbar level | Offset (mm) | | Axial displacement variation (mm) | | Testing load (N) | |
|---|---|---|---|---|---|---|---|---|
| | | | Flexion | Extension | Flexion | Extension | Flexion | Extension |
| 01 | M-68 | T12-L1 | 12.3 | 24.5 | -0.59 | -1.35 | 402 | |
| 02 | M-79 | L2-L3 | 15.1 | 30.1 | - | -0.61 | - | 387 |
| 03 | M-53 | L2-L3 | 13.1 | 26.3 | -1.40 | -0.73 | 402 | |
| | | L4-L5 | 13.6 | 27.2 | -2.21 | -0.15 | 402 | |
| 04 | F-35 | T12-L1 | 10.4 | 20.8 | -0.37 | -0.21 | 309 | |
| | | L2-L3 | 10.7 | 21.5 | -3.20 | -0.43 | 309 | |
| | | L4-L5 | 11.0 | 22.1 | - | -0.34 | - | 309 |
| 05 | F-68 | T12-L1 | 9.1 | 18.2 | -2.06 | -0.84 | 396* | |
| 06 | M-59 | L2-L3 | 10.9 | 21.8 | 0.49 | -0.02 | 326* | |
| | | L4-L5 | 11.6 | 23.2 | 0.59 | -0.52 | 326* | 140* |
| 07 | F-78 | L1-L2 | 12.9 | 25.8 | -0.46 | -0.09 | 348 | |
| | | L3-L4 | 13.4 | 26.9 | 1.05 | -0.69 | 348 | |
| 08 | M-79 | L1-L2 | 12.8 | 25.7 | -2.02 | -1.34 | 456 | |
| | | L3-L4 | 14.8 | 29.5 | -1.22 | -0.68 | 456 | |
| 09 | F-86 | L1-L2 | 13.6 | 27.2 | -1.17 | -0.56 | 265* | |
| | | L3-L4 | 15.8 | 31.5 | -0.92 | -0.61 | 265* | |
| 10 | M-71 | L1-L2 | 11.9 | 23.7 | -1.98 | -0.38 | 343 | |
| | | L3-L4 | 13.3 | 26.5 | - | -0.40 | - | 343 |
| 11 | M-68 | L2-L3 | 12.6 | 25.3 | -0.44 | -0.11 | 319 | |
| | | L4-L5 | 13.2 | 26.3 | -1.51 | -0.01 | 319 | |
| 12 | F-80 | L3-L4 | 13.9 | 27.9 | -0.63 | -0.42 | 378 | |
| 13 | M-64 | L1-L2 | 12.8 | 25.6 | -1.62 | -0.09 | 417 | |
| | | L4-L5 | 14.9 | 29.8 | -4.31 | 0.09 | 417 | |
| 14 | M-73 | L3-L4 | 16.6 | 33.1 | -2.12 | -0.57 | 515 | |
| 15 | F-74 | L1-L2 | 12.3 | 24.6 | -1.65 | -1.01 | 412 | |

*Reduced load to avoid damages

***Table 5.7.2 -*** *Hausdorff Distance (HD) of the registered DIC masks. Measurements evaluated the accuracy of repeated registrations by the same operator ($O_1T_1$ vs $O_1T_2$, $O_2T_1$ vs $O_2T_2$) and the registration accuracy between two operators ($O_1T_1$ vs $O_2T_1$, $O_1T_2$ vs $O_2T_2$). Results are presented as the mean of HDs over all the DIC masks (SD)*

| | | HD (mm) | | | |
|---|---|---|---|---|---|
| | **Compared surfaces** | **Min** | **Mean** | **Max** | **RMS** |
| *Intra-operator* | $O_1T_1$ vs $O_1T_2$ | 0.00 (0.00) | 0.10 (0.23) | 0.52 (0.79) | 0.13 (0.28) |
| | $O_2T_1$ vs $O_2T_2$ | 0.00 (0.01) | 0.07 (0.07) | 0.37 (0.38) | 0.10 (0.10) |
| *Inter-operator* | $O_1T_1$ vs $O_2T_1$ | 0.01 (0.03) | 0.18 (0.25) | 0.63 (0.87) | 0.21 (0.29) |
| | $O_1T_2$ vs $O_2T_2$ | 0.01 (0.04) | 0.15 (0.18) | 0.53 (0.65) | 0.18 (0.22) |

Min: minimum, Max: maximum, RMS: root mean square

***Table 5.7.3 -*** *Volumetric measurements done by operator one ($O_1$), at two times ($T_1$, $T_2$). The main result is $\Delta V = V_{discoplasty} - V_{nucleotomy}$ the volumetric change of the foramen induced by discoplasty*

| | | **Flexion** | | | | | | **Extension** | | | | | |
|---|---|---|---|---|---|---|---|---|---|---|---|---|---|
| | | **$O_1T_1$** | | | **$O_1T_2$** | | | **$O_1T_1$** | | | **$O_1T_2$** | | |
| **Specimen ID** | **Spine level** | **$V_{nucleotomy}$ ($mm^3$)** | **$V_{discoplasty}$ ($mm^3$)** | **$\Delta V$ ($mm^3$)** | **$V_{nucleotomy}$ ($mm^3$)** | **$V_{discoplasty}$ ($mm^3$)** | **$\Delta V$ ($mm^3$)** | **$V_{nucleotomy}$ ($mm^3$)** | **$V_{discoplasty}$ ($mm^3$)** | **$\Delta V$ ($mm^3$)** | **$V_{nucleotomy}$ ($mm^3$)** | **$V_{discoplasty}$ ($mm^3$)** | **$\Delta V$ ($mm^3$)** |
| 01 | T12-L1 | 28504 | 29863 | 1359 | 28405 | 29703 | 1298 | 28457 | 29023 | 566 | 28688 | 29205 | 517 |
| 02 | L2-L3 | - | - | - | - | - | - | 35724 | 36632 | 907 | 35354 | 36779 | 1425 |
| 03 | L2-L3 | 41312 | 41774 | 462 | 41240 | 41627 | 387 | 39025 | 39380 | 355 | 39078 | 39629 | 551 |
| 03 | L4-L5 | 31970 | 33614 | 1644 | 31358 | 33230 | 1872 | 29884 | 31628 | 1744 | 29728 | 31433 | 1705 |
| 04 | T12-L1 | 35301 | 35586 | 285 | 35224 | 35343 | 119 | 34562 | 35531 | 969 | 34560 | 36210 | 1650 |
| 04 | L2-L3 | 36256 | 35041 | -1215 | 36455 | 34775 | -1680 | 34037 | 34269 | 232 | 34030 | 34205 | 175 |
| 04 | L4-L5 | - | - | - | - | - | - | 33043 | 33027 | -16 | 32661 | 32340 | -321 |
| 05 | T12-L1 | 35235 | 36171 | 936 | 35701 | 36270 | 569 | 34889 | 35435 | 546 | 34879 | 35295 | 416 |
| 06 | L2-L3 | 30536 | 30599 | 63 | 30371 | 30770 | 399 | 28641 | 29124 | 483 | 28308 | 28877 | 569 |
| 06 | L4-L5 | 22497 | 23157 | 660 | 22576 | 23256 | 680 | 20836 | 22283 | 1447 | 20359 | 22273 | 1914 |
| 07 | L1-L2 | 28873 | 29601 | 728 | 29276 | 29512 | 236 | 28490 | 28501 | 11 | 28509 | 28653 | 144 |
| 07 | L3-L4 | 20188 | 22328 | 2140 | 22514 | 24621 | 2107 | 18619 | 21103 | 2484 | 17505 | 20736 | 3231 |
| 08 | L1-L2 | 28388 | 28801 | 413 | 28737 | 28620 | -117 | 26586 | 29735 | 3149 | 25777 | 29636 | 3859 |
| 08 | L3-L4 | 25795 | 23783 | -2012 | 23791 | 28274 | 4483 | 22603 | 27897 | 5294 | 22774 | 25658 | 2884 |
| 09 | L1-L2 | 28792 | 30097 | 1305 | 28895 | 29029 | 134 | 28361 | 29185 | 824 | 28310 | 29428 | 1118 |
| 09 | L3-L4 | - | - | - | - | - | - | 39407 | 43374 | 3967 | 39129 | 42791 | 3662 |
| 10 | L1-L2 | 30604 | 31207 | 603 | 30448 | 30365 | -83 | 28921 | 30079 | 1158 | 29385 | 30095 | 710 |
| 10 | L3-L4 | - | - | - | - | - | - | 34761 | 35513 | 752 | 34723 | 35127 | 404 |
| 11 | L2-L3 | 35317 | 35376 | 59 | 35222 | 35407 | 185 | 28445 | 28696 | 251 | 28608 | 28578 | -30 |
| 11 | L4-L5 | 31761 | 32543 | 782 | 32205 | 32738 | 533 | 24751 | 26304 | 1553 | 24230 | 26531 | 2301 |
| 12 | L3-L4 | 27576 | 27565 | -11 | 27777 | 27515 | -262 | 26558 | 26605 | 47 | 26576 | 26385 | -191 |
| 13 | L1-L2 | 29930 | 30645 | 715 | 29746 | 30707 | 961 | 29190 | 29788 | 598 | 29142 | 29697 | 555 |
| 13 | L4-L5 | 27969 | 33972 | 6003 | 27061 | 33551 | 6490 | 30532 | 32686 | 2154 | 30238 | 32262 | 2024 |
| 14 | L3-L4 | 32759 | 33865 | 1106 | 33169 | 33714 | 545 | 30438 | 31257 | 819 | 31033 | 31471 | 438 |
| 15 | L1-L2 | 37114 | 37309 | 195 | 36928 | 37031 | 103 | 35418 | 35953 | 535 | 35361 | 35999 | 638 |
| **Mean** | | | | **772** | | | **903** | | | **1233** | | | **1214** |
| **SD** | | | | **1499** | | | **1737** | | | **1304** | | | **1208** |

***Table 5.7.4 -*** *Volumetric measurements done by operator two ($O_2$), at two times ($T_1$, $T_2$)*

| | | Flexion | | | | | | Extension | | | | | |
|---|---|---|---|---|---|---|---|---|---|---|---|---|---|
| | | $O_2T_1$ | | | $O_2T_2$ | | | $O_2T_1$ | | | $O_2T_2$ | | |
| Specimen ID | Spine level | $V_{nucleotomy}$ ($mm^3$) | $V_{discoplasty}$ ($mm^3$) | $\Delta V$ ($mm^3$) | $V_{nucleotomy}$ ($mm^3$) | $V_{discoplasty}$ ($mm^3$) | $\Delta V$ ($mm^3$) | $V_{nucleotomy}$ ($mm^3$) | $V_{discoplasty}$ ($mm^3$) | $\Delta V$ ($mm^3$) | $V_{nucleotomy}$ ($mm^3$) | $V_{discoplasty}$ ($mm^3$) | $\Delta V$ ($mm^3$) |
| 01 | T12-L1 | 28743 | 29460 | 717 | 28443 | 29266 | 823 | 28292 | 28718 | 426 | 28078 | 28529 | 451 |
| 02 | L2-L3 | - | - | - | - | - | - | 36058 | 37227 | 1169 | 36341 | 37413 | 1072 |
| 03 | L2-L3 | 41079 | 41547 | 468 | 41306 | 41713 | 407 | 38420 | 38873 | 453 | 38470 | 38990 | 520 |
| 03 | L4-L5 | 31251 | 32946 | 1695 | 31150 | 33096 | 1946 | 29259 | 30762 | 1503 | 29560 | 31451 | 1891 |
| 04 | T12-L1 | 34762 | 35397 | 635 | 34684 | 35076 | 392 | 34248 | 35040 | 792 | 34965 | 35838 | 873 |
| 04 | L2-L3 | 36243 | 34568 | -1675 | 36192 | 34367 | -1825 | 33936 | 34526 | 590 | 33928 | 34202 | 274 |
| 04 | L4-L5 | - | - | - | - | - | - | 31305 | 32807 | 1502 | 31563 | 32475 | 912 |
| 05 | T12-L1 | 36198 | 36568 | 370 | 35864 | 36440 | 576 | 35370 | 35749 | 379 | 35212 | 35513 | 301 |
| 06 | L2-L3 | 30207 | 30529 | 322 | 30416 | 30441 | 25 | 29285 | 29815 | 530 | 29062 | 29108 | 46 |
| 06 | L4-L5 | 25322 | 25872 | 550 | 26188 | 26522 | 334 | 23942 | 25146 | 1204 | 24697 | 25819 | 1122 |
| 07 | L1-L2 | 29254 | 29729 | 475 | 29043 | 29333 | 290 | 28322 | 28237 | -85 | 27941 | 27650 | -291 |
| 07 | L3-L4 | 24447 | 27561 | 3114 | 24169 | 28289 | 4120 | 23137 | 25225 | 2088 | 23465 | 25314 | 1849 |
| 08 | L1-L2 | 28414 | 28469 | 55 | 28557 | 28414 | -143 | 25641 | 29475 | 3834 | 26050 | 29291 | 3241 |
| 08 | L3-L4 | 33557 | 36963 | 3406 | 33225 | 37394 | 4169 | 29945 | 34579 | 4634 | 30502 | 35665 | 5163 |
| 09 | L1-L2 | 29191 | 29347 | 156 | 28715 | 29091 | 376 | 28306 | 29994 | 1688 | 28453 | 29909 | 1456 |
| 09 | L3-L4 | - | - | - | - | - | - | 36201 | 35706 | -495 | 34835 | 37240 | 2405 |
| 10 | L1-L2 | 34916 | 34926 | 10 | 35032 | 35591 | 559 | 33781 | 34450 | 669 | 34237 | 34908 | 671 |
| 10 | L3-L4 | - | - | - | - | - | - | 34014 | 35068 | 1054 | 34226 | 34835 | 609 |
| 11 | L2-L3 | 35344 | 35734 | 390 | 35545 | 35546 | 1 | 33318 | 33425 | 107 | 33475 | 33581 | 106 |
| 11 | L4-L5 | 32407 | 33726 | 1319 | 31944 | 33135 | 1191 | 28807 | 31128 | 2321 | 28893 | 30898 | 2005 |
| 12 | L3-L4 | 27479 | 27205 | -274 | 27426 | 27355 | -71 | 26376 | 26587 | 211 | 26114 | 26442 | 328 |
| 13 | L1-L2 | 29984 | 30716 | 732 | 30064 | 30667 | 603 | 29015 | 29872 | 857 | 28949 | 29800 | 851 |
| 13 | L4-L5 | 30625 | 33995 | 3370 | 31063 | 34065 | 3002 | 31180 | 32857 | 1677 | 30710 | 33100 | 2390 |
| 14 | L3-L4 | 32435 | 33892 | 1457 | 32637 | 33867 | 1230 | 30331 | 31368 | 1037 | 30053 | 31263 | 1210 |
| 15 | L1-L2 | 36993 | 36865 | -128 | 36954 | 36777 | -177 | 35004 | 35953 | 949 | 35106 | 35880 | 774 |
| **Mean** | | | | **817** | | | **849** | | | **1164** | | | **1209** |
| **SD** | | | | **1243** | | | **1426** | | | **1144** | | | **1185** |

***Table 5.7.5*** *- Volumes and changes based on the measurements of $O_1$ and $O_2$ at $T_1$ and $T_2$ ($O_1T_1+O_1T_2+O_2T_1+O_2T_2/4$) for the 15 specimens*

| | | Flexion | | | | | Extension | | | | |
|---|---|---|---|---|---|---|---|---|---|---|---|
| **Specimen ID** | **Spine level** | **Cylinder radius (mm)** | **Mean $V_{nucleotomy}$ ($mm^3$)** | **Mean $V_{discoplasty}$ ($mm^3$)** | **Mean ΔV ($mm^3$)** | **SD ΔV ($mm^3$)** | **Cylinder radius (mm)** | **Mean $V_{nucleotomy}$ ($mm^3$)** | **Mean $V_{discoplasty}$ ($mm^3$)** | **Mean ΔV ($mm^3$)** | **SD ΔV ($mm^3$)** |
| 01 | T12-L1 | 11 | 28524 | 29573 | 1049 | 326 | 11 | 28379 | 28869 | 490 | 64 |
| 02 | L2-L3 | - | - | - | - | - | 13 | 35869 | 37013 | 1143 | 216 |
| 03 | L2-L3 | 13 | 41234 | 41665 | 431 | 40 | 13 | 38748 | 39218 | 470 | 87 |
| 03 | L4-L5 | 12 | 31432 | 33222 | 1789 | 143 | 12 | 29608 | 31319 | 1711 | 160 |
| 04 | T12-L1 | 12 | 34993 | 35351 | 358 | 216 | 12 | 34584 | 35655 | 1071 | 393 |
| 04 | L2-L3 | 12 | 36287 | 34688 | -1599 | 265 | 12 | 33983 | 34301 | 318 | 186 |
| 04 | L4-L5 | - | - | - | - | - | 12 | 32143 | 32662 | 519 | 839 |
| 05 | T12-L1 | 12 | 35750 | 36362 | 613 | 236 | 12 | 35088 | 35498 | 411 | 102 |
| 06 | L2-L3 | 11 | 30383 | 30585 | 202 | 186 | 11 | 28824 | 29231 | 407 | 243 |
| 06 | L4-L5 | 10 | 24146 | 24702 | 556 | 159 | 11 | 22459 | 23880 | 1422 | 356 |
| 07 | L1-L2 | 11 | 29112 | 29544 | 432 | 222 | 11 | 28316 | 28260 | -55 | 183 |
| 07 | L3-L4 | 10 | 22830 | 25700 | 2870 | 955 | 10 | 20682 | 23095 | 2413 | 605 |
| 08 | L1-L2 | 11 | 28524 | 28576 | 52 | 256 | 11 | 26014 | 29534 | 3521 | 378 |
| 08 | L3-L4 | 15 | 26456 | 31604 | 2512 | 3049 | 15 | 29092 | 30950 | 4494 | 1110 |
| 09 | L1-L2 | 11 | 28898 | 29391 | 493 | 552 | 11 | 28358 | 29629 | 1272 | 379 |
| 09 | L3-L4 | - | - | - | - | - | 13 | 37393 | 39778 | 2385 | 2035 |
| 10 | L1-L2 | 12 | 32750 | 33022 | 272 | 359 | 12 | 31581 | 32383 | 802 | 238 |
| 10 | L3-L4 | - | - | - | - | - | 12 | 34431 | 35136 | 705 | 273 |
| 11 | L2-L3 | 12 | 35357 | 35516 | 159 | 172 | 11 | 30962 | 31070 | 109 | 115 |
| 11 | L4-L5 | 12 | 32079 | 33036 | 956 | 363 | 11 | 26670 | 28715 | 2045 | 358 |
| 12 | L3-L4 | 11 | 27565 | 27410 | -155 | 133 | 11 | 26406 | 26505 | 99 | 225 |
| 13 | L1-L2 | 11 | 29931 | 30684 | 753 | 150 | 11 | 29074 | 29789 | 715 | 161 |
| 13 | L4-L5 | 12 | 29180 | 33896 | 4716 | 1784 | 12 | 30665 | 32726 | 2061 | 298 |
| 14 | L3-L4 | 12 | 32750 | 33835 | 1085 | 388 | 12 | 30464 | 31340 | 876 | 333 |
| 15 | L1-L2 | 12 | 36997 | 36996 | -2 | 179 | 12 | 35222 | 35946 | 724 | 179 |
| **Mean** | | | | | **835** | | | | | **1205** | |
| **Standard Deviation** | | | | | **1289** | | | | | **1106** | |

*Chapter 6*

# Conclusions

In this PhD project, a combination of *in vitro* testing, numerical approaches, and clinical observations were applied to the spine to explore its biomechanics following percutaneous cement discoplasty, a minimally invasive surgery to treat intervertebral disc degeneration. The anatomical geometry and the kinematics of the spine were measured using contactless tools: Digital Image Correlation and medical imaging.

The first part of the research started with an extensive review of the compound knowledge on the application of percutaneous cement discoplasty on the lumbar spine. The analysis of the few retrieved papers allowed specifying the surgical planning and highlighting the benefits of the surgery on patient outcome and stabilization of the spine. It also raised some questions about potential complications and the solutions to prevent them. Among them, one work presented an alternative filling material to improve the alien-biological material compatibility. However, the review of the literature emphasized the lack of investigation of the treated spine level biomechanics which could help to better understand failure mechanisms.

In order to fill this gap, a preliminary study was conducted on animal specimens to present a realistic way to test PCD biomechanics *in vitro*. Through the careful reproduction of the vacuum phenomenon in degenerated discs and of the cement injection, the loss and then recovery of disc height observed *in vivo* in degenerated and treated cases was also measured in bending conditions. The biomechanical behaviour of the segments in both disc conditions was also compared to the intact conditions, showing beneficial effect of discoplasty on the release of disc surface strains and the kinematics. These results showed a promising potential to investigate the surgery on human specimens and in loading configurations more demanding for the spine. The next step was therefore to apply the former methodology to human spines to establish the first rational on the biomechanical consequences of PCD on the treated segments. This goal was reached on 27 lumbar specimens, which were tested in two loading conditions (flexion and extension) challenging the neuroforamen space. The use of Digital Image Correlation allowed to measure the increase of the disc height and the partial stabilization induced by the surgery which were correlated to the cement thickness. The strain maps under loadings were also evaluated but did not indicate extreme behaviour of the surface tissue. This *in vitro* model of PCD can open the way to additional investigations under complementary loadings and on deeper disc tissue.

A complementary approach was used in the second part of this research, focusing on the assessment of the foramen changes. As low back pain is directly related to the foramen stenosis, the understanding of the mechanisms behind patient pain relief was targeted. A 3D *in silico* method was developed by the research group to quantify the foramen space from CT scan images. This way, the volumetric change in patients undergoing the surgery was measured pre- and postoperatively. The next step consisted in evaluating the foramen decompression under other functional loadings. Through the combination of this computational method with the *ex vivo* data obtained previously, the 3D geometry of the spine segments

was registered in flexion and extension positions allowing the quantification of the volumetric foramen change in these challenging alignments. A careful optimization of the registration allowed to define criteria on the experimental data acquisition to ensure the most precise 3D model.

All this work provided a reliable bench of tools and methods to investigate the biomechanics behind percutaneous discoplasty and a first overview of the main changes in the spine biomechanical behaviour. In the next years, more investigations on the surgery biomechanical outcome should be performed future directions could include: (i) applying more complex loading scenarios; (ii) exploring the mechanisms leading to surgical complication; (iii) exploring alternative surgical approaches; (iv) testing alternative injectable materials.

# Appendix 1:
# The effect of intervertebral disc simulated damage

by:

S. Montanari, C. Techens, L. Cristofolini

Included in appendix of the manuscript:

**Biomechanical consequences of cement discoplasty:**

**an *in vitro* study on thoraco-lumbar human spines**

C. Techens, S. Montanari, F. Bereczki, P. E. Eltes, A. Lazary, L. Cristofolini

## A1.1 Introduction

*In vitro* biomechanical investigation of percutaneous cement discoplasty (PCD) requires collateral lesions, such as annulus incision and disc material removal, to recreate the typical vacuum phenomenon (VP) of the degenerated discs that would require PCD. The mechanical impact and consequences of annulus lesions on spine biomechanics have not been completely assessed [117]–[121].

The aim of this set of experiments was to evaluate the consequences of intervertebral disc (IVD) lesions on the spine biomechanics, especially due to the incision of annulus fibrosus as those performed in the main paper, in order to:

i. Explore the artefacts induced by simulated disc lesions, in terms of disc height, stiffness and range of motion.

ii. Assess to what extent simulated nucleotomy affects the biomechanics of the IVD.

More specifically, this additional study aimed to assess if the lesion of the annulus required to remove the nucleus would compromise the biomechanics of the Functional Spinal Unit (FSU) significantly, compared to the alteration caused by the simulated disc degeneration.

## A1.2 Methods

### *A1.2.1 Specimens, imaging, and preparation*

Eight fresh cadaver thoraco-lumbar functional spine unit were extracted from six donors (Table A1.1). CT scans were performed for all the spines, (Aquilion, ONE, Toshiba, Bologna) in the same conditions of the main paper.

The FSUs were prepared following the same protocol as the main paper, except for the posterior processes, which were cut at the facet joints level. In addition, osteophytes were removed in specimens #1 and #2, ensuring not to damage the disc.

***Table A1.1*** *- Donors' data with testing parameters for flexion and extension*

| Specimen N° | Level | Sex – Age | Offset (mm) | | Applied Load (N) | Width of the slot (mm) |
|---|---|---|---|---|---|---|
| | | | Flexion | Extension | | |
| ***#1*** | T9 - T10 | F - 77 | 8.5 | 17.0 | 211 | 4.2 |
| ***#2*** | T11 - T12 | F - 77 | 9.3 | 18.6 | 211 | 6.2 |
| ***#3*** | T10 - T11 | M - 68 | 10.5 | 21.0 | 402 | 5.3 |
| ***#4*** | L4 - L5 | M - 79 | 17.3 | 34.6 | 388 | 10.5 |
| ***#5*** | T12 - L1 | M - 53 | 11.7 | 23.4 | 402 | 5.4 |
| ***#6*** | T10 - T11 | M - 59 | 13.1 | 26.2 | 495 | 5.6 |
| ***#7*** | T12 - L1 | M - 59 | 13.4 | 26.8 | 495 | 5.9 |
| ***#8*** | T10 - T11 | F - 58 | 8.2 | 16.4 | *300* | 5.9 |
| ***Mean*** | | 66 | 11.5 | 23.0 | 363 | 6.1 |
| ***SD*** | | 10.3 | 3.1 | 6.1 | 112.6 | 1.9 |
| ***Range*** | | 53 - 79 | 8.2 – 17.3 | 16.4 – 34.6 | 211 - 495 | 4.2 – 10.5 |

### *A1.2.2 Incremental creation of the defects in the disc*

In order to explore how the incisions on the annulus affect the biomechanics of the FSU, all the specimens were sequentially tested, through these five subsequent conditions (Fig. 7.1):

a) INT: the disc was in the native conditions (intact)

b) 2CUTS: two vertical cuts from the upper endplate to the lower endplate were made on the lateral side of the annulus fibrosus as deep as required to reach the nucleus. The two incisions were spaced by a mean of 6.1 mm (range 4.2 – 10.5 mm)

c) 4CUTS: two additional horizontal cuts were made along the endplates, connecting the first two cuts so as to form a square incision on the annulus tissue.

d) SQR: the square-shaped plug of annulus tissue was removed, leaving the nucleus visible.

e) NUCL: the nucleus pulposus was extracted with curette and surgical spoon through the window created in the previous condition. This final condition corresponded to the starting condition (NUCL) of the specimens tested for discoplasty in the main paper.

In order to minimize variability between testing session, the lesions 2CUTS, 4CUTS and SQR were created while the specimen was on the testing machine. Removing all the nucleus pulposus from the FSU on the testing machine was not possible. Therefore, the nucleotomy and the subsequent mechanical tests were performed later.

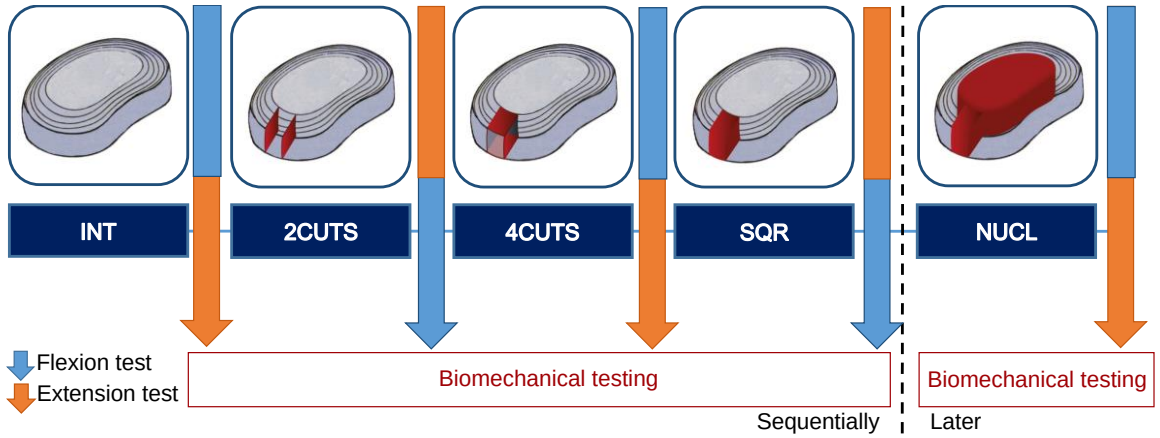


***Fig. A1.1 –*** *Different steps of treatment of the IVD (the red parts represent the cuts and the removed materials) and block diagram of the testing protocol: all the tests until SQR were performed at the same session, NUCL tests were performed later*

### *A1.2.3 Mechanical testing and measurement of displacements and strains with DIC*

The tests were sequentially performed, and the disc defect was increased after testing in both loading configurations (Fig. A1.1). The specimens were mechanically tested with the same protocol described in the main paper and undergoing the same loading configurations (Fig. 4.3 in the Chapter 4). For specimen #8, a load lower than the standard 50% BW was applied to avoid specimen damage. Axial load and displacement were acquired as in the main paper.

The displacements and strains were measured using Digital Image Correlation (DIC). The same hardware and parameters as in the main paper were used, the only difference being a slightly different grid spacing, which was set at 19 pixels to minimize the errors over the selected field of view.

### *A1.2.4 Data analysis and statistics*

The posterior disc height (PDH), ROM, stiffness parameters and the true principal strains over the specimen surface were extracted and computed from the last cycle of each test (Fig. 4.3), as described in the main paper. To reduce the inter-specimen variability influence, all the parameter values were normalized to the intact condition value, as in the main paper.

The normalized stiffness parameters, disc height, ROM, and median principal strains, both in flexion and in extension, were compared using the Friedman One-Way Repeated Measure Analysis of Variance by ranks. In case of significant trends ($p<0.05$), the individual conditions were compared using a Nemenyi post-hoc test.

## A1.3 Results

### *A1.3.1 Posterior disc height*

Posterior disc height was measured on DIC correlated images (Fig. 7.2). Normalized data showed a monotonic decrease from INT to NUCL both in flexion (-20% height) and extension (-23% height) (Table A1.2). The overall trend was statistically significant (Friedman test, p=0.036 in flexion and p=0.016 in extension). Relative comparison between the different disc conditions indicated that the only significant differences were between 4CUTS and NUCL in extension (Nemenyi test, p = 0.019). Large differences were observed also between nucleotomy and 2CUTS and 4CUTS in flexion and between nucleotomy and 2CUTS in extension, but they were poorly significant (Yemeni test, p=0.057).

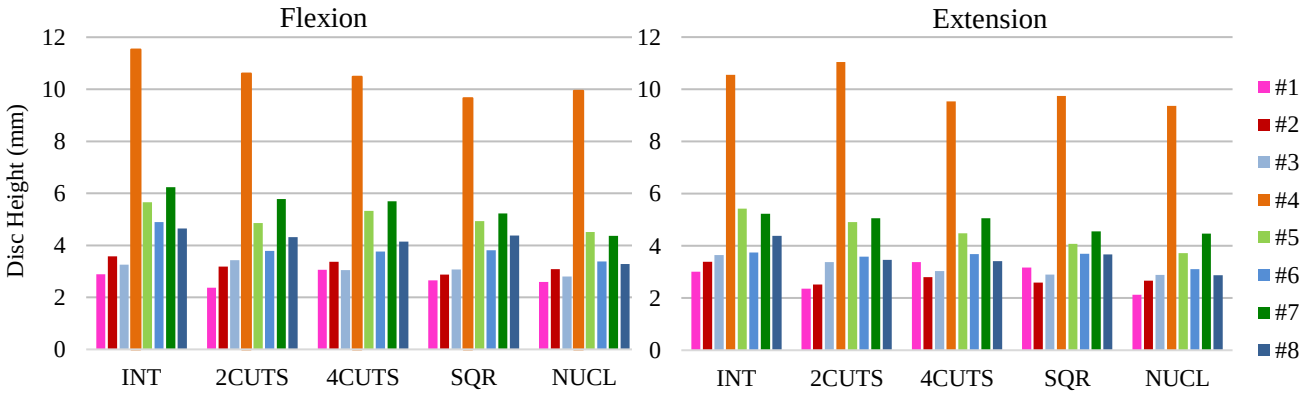


***Fig. A1.2 -*** *Disc height measured in the posterior region (PDH) in the different conditions, starting from intact (INT), and with progressive steps of incision (2CUTS, 4CUTS, SQR) in the annulus fibrosus, and after nucleotomy (NUCL). The mean values over three measurements for each of the eight specimens are plotted for flexion and extension*

***Table A1.2 –*** *Posterior disc height (PDH) in flexion and extension for the five conditions, normalized for each specimen with respect to the respective intact condition. The mean of eight specimens is reported. A value smaller than 1.00 indicates a decrease of the disc height with respect to the intact*

| | Posterior Disc Height | |
|---|---|---|
| | **Flexion** | **Extension** |
| *INT* | 1.00 | 1.00 |
| *2CUTS* | 0.90 | 0.89 |
| *4CUTS* | 0.92 | 0.91(*) |
| *SQR* | 0.87 | 0.87 |
| *NUCL* | 0.80 | 0.77 |

Note: The asterisks indicate where a statistically significant difference was found with respect to the intact (Nemenyi test) (*) p<0.05; (**) p<0.01; (***) p<0.001.

### *A1.3.2 Range of Motion*

From the measured three-dimensional motions, the component in the sagittal plane was extracted (Table A1.3). There was no statistically significant difference between the five conditions, both in flexion (Friedman test, p= 0.20) and in extension (Friedman test, p= 0.48). Despite this, a general increase of

the ROM due to the 2CUTS, and a decrease after nucleotomy were observed in flexion (Fig 7.3) and a generally decreasing trend of the ROM was observed in extension.

***Table A1.3 –*** *Range of motion (ROM) in flexion and extension for the five disc conditions, normalized for each specimen with respect to the respective intact conditions. The mean of eight specimens is reported. A value larger than 1.00 indicates an increased ROM with respect to the intact condition*

| | Range of motion | |
|---|---|---|
| | **Flexion** | **Extension** |
| *INT* | 1.00 | 1.00 |
| *2CUTS* | 1.09 | 0.98 |
| *4CUTS* | 1.03 | 1.16 |
| *SQR* | 1.04 | 1.06 |
| *NUCL* | 0.94 | 1.22 |

Note: The asterisks indicate where a statistically significant difference was found with respect to the intact (Nemenyi test) (*) p<0.05; (**) p<0.01; (***) p<0.001.

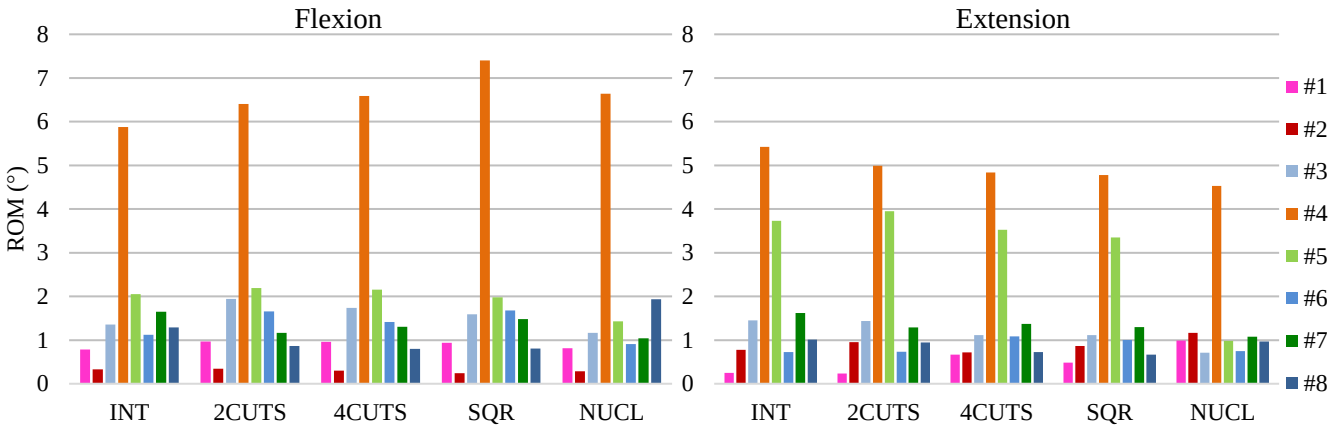


***Fig. A1.3 –*** *Range of Motion (ROM) in the different conditions, starting from intact (INT), and with progressive steps of incision (2CUTS, 4CUTS, SQR) in the annulus fibrosus, and after nucleotomy (NUCL). The median values over the five test repetitions are plotted for flexion and extension*

### *A1.3.3 Stiffness*

The load – displacement curves showed different trends between specimens and for each type of motion. In flexion, the load – displacement curves showed monotone or exponential shape for all specimens. An increase of the sigmoid-shape curve in the laxity zone was common to the specimens: usually the first part of the curve was linear. In extension, the specimens showed a linear behaviour except one specimen with an exponential one. Both in flexion and in extension, nucleotomy condition exhibited a comparable or lower slope respect to the others.

The transition displacement (***p***), transition load (***q***) and elastic stiffness (***E***) were extracted from the fit of the specimen loading curves (Table A1.4). Both in flexion and in extension, transition displacement showed similar and constant trend, except after nucleotomy (Friedman test: p= 0.26 in flexion, p= 0.68 in extension). The level of disc damage did not significantly impact transition load and elastic stiffness

(Friedman test: ***q***: p= 0.93 in flexion, p= 0.65 in extension; ***E***: p=0.75 in flexion, p= 0.60 in extension) (Fig. A1.4, A1.5, A1.6).

***Table A1.4 –*** *Transition displacement (p), transition load (q) and elastic stiffness (E) in the five discs damage conditions in flexion and in extension. The values were normalized against the intact condition. The mean between specimens is reported*

| | p | | q | | E | |
|---|---|---|---|---|---|---|
| | **Flexion** | **Extension** | **Flexion** | **Extension** | **Flexion** | **Extension** |
| *INT* | 1.00 | 1.00 | 1.00 | 1.00 | 1.00 | 1.00 |
| *2CUTS* | 0.77 | 0.95 | 0.77 | 1.18 | 0.96 | 1.02 |
| *4CUTS* | 0.75 | 0.88 | 0.75 | 0.93 | 0.97 | 1.03 |
| *SQR* | 0.67 | 0.88 | 0.69 | 0.96 | 1.02 | 1.06 |
| *NUCL* | 1.91 | 2.21 | 2.36 | 3.88 | 0.97 | 1.25 |

Note: The asterisks indicate where a statistically significant difference was found with respect to the intact (Nemenyi test) (*) p<0.05; (**) p<0.01; (***) p<0.001.

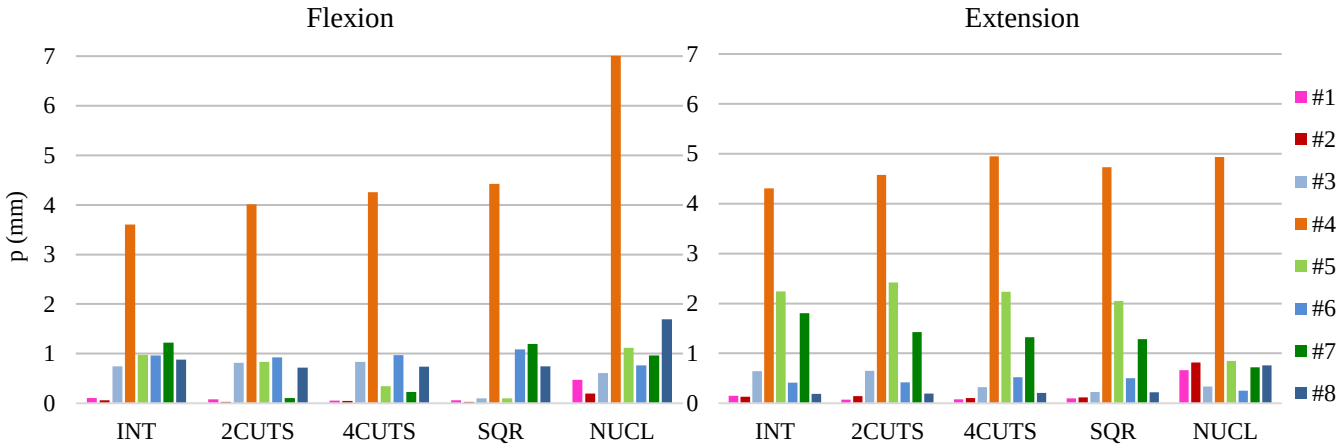


***Fig. A1.4 –*** *Transition displacement (p) in flexion and in extension in the different conditions, starting from intact (INT), and with progressive steps of incision (2CUTS, 4CUTS, SQR) in the annulus fibrosus, and after nucleotomy (NUCL). The median values over the five test repetitions are plotted for each of the eight specimens*

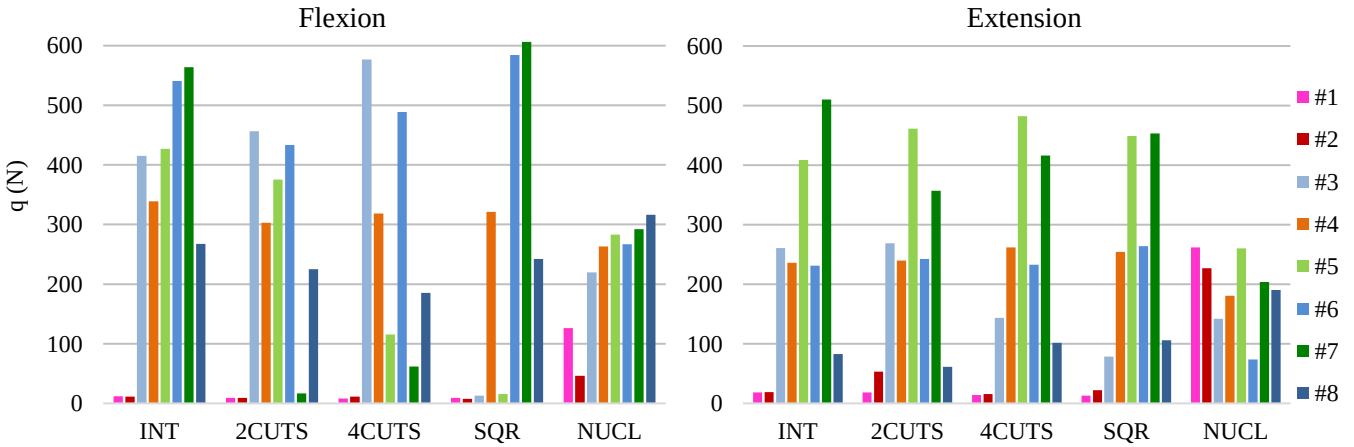


***Fig. A1.5 –*** *Transition load (q) in flexion and in extension in the different conditions, starting from intact (INT), and with progressive steps of incision (2CUTS, 4CUTS, SQR) in the annulus fibrosus, and after nucleotomy (NUCL). The median values over the five test repetitions are plotted for each of the eight specimens*

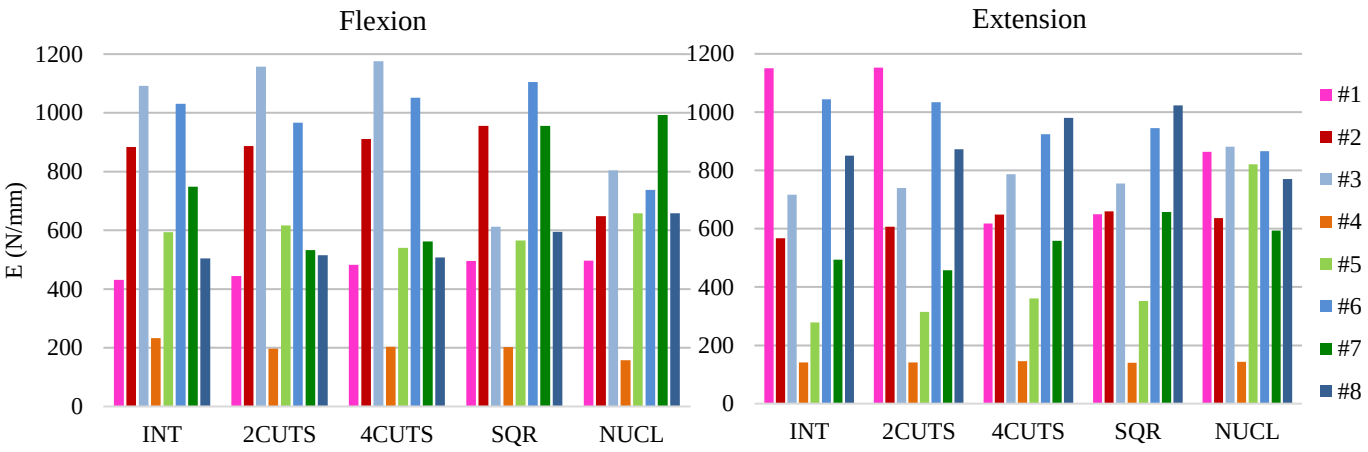


***Fig. A1.6 –*** *Elastic stiffness (E) in flexion and in extension in the different conditions, starting from intact (INT), and with progressive steps of incision (2CUTS, 4CUTS, SQR) in the annulus fibrosus, and after nucleotomy (NUCL). The median values over the five test repetitions are plotted for each of the eight specimens*

### *A1.3.4 Strain distribution*

The true maximum and minimum principal strains ($\varepsilon_1$ and $\varepsilon_2$) were extracted from all the tests at the peak load from the DIC correlations (Table A1.5). Both in flexion and in extension, the extreme strain values were in the disc while the strains in the vertebra were two orders of magnitude smaller. For both motions, the compressed part of the disc exhibited circumferential maximum and axial minimum principal strains whereas the stretched part of the disc showed circumferential maximum principal strains. In flexion, the maximum principal strain ($\varepsilon_1$) had a peak at mid-height of the disc, but did not follow any clear trend between disc conditions (Friedman test, p=0.79) (Fig. A1.7). With the increasing damage, the minimum principal strains ($\varepsilon_2$) located along the endplates in INT condition, migrated and concentrated covering the entire disc surface after NUCL condition (Friedman test, p= 0.06). In extension, most specimens showed constant maximum strains, and the extent of the lesion did not impact the maximum principal strain ($\varepsilon_1$) (Friedman test, p= 0.65) nor the minimum ones ($\varepsilon_2$) (p= 0.72).

***Table A1.5 –*** *Maximum and minimum principal strains ($\varepsilon_1$and $\varepsilon_2$) in flexion and in extension for the five conditions, normalized for each specimen with respect to the respective intact conditions. The mean of eight specimens is reported. A value larger than 1.00 indicates increased strains with respect to the intact condition*

| | $\varepsilon_1$ | | $\varepsilon_2$ | |
|---|---|---|---|---|
| | **Flexion** | **Extension** | **Flexion** | **Extension** |
| *INT* | 1.00 | 1.00 | 1.00 | 1.00 |
| *2CUTS* | 1.01 | 1.07 | 0.99 | 0.98 |
| *4CUTS* | 1.00 | 1.15 | 0.93 | 1.02 |
| *SQR* | 1.02 | 1.08 | 0.99 | 0.98 |
| *NUCL* | 0.92 | 0.97 | 3.68 | 1.48 |

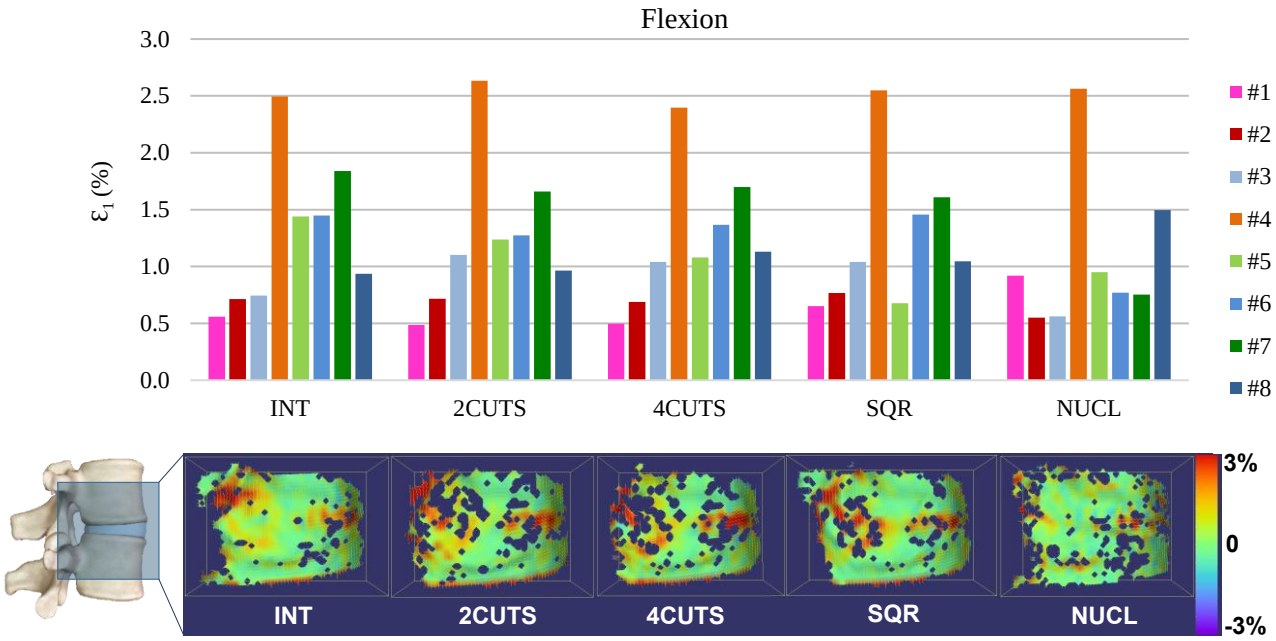


***Fig. A1.7 –*** *Top: maximum principal strain (Ɛ1), starting from intact (INT), and with progressive steps of incision (2CUTS, 4CUTS, SQR) in the annulus, and after nucleotomy (NUCL). The median over the five test repetitions is plotted for flexion for the eight specimens. Bottom: typical distribution of Ɛ1 on the disc surface in flexion. The dark spots are local non-correlated areas*

## A1.4 Discussion and conclusion

The posterior disc height was not affected by annulus damages between INT and SQR conditions, but PDH decreased after nucleotomy, confirming the clinical observations [20] and the results reported by Showalter *et al* [122]. The sequential execution of disc damage did not significantly impact the spine biomechanics in terms of range of motion, stiffness parameters and strains.

Similar to this study, Kuroki *et al.*, could not detect any significant difference in the flexion and extension range of motion after nucleotomy through a rectangular window in the annulus [9]. Lee *et al.* observed statistically significant differences between the range of motion in the intact and in the damaged disc, despite similar absolute values [124]. The variations of stiffness of the present study are in agreement with Green *et* Adams, as they reported that collagen fibres do not need to be continuous to reinforce the annulus and that the fibre-matrix interactions make a large contribution to stiffness [125]. In addition, Michalek *et* Iatridis, concluded in 2012 that, the lack of changes in bending stiffness suggests that acute annular tears are not sufficient to induce off-axis motion and instability [71]. Few studies investigated the strain distribution on the disc surface under the same condition. Ruspi *et al.* found that different portions of the intervertebral disc were subjected to compression or tension with different orientation of the strains [77]. The same was observed in this study: in the compressed side of the disc the minimum strains were axial, while circumferential maximum strains were located on the stretched side of the disc.

In conclusion, this study has shown that sequential damages of the annulus fibrosus does not significantly alter the spine biomechanics in terms of range of motion, stiffness, and strain distribution. The main effect caused by nucleotomy was the posterior disc height reduction due to the lack of support caused by the nucleus loss. The present findings therefore confirm the suitability of the model adopted in the main paper to simulate nucleotomy.

# Appendix 2:
# *In vivo* assessment of the cement distribution after percutaneous cement discoplasty

from the manuscript:

**A novel three-dimensional volumetric method to measure indirect decompression after percutaneous cement discoplasty**

P. E. Eltes, L. Kiss, F. Bereczki, Z. Szoverfi, C. Techens, G. Jakab, B. Hajnal, P. P. Varga, A. Lazary

Published in: *Journal of Orthopaedic Translation, 2021, 28: 131–139, https://doi.org/10.1016/j.jot.2021.02.003*



*The following sections are extracted from a published study I collaborated to. It is included for completeness, to fully describe the methods applied, the parts of the work I performed being included in Chapter 4.*

## A2.1 Abstract

Percutaneous cement discoplasty (PCD) is a minimally invasive surgical option to treat patients who suffer from the consequences of advanced disc degeneration. As the current two-dimensional methods can inappropriately measure the difference in the complex 3D anatomy of the spinal segment, our aim was to develop and apply a volumetric method to measure the geometrical change in the surgically treated segments.

Prospective clinical and radiological data of 10 patients who underwent single- or multilevel PCD was collected. Pre- and postoperative CT scan-based 3D reconstructions were performed. The injected PMMA (Polymethylmethacrylate) induced lifting of the cranial vertebra and the following volumetric change was measured by subtraction of the geometry of the spinal canal from a pre- and postoperatively predefined cylinder. The associations of the PMMA geometry and the volumetric change of the spinal canal with clinical outcome were determined.

Change in the spinal canal volume (ΔV) due to the surgery proved to be significant (mean $\Delta V = 2266.5 \pm 1172.2$ mm$^3$, $n = 16$; $p = 0.0004$). A significant, positive correlation was found between ΔV, the volume and the surface of the injected PMMA. A strong, significant association between pain intensity (low back and leg pain) and the magnitude of the volumetric increase of the spinal canal was shown ($\rho = 0.772$, $p = 0.009$ for LBP and $\rho = 0.693$, $p = 0.026$ for LP).

The developed method is accurate, reproducible, and applicable for the analysis of any other spinal surgical method. The volume and surface area of the injected PMMA have a predictive power on the extent of the indirect spinal canal decompression. The larger the ΔV the higher clinical benefit was achieved with the PCD procedure.

The developed method has the potential to be integrated into clinical software's to evaluate the efficacy of different surgical procedures based on indirect decompression effect such as PCD, anterior lumbar interbody fusion (ALIF), lateral lumbar interbody fusion (LLIF), oblique lumbar interbody fusion (OLIF), extreme lateral interbody fusion (XLIF). The intraoperative use of the method will allow the surgeon to respond if the decompression does not reach the desired level.

## A2.2 Introduction

The intervertebral disc degeneration (IDD) leads to biomechanical and structural changes of the spine [82]. The degree of IDD can be defined by the MRI based Pfirrmann grading system [17], where the terminal disc degeneration (Pfirrmann V) is characterised by total disorganisation of the intervertebral tissue, the complete resorption of the nucleus pulposus and in many cases causing a vacuum phenomenon [24], [83], [84]. Discs act as transmitting units and shock absorbers, distributing the load of body weight and muscle activity through the spinal column [126]; therefore, degeneration related structural changes will lead to biomechanical dysfunctions [85], such as segmental instability. Decreasing disc height will generate continuously diminishing spinal canal dimensions which further deteriorate by dynamic changes of the neuroforamen due to movement. Lumbar spinal stenosis can lead to the development of chronic radiculopathy causing local and irradiating pain typically provoked by axial loading [23]. Surgical treatment possibilities of segmental instability in elderly patients are limited due to patients' age, comorbidities and frailty. Therefore, minimally invasive surgical (MIS) procedures have become the preferred options. Percutaneous cement discoplasty (PCD) is a MIS procedure, where the vacuum space in the intervertebral disc is filled out with percutaneously injected PMMA (Polymethylmethacrylate), which provides a segmental stabilizing effect and indirect decompression of the neuronal elements due to the increase of the spinal canal dimensions. The technical details, the clinical effect and safety issues of the procedure have been previously published and the usage of the technique has also been supported by a prospective radiological study [20], [21], [33], [36].

Even though the spinal canal is a complex 3D geometry, the common description of its dimensions and the evaluation of the indirect decompression effect are based on 2D parameters. Measurements of disc height, foramen height/diameter, foramen cross-sectional area, central canal diameter, central canal cross-sectional area, or segmental lordosis angle therefore can possibly be biased [127]–[129]. However, the changes in the spinal canal (central canal and neuroforamen) dimensions have been quantified by only a few authors so far [130], [131], because of the challenging methodological issues.

Navarro [130] in his study reveals the usefulness of advanced computational methods by demonstrating that volumetric analysis of the anatomical change can better predict the clinical outcome of Extreme Lateral Interbody Fusion (XLIF) compared to conventional 2D methods [132], [133]. The developed computer algorithm by Gates and his colleagues [131] was used to investigate patient who underwent lateral retroperitoneal transpsoas interbody fusion (LIF) based on the pre and postoperative magnetic resonance images (MRI). To accurately calculate the changes of the spinal canal after a surgical procedure such as PCD, we aimed to develop a generalisable method based on patient-specific volumetric measurements, using 3D computational methods.

## A2.3 Methods

### *A2.3.1 Clinical cohort and CT scan acquisition*

We performed a retrospective analysis of prospectively collected data involving 10 consecutive patients (74 ± 7.7 years old), who underwent primary single or multilevel PCD at a tertiary care spine referral centre (Table 4.1). All patients suffered from low back pain and leg pain, due to advanced disc degeneration, and forward bending of the lumbar spine decreased the pain level, during physical examination.

All presented operative procedures were performed by a single surgeo***n*** (GJ). Preoperative (preop), and postoperative (postop) 6-month follow-up results were collected and analysed using the Oswestry Disability Index (ODI) for spine specific function and with the visual analogue scale (VAS) for leg pain (LP) and low back pain (LBP). Patients participating in the study were informed and their written consent was obtained. The study was approved by the National Ethics Committee of Hungary, the National Institute of Pharmacy and Nutrition (reference number: OGYEI/163–4/2019). Quantitative Computed Tomography (QCT) scans were performed pre- and postoperatively, with a Hitachi Presto CT machine using an inline calibration phantom, and a protocol previously defined in the MySpine study (ICT-2009.5.3 VPH, Project ID: 269909) with an intensity of 225 mA and voltage of 120 kV [89], [90]. Images were reconstructed with a voxel size of 0.6x0.6x0.6 mm3. Based on the QCT images, Hounsfield Units can be converted into bone mineral density (BMD) equivalent values, which are necessary for creating finite element (FE) models. In this study the QCT images were used as conventional CT images without any conversion. The data were exported from the hospital's PACS into DICOM file format. To comply with the ethical approval and the patient data protection, anonymization of the DICOM data was performed using the freely available Clinical Trial Processor software (Radiological Society of North America, https://www.rsna.org/ctp.aspx) [91].

### *A2.3.2 Definition of pre- and postop motion segments' 3D geometry*

In order to establish the 3D vertebral geometry of the pre- and postop motion segments and the injected polymethyl methacrylate (PMMA) geometry, a segmentation process was performed on the 2D CT images [133]. 16 motion segments were treated and analysed in cohort of 10 patients. The thresholding algorithm and manual segmentation tools (erase, paint, fill etc.) in Mimics® image analysis software (Mimics Research, Mimics Innovation Suite v21.0, Materialise, Leuven, Belgium) were used. (Fig. A.1). During the segmentation process the bone volume was first separated from the surrounding soft tissue by thresholding of the Hounsfield units' levels. The resulting masks (group of voxels) where homogenously filled by preserving the outer contour of the geometrical border in 2D. From the mask, a triangulated surface mesh was automatically generated. On the 3D geometries surface smoothing was carried out (iteration: 6, smooth factor: 0.7, with shrinkage compensation). Furthermore, uniform

remeshing process was applied (target triangle edge length 0.6 mm, sharp edge preservation, sharp edge angle 60°) for all the vertebrae and PMMA geometries. To evaluate the accuracy of the segmentation process, we calculated the Dice Similarity Index (DSI) [89], [90]. The DSI quantifies the relative volume overlap between two segmentation procedures as follows: $DSI = \frac{2*V(I_1 \cap I_2)}{V(I_1)+V(I_2)}$, $V$ is the volume of the voxels inside the binary mask (number of voxels multiplied with the voxel size; in $mm^3$), and $I_1$ and $I_2$ are the binary masks from two segmentation processes (performed by two investigators (I), 1 and 2). The DSI values range between 0 - 1, where 1 denotes a perfect match. Accuracy of the vertebral geometry segmentation was evaluated by a random (Microsoft Office Professional Plus 2016, Excel, RANDBETWEEN function) selection of 6 preoperative and 6 postoperative vertebral geometries. All 12 vertebras were segmented by the two investigators ($I_1$ and $I_2$) and the two segmentations were compared after then the DSI was defined. The PMMA segmentation evaluation was done by repeating all the 16 measurements by $I_2$ and then the DSI was calculated.

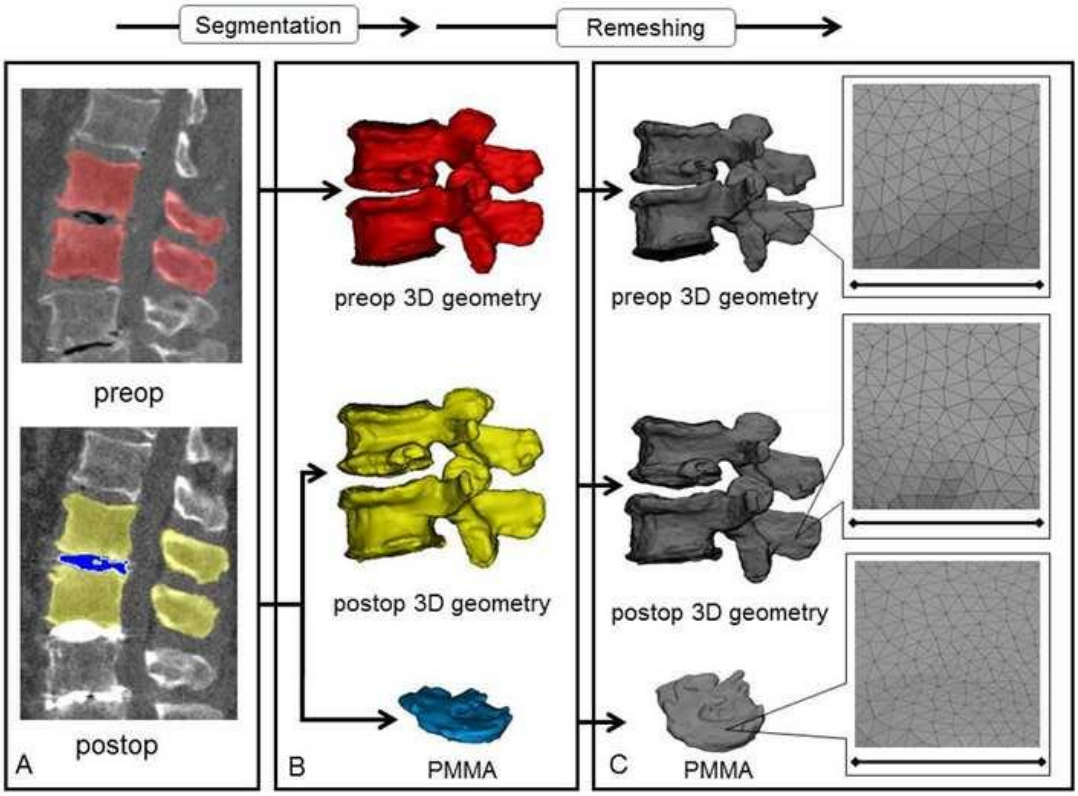


***Fig. A2.1 -*** *3D geometry definition of pre- and postoperative motion segment geometries and of the injected PMMA geometry. A: During the segmentation process the bone volume is first separated from the surrounding soft tissue by thresholding of the Hounsfield units' levels of the 2D CT images (sagittal view). The resulting red, yellow and blue masks represent the volumes of the pre- and postoperative vertebrae, and the PMMA respectively. B: From the mask, a triangulated surface mesh is generated, and smoothing is applied (iteration: 6, smooth factor: 0.7, with shrinkage compensation). C: Uniform remeshing was applied (target triangle edge length: 0.6 mm, sharp edge preservation, sharp edge angle: 60). Scale bar length is 5 mm*

### *A2.3.3 PMMA geometry visualisation and thickness measurement*

The 3D geometry of the intervertebral PMMA for the 16 treated motion segments were defined during the segmentation process by a uniformly remeshed triangulated surface mesh (Fig. 5.1). The surface mesh defines the geometry and determines the surface and volume of the investigated object. Thickness measurement was performed and visualised by using contour plots by applying the 3-matic® software (Mimics Innovation Suite v21.0, Materialise, Leuven, Belgium). Thickness was defined at the level of every triangle element of the surface mesh as the perpendicular distance from the element midpoint to the other wall (surface) of the geometry.

## A2.4 Results

### *A2.4.1 Evaluation of the segmentation procedure*

To evaluate the accuracy of our segmentation process we used the DSI for 6 randomly selected geometries (Appendix 5.6.1). The obtained DSI values for both pre- and postoperative geometries were $0.96 \pm 0.02$ and $0.90 \pm 0.07$, respectively ($n = 6$) and showed negligible variance, thus indicating a high accuracy of our segmentation method for all segmented geometries [134]. Next, to assess the injected PMMA cement geometries we first evaluated the PMMA geometry distribution over the caudal vertebra endplate of the motion segments visually in the same 3D view (Fig. 5.4). Because the degenerative processes are not only age dependent, but also rely on the musculoskeletal status of each patient, the variations of intervertebral disc degeneration will be widely different. Accordingly, we found that the injected volumes are arranged patient-specifically to widely differing 3D shapes (Fig. 5.4). Because of this large variance, is unlikely for a random subset to be representative of the whole; therefore, we chose to validate the segmentation process on all injected PMMA volumes instead. We calculated the DSI as above described for the 16 segmented geometries (Appendix 5.6.2). Again, the DSI values were very high for all segmented geometries (mean: $0.93 \pm 0.035$, $n = 16$) demonstrating the precision of our segmentation method also in the case of the injected PMMA geometries.

## A2.5 Conclusion

Patient specific computational methods provide accurate information about the unique and complex geometrical/anatomical relations caused by intervertebral disc degeneration. In the present study, the 3D geometrical change of the spinal canal and the indirect decompression effect of PCD, a minimally invasive surgical procedure, was investigated with a new computational 3D volumetric measurement method. Significant associations have been explored between indirect decompression and clinical improvement. Due to its relative simplicity, we suggest the application of our measurement method for

the scientific and clinical analysis of other surgical procedures based on indirect decompression effect such as: ALIF, LLIF, OLIF, XLIF.

## A2.6 Appendix

***Appendix A2.6.1 -*** *Evaluation of the accuracy of the segmentation process by two investigators ($I_1$, $I_2$) via Dice Similarity Index (DSI)*

| **preop** | | | **postop** | | |
|---|---|---|---|---|---|
| ***Patient ID*** | ***Vertebra*** | ***DSI*** | ***Patient ID*** | ***Vertebra*** | ***DSI*** |
| **P01** | L4 | 0.97 | P01 | L5 | 0.96 |
| **P02** | L3 | 0.98 | P02 | L4 | 0.83 |
| **P04** | L4 | 0.96 | P05 | L5 | 0.96 |
| **P06** | L2 | 0.99 | P07 | L4 | 0.91 |
| **P08** | L3 | 0.96 | P08 | L5 | 0.81 |
| **P09** | L1 | 0.93 | P09 | T12 | 0.96 |
| **mean DSI** 0.96 ±0.02 | | | **mean DSI** 0.90 ±0.07 | | |

***Appendix A2.6.2 -*** *Dice Similarity Index (DSI) values for the segmented PMMA geometries by two investigators ($I_1$, $I_2$)*

| **DSI PMMA geometry** | | |
|---|---|---|
| ***Patient ID*** | ***Treated Segment*** | ***DSI*** |
| **P01** | L4-L5 | 0.90 |
| **P02** | L2-L3 | 0.94 |
| | L3-L4 | 0.91 |
| | L4-L5 | 0.92 |
| **P03** | L5-S1 | 0.89 |
| **P04** | L3-L4 | 0.96 |
| **P05** | L5-S1 | 0.95 |
| **P06** | L1-L2 | 0.85 |
| **P07** | L2-L3 | 0.97 |
| | L3-L4 | 0.97 |
| | L4-L5 | 0.90 |
| **P08** | L3-L4 | 0.95 |
| | L4-L5 | 0.96 |
| **P09** | Th12-L1 | 0.94 |
| | L1-L2 | 0.91 |
| **P10** | L1-L2 | 0.96 |
| **mean DSI** 0.93 ±0.035 | | |

# Bibliography


[1] N. Newell, J. Little, A. Christou, M. Adams, C. Adam, and S. Masouros, 'Biomechanics of the human intervertebral disc: A review of testing techniques and results', *J. Mech. Behav. Biomed. Mater.*, vol. 69, pp. 420–434, May 2017, doi: 10.1016/j.jmbbm.2017.01.037.

[2] I. M. Shapiro and M. V. Risbud, 'Introduction to the Structure, Function, and Comparative Anatomy of the Vertebrae and the Intervertebral Disc', in *The Intervertebral Disc: Molecular and Structural Studies of the Disc in Health and Disease*, I. M. Shapiro and M. V. Risbud, Eds. Vienna: Springer, 2014, pp. 3–15. doi: 10.1007/978-3-7091-1535-0_1.

[3] H. Yamada, *Strength of biological materials*. Baltimore: Williams & Wilkins, 1970.

[4] M. A. Adams and P. J. Roughley, 'What is Intervertebral Disc Degeneration, and What Causes It?', *Spine*, vol. 31, no. 18, pp. 2151–2161, Aug. 2006, doi: 10.1097/01.brs.0000231761.73859.2c.

[5] G. Armbrecht *et al.*, 'Degenerative inter-vertebral disc disease osteochondrosis intervertebralis in Europe: prevalence, geographic variation and radiological correlates in men and women aged 50 and over', *Rheumatology*, vol. 56, no. 7, pp. 1189–1199, Jul. 2017, doi: 10.1093/rheumatology/kex040.

[6] C. S. Parenteau, E. C. Lau, I. C. Campbell, and A. Courtney, 'Prevalence of spine degeneration diagnosis by type, age, gender, and obesity using Medicare data', *Sci. Rep.*, vol. 11, no. 1, p. 5389, Mar. 2021, doi: 10.1038/s41598-021-84724-6.

[7] Y. Wang and M. C. Battié, 'Epidemiology of Lumbar Disc Degeneration', in *The Intervertebral Disc: Molecular and Structural Studies of the Disc in Health and Disease*, I. M. Shapiro and M. V. Risbud, Eds. Vienna: Springer, 2014, pp. 139–156. doi: 10.1007/978-3-7091-1535-0_9.

[8] D. Samartzis, J. Karppinen, F. Mok, D. Y. T. Fong, K. D. K. Luk, and K. M. C. Cheung, 'A Population-Based Study of Juvenile Disc Degeneration and Its Association with Overweight and Obesity, Low Back Pain, and Diminished Functional Status', *JBJS*, vol. 93, no. 7, pp. 662–670, Apr. 2011, doi: 10.2106/JBJS.I.01568.

[9] '6. Priority diseases and reasons for inclusion', in *WHO | Priority Medicines for Europe and the World Update Report*, 2013. [Online]. Available: https://www.who.int/medicines/areas/priority_medicines/Ch6_24LBP.pdf

[10] P.-P. A. Vergroesen *et al.*, 'Mechanics and biology in intervertebral disc degeneration: a vicious circle', *Osteoarthritis Cartilage*, vol. 23, no. 7, pp. 1057–1070, Jul. 2015, doi: 10.1016/j.joca.2015.03.028.

[11] C.-Q. Zhao, L.-M. Wang, L.-S. Jiang, and L.-Y. Dai, 'The cell biology of intervertebral disc aging and degeneration', *Ageing Res. Rev.*, vol. 6, no. 3, pp. 247–261, Oct. 2007, doi: 10.1016/j.arr.2007.08.001.

[12] J. Antoniou *et al.*, 'The human lumbar intervertebral disc: evidence for changes in the biosynthesis and denaturation of the extracellular matrix with growth, maturation, ageing, and degeneration.', *J. Clin. Invest.*, vol. 98, no. 4, pp. 996–1003, Aug. 1996, doi: 10.1172/JCI118884.

[13] P. J. Roughley, L. I. Melching, T. F. Heathfield, R. H. Pearce, and J. S. Mort, 'The structure and degradation of aggrecan in human intervertebral disc', *Eur. Spine J.*, vol. 15, no. 3, pp. 326–332, Aug. 2006, doi: 10.1007/s00586-006-0127-7.

[14] P.-P. A. Vergroesen, A. J. van der Veen, B. J. van Royen, I. Kingma, and T. H. Smit, 'Intradiscal pressure depends on recent loading and correlates with disc height and compressive stiffness', *Eur. Spine J.*, vol. 23, no. 11, pp. 2359–2368, Nov. 2014, doi: 10.1007/s00586-014-3450-4.

[15] P. Brinckmann and H. Grootenboer, 'Change of disc height, radial disc bulge, and intradiscal pressure from discectomy. An in vitro investigation on human lumbar discs', *Spine*, vol. 16, no. 6, pp. 641–646, Jun. 1991, doi: 10.1097/00007632-199106000-00008.

[16] K. Olmarker, 'Back Pain and Disc Degeneration: Are They Really Linked?', in *The Intervertebral Disc: Molecular and Structural Studies of the Disc in Health and Disease*, I. M. Shapiro and M. V. Risbud, Eds. Vienna: Springer, 2014, pp. 261–275. doi: 10.1007/978-3-7091-1535-0_16.

[17] C. W. Pfirrmann, A. Metzdorf, M. Zanetti, J. Hodler, and N. Boos, ‘Magnetic resonance classification of lumbar intervertebral disc degeneration’, *Spine*, vol. 26, no. 17, pp. 1873–1878, Sep. 2001, doi: 10.1097/00007632-200109010-00011.
[18] Y. Yanagawa *et al.*, ‘Vacuum phenomenon’, *Emerg. Radiol.*, vol. 23, no. 4, pp. 377–382, Aug. 2016, doi: 10.1007/s10140-016-1401-6.
[19] A. A. Momin and M. P. Steinmetz, ‘Evolution of Minimally Invasive Lumbar Spine Surgery’, *World Neurosurg.*, vol. 140, pp. 622–626, Aug. 2020, doi: 10.1016/j.wneu.2020.05.071.
[20] P. P. Varga, G. Jakab, I. B. Bors, A. Lazary, and Z. Szövérfi, ‘Experiences with PMMA cement as a stand-alone intervertebral spacer: Percutaneous cement discoplasty in the case of vacuum phenomenon within lumbar intervertebral discs’, *Orthopade*, vol. 44 Suppl 1, pp. S1-7, Nov. 2015, doi: 10.1007/s00132-014-3060-1.
[21] L. Kiss, P. P. Varga, Z. Szoverfi, G. Jakab, P. E. Eltes, and A. Lazary, ‘Indirect foraminal decompression and improvement in the lumbar alignment after percutaneous cement discoplasty’, *Eur. Spine J.*, Apr. 2019, doi: 10.1007/s00586-019-05966-7.
[22] K. Yamada *et al.*, ‘Targeted Therapy for Low Back Pain in Elderly Degenerative Lumbar Scoliosis: A Cohort Study’, *Spine*, vol. 41, no. 10, pp. 872–879, May 2016, doi: 10.1097/BRS.0000000000001524.
[23] S. Y. Lee, T.-H. Kim, J. K. Oh, S. J. Lee, and M. S. Park, ‘Lumbar Stenosis: A Recent Update by Review of Literature’, *Asian Spine J.*, vol. 9, no. 5, pp. 818–828, Sep. 2015, doi: 10.4184/asj.2015.9.5.818.
[24] K. Morishita, Y. Kasai, and A. Uchida, ‘Clinical Symptoms of Patients With Intervertebral Vacuum Phenomenon’, *The Neurologist*, vol. 14, no. 1, pp. 37–39, Jan. 2008, doi: 10.1097/NRL.0b013e3180dc9992.
[25] K. Roosen, ‘[Bone cement as replacement material of cervical disks]’, *Fortschr. Med.*, vol. 100, no. 45, pp. 2120–2126, Dec. 1982.
[26] C. B. Bärlocher, A. Barth, J. K. Krauss, R. Binggeli, and R. W. Seiler, ‘Comparative evaluation of microdiscectomy only, autograft fusion, polymethylmethacrylate interposition, and threaded titanium cage fusion for treatment of single-level cervical disc disease: a prospective randomized study in 125 patients’, *Neurosurg. Focus*, vol. 12, no. 1, pp. 1–7, Jan. 2002, doi: 10.3171/foc.2002.12.1.5.
[27] M. C. Korinth, A. Krüger, M. F. Oertel, and J. M. Gilsbach, ‘Posterior foraminotomy or anterior discectomy with polymethyl methacrylate interbody stabilization for cervical soft disc disease: results in 292 patients with monoradiculopathy’, *Spine*, vol. 31, no. 11, pp. 1207–1214; discussion 1215-1216, May 2006, doi: 10.1097/01.brs.0000217604.02663.59.
[28] H.-J. Wilke, A. Kettler, and L. Claes, ‘Primary stabilizing effect of interbody fusion devices for the cervical spine: an in vitro comparison between three different cage types and bone cement’, *Eur. Spine J.*, vol. 9, no. 5, pp. 410–416, Oct. 2000, doi: 10.1007/s005860000168.
[29] H. J. Wilke, A. Kettler, C. Goetz, and L. Claes, ‘Subsidence Resulting From Simulated Postoperative Neck Movements: An In Vitro Investigation With a New Cervical Fusion Cage’, *Spine*, vol. 25, no. 21, pp. 2762–2770, Nov. 2000.
[30] A. Kettler, H.-J. Wilke, and L. Claes, ‘Effects of neck movements on stability and subsidence in cervical interbody fusion: an in vitro study’, *J. Neurosurg. Spine*, vol. 94, no. 1, pp. 97–107, Jan. 2001, doi: 10.3171/spi.2001.94.1.0097.
[31] B. Wang, L. Shan, and D. Hao, ‘Letter to the Editor concerning “Percutaneous cement discoplasty for the treatment of advanced degenerative disk disease in elderly patients” by Sola C, Camino Willhuber G, Kido G et al. Eur Spine J (2018): Doi 10.1007/s00586-018-5547-7’, *Eur. Spine J.*, vol. 27, no. 7, pp. 1665–1666, Jul. 2018, doi: 10.1007/s00586-018-5642-9.
[32] G. Camino Willhuber and C. Sola, ‘Answer to the Letter to the Editor of Biao Wang et al. concerning “Percutaneous cement discoplasty for the treatment of advanced degenerative disk disease in elderly patients” by Sola C, Camino Willhuber G, Kido G et al. Eur Spine J (2018): doi:10.1007/s00586-018-5547-7’, *Eur. Spine J.*, vol. 27, no. 7, pp. 1667–1668, Jul. 2018, doi: 10.1007/s00586-018-5643-8.
[33] C. Sola *et al.*, ‘Percutaneous cement discoplasty for the treatment of advanced degenerative disk disease in elderly patients’, *Eur. Spine J.*, Mar. 2018, doi: 10.1007/s00586-018-5547-7.

[34] G. Camino Willhuber *et al.*, 'Development of a New Therapy-Oriented Classification of Intervertebral Vacuum Phenomenon With Evaluation of Intra- and Interobserver Reliabilities', *Glob. Spine J.*, p. 2192568220913006, Mar. 2020, doi: 10.1177/2192568220913006.
[35] K. Yamada *et al.*, 'Long-term outcome of targeted therapy for low back pain in elderly degenerative lumbar scoliosis', *Eur. Spine J.*, Mar. 2021, doi: 10.1007/s00586-021-06805-4.
[36] G. C. Willhuber *et al.*, 'Percutaneous Cement Discoplasty for the Treatment of Advanced Degenerative Disc Conditions: A Case Series Analysis':, *Glob. Spine J.*, Sep. 2019, doi: 10.1177/2192568219873885.
[37] G. Camino-Willhuber *et al.*, 'Percutaneous Cement Discoplasty for Degenerative Low Back Pain with Vacuum Phenomenon: A Multicentric Study with a Minimum of 2 Years of Follow-Up', *World Neurosurg.*, Aug. 2021, doi: 10.1016/j.wneu.2021.08.042.
[38] P. E. Eltes *et al.*, 'A novel three-dimensional volumetric method to measure indirect decompression after percutaneous cement discoplasty', *J. Orthop. Transl.*, vol. 28, pp. 131–139, May 2021, doi: 10.1016/j.jot.2021.02.003.
[39] C. Techens, M. Palanca, P. E. Éltes, Á. Lazáry, and L. Cristofolini, 'Testing the impact of discoplasty on the biomechanics of the intervertebral disc with simulated degeneration: An in vitro study', *Med. Eng. Phys.*, vol. 84, pp. 51–59, Oct. 2020, doi: 10.1016/j.medengphy.2020.07.024.
[40] L. Yang *et al.*, 'Mineralized collagen-modified PMMA cement enhances bone integration and reduces fibrous encapsulation in the treatment of lumbar degenerative disc disease', *Regen. Biomater.*, vol. 7, no. 2, pp. 181–193, Mar. 2020, doi: 10.1093/rb/rbz044.
[41] R. Rasik Patel, 'Does Patient-Specific Implant Design Reduce Subsidence Risk in Lumbar Interbody Fusion? A Bottom up Analysis of Methods to Reduce Vertebral Endplate Stress - ProQuest', University of Colorado, 2018. Accessed: Oct. 11, 2021. [Online]. Available: https://www.proquest.com/openview/92cfead951fba3229030648f0c55ec1b/1?pq-origsite=gscholar&cbl=18750&diss=y
[42] I. Oda, K. Abumi, B.-S. Yu, H. Sudo, and A. Minami, 'Types of Spinal Instability That Require Interbody Support in Posterior Lumbar Reconstruction: An In Vitro Biomechanical Investigation. [Miscellaneous Article]', *Spine*, vol. 28, no. 14, pp. 1573–1580, Jul. 2003.
[43] P. Moissonnier, L. Desquilbet, D. Fitzpatrick, and F. Bernard, 'Radiography and biomechanics of sixth and seventh cervical vertebrae segments after disc fenestration and after insertion of an intervertebral body spacer', *Vet. Comp. Orthop. Traumatol.*, vol. 27, no. 1, pp. 54–61, 2014, doi: 10.3415/VCOT-11-11-0159.
[44] X. Li, Y. Song, and H. Duan, 'Reconstruction of Segmental Stability of Goat Cervical Spine with Poly (D, L-lactic acid) Cage', *Orthop. Surg.*, vol. 7, no. 3, pp. 266–272, 2015, doi: 10.1111/os.12192.
[45] F. Kandziora, R. Pflugmacher, M. Scholz, T. D. Eindorf, K. J. Schnake, and N. P. Haas, 'Bioabsorbable Interbody Cages in a Sheep Cervical Spine Fusion Model.', *Spine*, vol. 29, no. 17, pp. 1845–1855, Sep. 2004.
[46] F. Kandziora *et al.*, 'Comparison of BMP-2 and combined IGF-I/TGF-ß1 application in a sheep cervical spine fusion model', *Eur. Spine J.*, vol. 11, no. 5, pp. 482–493, Oct. 2002, doi: 10.1007/s00586-001-0384-4.
[47] Y. Gu, Z. Yao, L. Jia, J. Qi, and J. Wang, 'In vivo experimental study of hat type cervical intervertebral fusion cage (HCIFC)', *Int. Orthop.*, vol. 34, no. 8, pp. 1251–1259, Dec. 2010, doi: 10.1007/s00264-010-0978-8.
[48] Z. Chunguang *et al.*, 'Evaluation of Bioabsorbable Multiamino Acid Copolymer/α-Tri-Calcium Phosphate Interbody Fusion Cages in a Goat Model':, *Spine*, vol. 36, no. 25, pp. E1615–E1622, Dec. 2011, doi: 10.1097/BRS.0b013e318210ca32.
[49] M. J. Allen, Y. Hai, N. R. Ordway, C.-K. Park, B. Bai, and H. A. Yuan, 'Assessment of a synthetic anterior cervical ligament in a spinal fusion model in sheep', *Spine J.*, vol. 2, no. 4, pp. 261–266, Jul. 2002, doi: 10.1016/S1529-9430(02)00188-2.
[50] S. E. Emery, D. A. Fuller, and S. D. Stevenson, 'Ceramic Anterior Spinal Fusion: Biologic and Biomechanical Comparison in a Canine Model. [Miscellaneous Article]', *Spine*, vol. 21, no. 23, pp. 2713–2719, Dec. 1996.

[51] H.-J. Wilke, F. Heuer, C. Neidlinger-Wilke, and L. Claes, 'Is a collagen scaffold for a tissue engineered nucleus replacement capable of restoring disc height and stability in an animal model?', *Eur. Spine J.*, vol. 15, no. 3, pp. 433–438, Aug. 2006, doi: 10.1007/s00586-006-0177-x.
[52] G. Vadalà *et al.*, 'A Nucleotomy Model with Intact Annulus Fibrosus to Test Intervertebral Disc Regeneration Strategies', *Tissue Eng. Part C Methods*, vol. 21, no. 11, pp. 1117–1124, 2015, doi: http://dx.doi.org/10.1089/ten.tec.2015.0086.
[53] G. Vadalà *et al.*, 'The Transpedicular Approach As an Alternative Route for Intervertebral Disc Regeneration':, *Spine*, vol. 38, no. 6, pp. E319–E324, Mar. 2013, doi: 10.1097/BRS.0b013e318285bc4a.
[54] M. Shea, T. Y. Takeuchi, R. H. Wittenberg, A. A. White, and W. C. Hayes, 'A Comparison of the Effects of Automated Percutaneous Diskectomy and Conventional Diskectomy on Intradiscal Pressure, Disk Geometry, and Stiffness':, *J. Spinal Disord.*, vol. 7, no. 4, p. 317???325, Aug. 1994, doi: 10.1097/00002517-199408000-00005.
[55] W. Johannessen, J. M. Cloyd, G. D. O'Connell, E. J. Vresilovic, and D. M. Elliott, 'Trans-Endplate Nucleotomy Increases Deformation and Creep Response in Axial Loading', *Ann. Biomed. Eng.*, vol. 34, no. 4, pp. 687–696, Apr. 2006, doi: 10.1007/s10439-005-9070-8.
[56] J. S. Tan and S. Uppuganti, 'Cumulative Multiple Freeze-Thaw Cycles and Testing Does Not Affect Subsequent Within-Day Variation in Intervertebral Flexibility of Human Cadaveric Lumbosacral Spine', *SPINE*, vol. 37, no. 20, pp. E1238–E1242, 2012, doi: 10.1097/BRS.0b013e31826111a3.
[57] J. M. Cottrell, M. C. H. van der Meulen, J. M. Lane, and E. R. Myers, 'Assessing the Stiffness of Spinal Fusion in Animal Models', *HSS J.*, vol. 2, no. 1, pp. 12–18, Feb. 2006, doi: 10.1007/s11420-005-5123-7.
[58] J. P. Dickey and D. J. Kerr, 'Effect of specimen length: are the mechanics of individual motion segments comparable in functional spinal units and multisegment specimens?', *Med. Eng. Phys.*, vol. 25, no. 3, pp. 221–227, Apr. 2003, doi: 10.1016/S1350-4533(02)00152-2.
[59] F. Russo *et al.*, 'Biomechanical Evaluation of Transpedicular Nucleotomy With Intact Annulus Fibrosus':, *SPINE*, vol. 42, no. 4, pp. E193–E201, Feb. 2017, doi: 10.1097/BRS.0000000000001762.
[60] D. J. Sucato, 'Thoracoscopic Discectomy and Fusion in an Animal Model: Safe and Effective When Segmental Blood Vessels Are Spared.', *SPINE*, vol. 27, no. 8, pp. 880–886, 2002.
[61] M. Palanca, M. Marco, M. L. Ruspi, and L. Cristofolini, 'Full-field strain distribution in multi-vertebra spine segments: An in vitro application of digital image correlation', *Med. Eng. Phys.*, vol. 52, pp. 76–83, Feb. 2018, doi: 10.1016/j.medengphy.2017.11.003.
[62] M. Palanca, T. M. Brugo, and L. Cristofolini, 'Use of Digital Image Correlation to investigate the Biomechanics of the Vertebra', *J. Mech. Med. Biol.*, vol. 15, no. 02, p. 1540004, Apr. 2015, doi: 10.1142/S0219519415400047.
[63] H.-J. Wilke, K. Wenger, and L. Claes, 'Testing criteria for spinal implants: recommendations for the standardization of in vitro stability testing of spinal implants', *Eur. Spine J.*, vol. 7, no. 2, pp. 148–154, May 1998, doi: 10.1007/s005860050045.
[64] S. M. Ross, 'Peirce's criterion for the elimination of suspect experimental data', *J. Eng. Technol.*, pp. 1–12, 2003.
[65] J. T. Lysack, J. P. Dickey, G. A. Dumas, and D. Yen, 'A continuous pure moment loading apparatus for biomechanical testing of multi-segment spine specimens', *J. Biomech.*, vol. 33, no. 6, pp. 765–770, Jun. 2000, doi: 10.1016/S0021-9290(00)00021-X.
[66] Busscher, 'Comparative anatomical dimensions of the complete human and porcine spine', 2010.
[67] C. Daly, P. Ghosh, G. Jenkin, D. Oehme, and T. Goldschlager, 'A Review of Animal Models of Intervertebral Disc Degeneration: Pathophysiology, Regeneration, and Translation to the Clinic', *BioMed Res. Int.*, vol. 2016, 2016, doi: 10.1155/2016/5952165.
[68] H.-J. Wilke, J. Geppert, and A. Kienle, 'Biomechanical in vitro evaluation of the complete porcine spine in comparison with data of the human spine', *Eur. Spine J.*, vol. 20, no. 11, pp. 1859–1868, Nov. 2011, doi: 10.1007/s00586-011-1822-6.
[69] J. P. Dickey, G. A. Dumas, and D. A. Bednar, 'Comparison of porcine and human lumbar spine flexion mechanics*', *Vet. Comp. Orthop. Traumatol.*, vol. 16, no. 01, pp. 44–49, 2003, doi: 10.1055/s-0038-1632753.

[70] I. Busscher, A. J. van der Veen, J. H. van Dieen, I. Kingma, G. J. Verkerke, and A. G. Veldhuizen, 'In Vitro Biomechanical Characteristics of the Spine A Comparison Between Human and Porcine Spinal Segments', *SPINE*, vol. 35, no. 2, pp. E35–E42, Jan. 2010, doi: 10.1097/BRS.0b013e3181b21885.
[71] A. J. Michalek and J. C. Iatridis, 'Height and torsional stiffness are most sensitive to annular injury in large animal intervertebral discs', *Spine J.*, vol. 12, no. 5, pp. 425–432, May 2012, doi: 10.1016/j.spinee.2012.04.001.
[72] R. E. Thompson, M. J. Pearcy, and T. M. Barker, 'The mechanical effects of intervertebral disc lesions', *Clin. Biomech.*, vol. 19, no. 5, pp. 448–455, Jun. 2004, doi: 10.1016/j.clinbiomech.2004.01.012.
[73] A. G. Patwardhan, R. M. Havey, K. P. Meade, B. Lee, and B. Dunlap, 'A Follower Load Increases the Load-Carrying Capacity of the Lumbar Spine in Compression.', *SPINE*, vol. 24, no. 10, pp. 1003–1009, 1999.
[74] A. G. Patwardhan, K. P. Meade, and B. Lee, 'A Frontal Plane Model of the Lumbar Spine Subjected to a Follower Load: Implications for the Role of Muscles', *J. Biomech. Eng.*, vol. 123, no. 3, pp. 212–217, Jun. 2001, doi: 10.1115/1.1372699.
[75] M. A. Adams, S. May, B. J. C. Freeman, H. P. Morrison, and P. Dolan, 'Effects of Backward Bending on Lumbar Intervertebral Discs: Relevance to Physical Therapy Treatments for Low Back Pain.', *SPINE*, vol. 25, no. 4, pp. 431–437, 2000.
[76] M. Al-Rawahi, J. Luo, P. Pollintine, P. Dolan, and M. A. Adams, 'Mechanical Function of Vertebral Body Osteophytes, as Revealed by Experiments on Cadaveric Spines':, *Spine*, vol. 36, no. 10, pp. 770–777, May 2011, doi: 10.1097/BRS.0b013e3181df1a70.
[77] M. L. Ruspi, M. Palanca, C. Faldini, and L. Cristofolini, 'Full-field in vitro investigation of hard and soft tissue strain in the spine by means of Digital Image Correlation', *Muscles Ligaments Tendons J.*, vol. 7, no. 4, pp. 538–545, Apr. 2018, doi: 10.11138/mltj/2017.7.4.538.
[78] M. Adams and P. Dolan, 'Time-dependent changes in the lumbar spine's resistancc to bending', *Clin. Biomech.*, vol. 11, no. 4, pp. 194–200, Jun. 1996, doi: 10.1016/0268-0033(96)00002-2.
[79] M. G. Gardner-Morse and I. A. Stokes, 'Physiological axial compressive preloads increase motion segment stiffness, linearity and hysteresis in all six degrees of freedom for small displacements about the neutral posture', *J. Orthop. Res.*, vol. 21, no. 3, pp. 547–552, Jan. 2003, doi: 10.1016/S0736-0266(02)00199-7.
[80] V. Fuster, 'Changing Demographics: A New Approach to Global Health Care Due to the Aging Population', *J. Am. Coll. Cardiol.*, vol. 69, no. 24, pp. 3002–3005, Jun. 2017, doi: 10.1016/j.jacc.2017.05.013.
[81] M. G. Fehlings *et al.*, 'The Aging of the Global Population: The Changing Epidemiology of Disease and Spinal Disorders', *Neurosurgery*, vol. 77, no. suppl_1, pp. S1–S5, Oct. 2015, doi: 10.1227/NEU.0000000000000953.
[82] I. M. Shapiro and M. V. Risbud, Eds., *The Intervertebral Disc: Molecular and Structural Studies of the Disc in Health and Disease*. Wien: Springer-Verlag, 2014. doi: 10.1007/978-3-7091-1535-0.
[83] F. Knutsson, 'The Vacuum Phenomenon in the Intervertebral Discs', *Acta Radiol.*, vol. os-23, no. 2, pp. 173–179, Mar. 1942, doi: 10.1177/028418514202300207.
[84] E. Samuel, 'Vacuum Intervertebral Discs', *Br. J. Radiol.*, vol. 21, no. 247, 1948, doi: 10.1259/0007-1285-21-247-337.
[85] N. Inoue and A. A. Espinoza Orías, 'Biomechanics of Intervertebral Disk Degeneration', *Orthop. Clin. North Am.*, vol. 42, no. 4, pp. 487–499, Oct. 2011, doi: 10.1016/j.ocl.2011.07.001.
[86] J. Yue, R. Guyer, J. P. Johnson, L. Khoo, and S. Hochschuler, *The Comprehensive Treatment of the Aging Spine - 1st Edition - Minimally Invasive and Advanced Techniques*, Saunders. 2010. Accessed: Jan. 26, 2021. [Online]. Available: https://www.elsevier.com/books/the-comprehensive-treatment-of-the-aging-spine/9781437703733
[87] J. F. Behrsin and C. A. Briggs, 'Ligaments of the lumbar spine: a review', *Surg. Radiol. Anat.*, vol. 10, no. 3, pp. 211–219, Sep. 1988, doi: 10.1007/BF02115239.
[88] M. Palanca *et al.*, 'The strain distribution in the lumbar anterior longitudinal ligament is affected by the loading condition and bony features: An in vitro full-field analysis', *PloS One*, vol. 15, no. 1, p. e0227210, 2020, doi: 10.1371/journal.pone.0227210.

[89] I. Castro-Mateos, J. M. Pozo, A. Lazary, and A. Frangi, '3D Vertebra Segmentation by Feature Selection Active Shape Model', in *Recent Advances in Computational Methods and Clinical Applications for Spine Imaging*, J. Yao, B. Glocker, T. Klinder, and S. Li, Eds. Cham: Springer International Publishing, 2015, pp. 241–245. doi: 10.1007/978-3-319-14148-0_22.
[90] M. van Rijsbergen *et al.*, 'Comparison of patient-specific computational models vs. clinical follow-up, for adjacent segment disc degeneration and bone remodelling after spinal fusion', *PLOS ONE*, vol. 13, no. 8, p. e0200899, Aug. 2018, doi: 10.1371/journal.pone.0200899.
[91] K. Y. E. Aryanto, M. Oudkerk, and P. M. A. van Ooijen, 'Free DICOM de-identification tools in clinical research: functioning and safety of patient privacy', *Eur. Radiol.*, vol. 25, no. 12, pp. 3685–3695, Dec. 2015, doi: 10.1007/s00330-015-3794-0.
[92] P. E. Eltes *et al.*, 'Geometrical accuracy evaluation of an affordable 3D printing technology for spine physical models.', *J. Clin. Neurosci. Off. J. Neurosurg. Soc. Australas.*, vol. 72, pp. 438–446, Jan. 2020, doi: 10.1016/j.jocn.2019.12.027.
[93] H.-J. Wilke, 'Is It Possible to Simulate Physiologic Loading Conditions by Applying Pure Moments? A Comparison of In Vivo and In Vitro Load Components in an Internal Fixator', *SPINE*, vol. 26, no. 6, pp. 636–642, doi: 10.1097/00007632-200103150-00014.
[94] Bergmann, G. (ed.), Charité Universitaetsmedizin Berlin, 'OrthoLoad', 2008. https://orthoload.com/database/ (accessed Feb. 04, 2022).
[95] G. Lionello, C. Sirieix, and M. Baleani, 'An effective procedure to create a speckle pattern on biological soft tissue for digital image correlation measurements', *J. Mech. Behav. Biomed. Mater.*, vol. 39, pp. 1–8, Nov. 2014, doi: 10.1016/j.jmbbm.2014.07.007.
[96] M. Palanca, G. Tozzi, and L. Cristofolini, 'The use of digital image correlation in the biomechanical area: a review', *Int. Biomech.*, vol. 3, no. 1, pp. 1–21, Jan. 2016, doi: 10.1080/23335432.2015.1117395.
[97] F. Morosato, F. Traina, and L. Cristofolini, 'Effect of different motor tasks on hip cup primary stability and on the strains in the periacetabular bone: An in vitro study', *Clin. Biomech.*, vol. 70, pp. 137–145, Dec. 2019, doi: 10.1016/j.clinbiomech.2019.08.005.
[98] M. Tanaka, C. Weisenbach, M. Miller, and L. Kuxhaus, 'A Continuous Method to Compute Model Parameters for Soft Biological Materials', *J. Biomech. Eng.*, vol. 133, p. 074502, Jul. 2011, doi: 10.1115/1.4004412.
[99] J. D. Evans, *Straightforward statistics for the behavioral sciences*. Pacific Grove: Brooks/Cole Pub. Co., 1996.
[100] A. F. Tencer, A. M. Ahmed, and D. L. Burke, 'Some static mechanical properties of the lumbar intervertebral joint, intact and injured', *J. Biomech. Eng.*, vol. 104, no. 3, pp. 193–201, Aug. 1982, doi: 10.1115/1.3138348.
[101] R. G. Long, O. M. Torre, W. W. Hom, D. J. Assael, and J. C. Iatridis, 'Design Requirements for Annulus Fibrosus Repair: Review of Forces, Displacements, and Material Properties of the Intervertebral Disk and a Summary of Candidate Hydrogels for Repair', *J. Biomech. Eng.*, vol. 138, no. 2, Feb. 2016, doi: 10.1115/1.4032353.
[102] F. Heuer, H. Schmidt, Z. Klezl, L. Claes, and H.-J. Wilke, 'Stepwise reduction of functional spinal structures increase range of motion and change lordosis angle', *J. Biomech.*, vol. 40, no. 2, pp. 271–280, Jan. 2007, doi: 10.1016/j.jbiomech.2006.01.007.
[103] F. Heuer, H. Schmidt, and H.-J. Wilke, 'Stepwise reduction of functional spinal structures increase disc bulge and surface strains', *J. Biomech.*, vol. 41, no. 9, pp. 1953–1960, Jan. 2008, doi: 10.1016/j.jbiomech.2008.03.023.
[104] I. Posner, A. A. White, W. T. Edwards, and W. C. Hayes, 'A biomechanical analysis of the clinical stability of the lumbar and lumbosacral spine', *Spine*, vol. 7, no. 4, pp. 374–389, Aug. 1982, doi: 10.1097/00007632-198207000-00008.
[105] J. Janevic, J. A. Ashton-Miller, and A. B. Schultz, 'Large compressive preloads decrease lumbar motion segment flexibility', *J. Orthop. Res. Off. Publ. Orthop. Res. Soc.*, vol. 9, no. 2, pp. 228–236, Mar. 1991, doi: 10.1002/jor.1100090211.
[106] D. Spenciner, D. Greene, J. Paiva, M. Palumbo, and J. Crisco, 'The multidirectional bending properties of the human lumbar intervertebral disc', *Spine J.*, vol. 6, no. 3, pp. 248–257, May 2006, doi: 10.1016/j.spinee.2005.08.020.

[107] K. L. Markolf, ‘Deformation of the Thoracolumbar Intervertebral Joints in Response to External Loads: A biomechanical study using autopsy material’, *JBJS*, vol. 54, no. 3, pp. 511–533, Apr. 1972.
[108] D. B. Amin, D. Sommerfeld, I. M. Lawless, R. M. Stanley, B. Ding, and J. J. Costi, ‘Effect of degeneration on the six degree of freedom mechanical properties of human lumbar spine segments’, *J. Orthop. Res.*, vol. 34, no. 8, pp. 1399–1409, 2016, doi: 10.1002/jor.23334.
[109] S. A. Zirbel, D. K. Stolworthy, L. L. Howell, and A. E. Bowden, ‘Intervertebral disc degeneration alters lumbar spine segmental stiffness in all modes of loading under a compressive follower load’, *Spine J.*, vol. 13, no. 9, pp. 1134–1147, Sep. 2013, doi: 10.1016/j.spinee.2013.02.010.
[110] P. Eysel, J.-D. Rompe, R. Schoenmayr, and J. Zoellner, ‘Biomechanical Behaviour of a Prosthetic Lumbar Nucleus’, *Acta Neurochir. (Wien)*, vol. 141, no. 10, pp. 1083–1087, Oct. 1999, doi: 10.1007/s007010050486.
[111] D. McNally, J. Naylor, and S. Johnson, ‘An in vitro biomechanical comparison of Cadisc™-L with natural lumbar discs in axial compression and sagittal flexion’, *Eur. Spine J.*, vol. 21, no. 5, pp. 612–617, Jun. 2012, doi: 10.1007/s00586-012-2249-4.
[112] C. H. Flamme, N. von der Heide, C. Heymann, and C. Hurschler, ‘Primary stability of anterior lumbar stabilization: interdependence of implant type and endplate retention or removal’, *Eur. Spine J.*, vol. 15, no. 6, pp. 807–818, Jun. 2006, doi: 10.1007/s00586-005-0993-4.
[113] C. Techens, S. Montanari, F. Bereczki, P. E. Eltes, and Á. Lazáry, ‘Biomechanical consequences of cement discoplasty: an in vitro study on thoracolumbar human spines’, *PLOS ONE*, submitted.
[114] F. Bernardini, J. Mittleman, H. Rushmeier, C. Silva, and G. Taubin, ‘The ball-pivoting algorithm for surface reconstruction’, *IEEE Trans. Vis. Comput. Graph.*, vol. 5, no. 4, pp. 349–359, Oct. 1999, doi: 10.1109/2945.817351.
[115] P. Cignoni, C. Rocchini, and R. Scopigno, ‘Metro: Measuring Error on Simplified Surfaces’, *Comput. Graph. Forum*, vol. 17, no. 2, pp. 167–174, 1998, doi: 10.1111/1467-8659.00236.
[116] M. Palanca *et al.*, ‘Type, size, and position of metastatic lesions explain the deformation of the vertebrae under complex loading conditions’, *Bone*, vol. 151, p. 116028, Oct. 2021, doi: 10.1016/j.bone.2021.116028.
[117] W. H. Kirkaldy-Willis and H. F. Farfan, ‘Instability of the lumbar spine’, *Clin. Orthop.*, no. 165, pp. 110–123, May 1982.
[118] N. Tanaka, H. S. An, T.-H. Lim, A. Fujiwara, C.-H. Jeon, and V. M. Haughton, ‘The relationship between disc degeneration and flexibility of the lumbar spine’, *Spine J.*, vol. 1, no. 1, pp. 47–56, Jan. 2001, doi: 10.1016/S1529-9430(01)00006-7.
[119] R. E. Thompson, M. J. Pearcy, K. J. Downing, B. A. Manthey, I. H. Parkinson, and N. L. Fazzalari, ‘Disc lesions and the mechanics of the intervertebral joint complex’, *Spine*, vol. 25, no. 23, pp. 3026–3035, Dec. 2000, doi: 10.1097/00007632-200012010-00010.
[120] R. E. Thompson, M. J. Pearcy, and T. M. Barker, ‘The mechanical effects of intervertebral disc lesions’, *Clin. Biomech.*, vol. 19, no. 5, pp. 448–455, Jun. 2004, doi: 10.1016/j.clinbiomech.2004.01.012.
[121] F. Galbusera, M. van Rijsbergen, K. Ito, J. M. Huyghe, M. Brayda-Bruno, and H.-J. Wilke, ‘Ageing and degenerative changes of the intervertebral disc and their impact on spinal flexibility’, *Eur. Spine J. Off. Publ. Eur. Spine Soc. Eur. Spinal Deform. Soc. Eur. Sect. Cerv. Spine Res. Soc.*, vol. 23 Suppl 3, pp. S324-332, Jun. 2014, doi: 10.1007/s00586-014-3203-4.
[122] B. L. Showalter, N. R. Malhotra, E. J. Vresilovic, and D. M. Elliott, ‘Nucleotomy reduces the effects of cyclic compressive loading with unloaded recovery on human intervertebral discs’, *J. Biomech.*, vol. 47, no. 11, pp. 2633–2640, Aug. 2014, doi: 10.1016/j.jbiomech.2014.05.018.
[123] H. Kuroki, V. K. Goel, S. A. Holekamp, N. A. Ebraheim, S. Kubo, and N. Tajima, ‘Contributions of flexion-extension cyclic loads to the lumbar spinal segment stability following different discectomy procedures’, *Spine*, vol. 29, no. 3, pp. E39-46, Feb. 2004, doi: 10.1097/01.brs.0000106683.84600.e5.
[124] T. Lee, T.-H. Lim, S.-H. Lee, J.-H. Kim, and J. Hong, ‘Biomechanical function of a balloon nucleus pulposus replacement system: A human cadaveric spine study’, *J. Orthop. Res. Off. Publ. Orthop. Res. Soc.*, vol. 36, no. 1, pp. 167–173, Jan. 2018, doi: 10.1002/jor.23607.

[125] T. P. Green, M. A. Adams, and P. Dolan, ‘Tensile properties of the annulus fibrosus II. Ultimate tensile strength and fatigue life’, *Eur. Spine J. Off. Publ. Eur. Spine Soc. Eur. Spinal Deform. Soc. Eur. Sect. Cerv. Spine Res. Soc.*, vol. 2, no. 4, pp. 209–214, Dec. 1993, doi: 10.1007/BF00299448.
[126] M. D. Humzah and R. W. Soames, ‘Human intervertebral disc: Structure and function’, *Anat. Rec.*, vol. 220, no. 4, pp. 337–356, 1988, doi: 10.1002/ar.1092200402.
[127] J. Steurer, S. Roner, R. Gnannt, and J. Hodler, ‘Quantitative radiologic criteria for the diagnosis of lumbar spinal stenosis: a systematic literature review’, *BMC Musculoskelet. Disord.*, vol. 12, no. 1, p. 175, Jul. 2011, doi: 10.1186/1471-2474-12-175.
[128] G. Andreisek *et al.*, ‘A Systematic Review of Semiquantitative and Qualitative Radiologic Criteria for the Diagnosis of Lumbar Spinal Stenosis’, *Am. J. Roentgenol.*, vol. 201, no. 5, pp. W735–W746, Nov. 2013, doi: 10.2214/AJR.12.10163.
[129] H. Yoshihara, ‘Indirect decompression in spinal surgery’, *J. Clin. Neurosci.*, vol. 44, pp. 63–68, Oct. 2017, doi: 10.1016/j.jocn.2017.06.061.
[130] R. Navarro-Ramirez *et al.*, ‘A New Volumetric Radiologic Method to Assess Indirect Decompression After Extreme Lateral Interbody Fusion Using High-Resolution Intraoperative Computed Tomography’, *World Neurosurg.*, vol. 109, pp. 59–67, Jan. 2018, doi: 10.1016/j.wneu.2017.07.155.
[131] T. A. Gates, R. R. Vasudevan, K. J. Miller, V. Stamatopoulou, and S. A. Mindea, ‘A novel computer algorithm allows for volumetric and cross-sectional area analysis of indirect decompression following transpsoas lumbar arthrodesis despite variations in MRI technique’, *J. Clin. Neurosci.*, vol. 21, no. 3, pp. 499–502, Mar. 2014, doi: 10.1016/j.jocn.2013.05.007.
[132] G. Lang *et al.*, ‘Potential and Limitations of Neural Decompression in Extreme Lateral Interbody Fusion—A Systematic Review’, *World Neurosurg.*, vol. 101, pp. 99–113, May 2017, doi: 10.1016/j.wneu.2017.01.080.
[133] J. Sato *et al.*, ‘Radiographic evaluation of indirect decompression of mini-open anterior retroperitoneal lumbar interbody fusion: oblique lateral interbody fusion for degenerated lumbar spondylolisthesis’, *Eur. Spine J.*, vol. 26, no. 3, pp. 671–678, Mar. 2017, doi: 10.1007/s00586-015-4170-0.
[134] J. Yao *et al.*, ‘A multi-center milestone study of clinical vertebral CT segmentation’, *Comput. Med. Imaging Graph.*, vol. 49, pp. 16–28, Apr. 2016, doi: 10.1016/j.compmedimag.2015.12.006.

# Acknowledgement

The past three years have been a long adventure and I would like to thank the people who walked beside me, people who provided help, support or challenged me, but in the end who considerably contributed to this journey.

First, I would like to thank my team, Jennifer, Denata, Jose, Cameron, and Marco. Although we were not physically together, our group has been a place to share our struggles, victories, and memories which made this PhD unforgettable. You were always a source of resilience, support, advice, and listening. Thank you for that.

Jennifer, how not to mention your great company. Without you, I would have been cold, serious, lost in so many occasions, hungry, alone in quarantine, homeless, and with no umbrellas! Thanks for introducing me to Budapest and easing my adaptation. More than a colleague, I am happy to have met a friend. I hope our ways will cross again somewhere around the globe.

Thank you Sara, you were my hands, my brain, and my memory during these months of tests. Working with you was a daily pleasure, and I am grateful for the dedication you put in this project. I could always rely on your hard work, perpetual enthusiasm, and rigour.

Toti, you taught me how to properly dislocate a spine (prepare specimens I mean!) and now I can safely jog around the world. More seriously, thank you for showing me everything, rushing down each time the paint gun was not correctly working. Your help was crucial for the success of this work.

I would like to thank Federico for always bringing sunshine and smile to the room. I won't forget our endless mathematical debates in the middle of corridors. Having you around made science exciting, limitless, and even funnier.

Marco, thank you for your kindness and your sensibility. You were a great teacher and a fantastic co-worker. It is always difficult to find people who share our work method. With you, 'work hard, play hard' was just the same thing at once. No need to mention your priceless contribution to make the lab a fashion place.

Luca, where to start… Thank you for offering me this opportunity. I did not know where I was going, and that was a life changing experience in so many ways. I could not have hoped for a better supervision. I remember at the interview I asked you to describe yourself and you answered you tried to be always available. But this was even a euphemism. Thank you for the late meetings, the always deep feedbacks despite the short deadlines, you were there whenever the day. More than the professor, I met an amazing person. Thank you for your humanity, you made this relationship a safe place where it was easy to

express opinions, disagreements, or troubles, and always brought wise solutions. That is truly inspiring. In short, I am grateful for the tremendous support, attention, trust, kindness you showed.

I would like to also mention Samuele, Cristina and Roberta for their warm welcoming and company in Bologna, Miguel and Guillermo for their help in the research and their companionship. Particular thanks to Samuele for his linguistic advices!

Peter, thank you for welcoming me in your team. You have always done everything to provide me with the best working environment. Our collaboration was shorter than expected but it was very rewarding, and I will keep good memories of Budapest. Thank you for your trust, and even if we did not often run into each other, I could always feel your support.

Thank you also to Aron for your very supportive comments which always lifted my spirit. Thank you for including me in Budapest's team as if I was a full-time member of the lab.

I would like to highlight the tremendous help of Ferenc. You provided a great support, gave a lot of your time for my project. I am grateful for your dedication even when you were doubting the outcome.

Thank you also to Agoston, Beni, and Mate for the company and the cheering-up in the lab. I was happy to have met you, and I wish you the best luck for your PhDs.

Many thanks to Fabrizio, this unexpected encounter from life, which led to me signing up for this project. You advised me, encouraged me to follow my intuitions, and definitively omitted to mention the exhaustion of the job!

I need to mention my sister, Lise, who called every time she knew I was sad or lonely. Your youth is refreshing and your analyses always relevant.

Mathieu thanks for your patience, for giving me the time I needed and waiting on me. I know it was not always easy for you and you did not spend the last three years exactly the way you would have chosen. You showed your usual understanding whether I was busy or needed company. If my life goes like an electron, you bring the stability I need to hold the rest together (one would say the spine!). Despite appearances, you were my home for the past three years, and not just because I tend to keep my luggage at your place!

Finally, I would like to thank me. I want to remember what the journey was like and not the easy, happy trip you will picture soon. This is the completion of a crazy objective in an eleven-year-old girl mind. Besides the science and being called doctor (let's be honest, it is fancy), you started this adventure because you needed to gain strength and confidence, to become self-sufficient. Three years later, you reached the most important goals. I want you to be proud because you evolved so much during this time, became an adult, and more important because this thesis is the result of your perseverance and resilience. You made it happen.

I probably forgot a lot of people, sorry for that. Thank you all for colouring these past three years and for your inspiration.

Sincerely,

Chloé